Analysis of the Lee-Yang Zeros in Lattice Compact QED with Scalars and Fermions in 3D and in Lattice Non-Compact QED in 4D

Nektarios Psycharis

Thesis submitted to
the University of Glasgow
for the degree of Doctor of Philosophy
in December 1998

This Thesis is dedicated to my Parents Ioannis and Anastasia in recognition of their financial support without which I could not had finished my studies and to Katerina for her support and encouragement and for helping me to put things in perspective.

"As you set out for Ithaka hope your road is a long one, full of adventure, full of discovery. Laistrygonians, Cyclops, angry Poseidon–don't be afraid of them: you'll never find things like that on your way as long as you keep your thoughts raised high, as long as a rare excitement stirs your spirit and your body".

Kostas Kavafis

Acknowledgements

Firstly I would like to thank my supervisor Dr. Ian Barbour for his supervision and his patient guidance during my thesis. I also appreciated the advice of Dr. Christine Davies. I would also like to thank all the people in the Department of Physics and Astronomy who have helped to make my Postgraduate studies in Glasgow such a pleasurable experience. I also appreciated the financial support from the University of Glasgow during the last stages of my studies. I would also like to thank Dr. Andrew Davies for his help and Dr. David Sutherland for his comments in the introduction.

It has been a great source of stimulation to work in collaboration with Professor Jiri Jersak and Dr. Wolfgang Franzki who contributed significantly to my understanding of Lattice QED with fermions and scalars. I would also like to thank Professor Dario Bini for useful discussions regarding the multi-precision package for the calculation of the Lee-Yang zeros.

I would also like to thank the Glasgow Postdocs: Hugh Shanahan, Sara Collins, Joachim Hein Arifa Ali-Khan, Peter Boyle , Spyros Manolopoulos, Paul McNamara, Geppo Cagnoli and Manfred Oevers who have proved to be an invaluable source of information.

I have enjoyed the company of the Postgraduate students including Paul and Susan who helped me considerably during my first year; Mark G., David, Steven, Mark C. ,Gordon, Alessandro U., Alessandro T., Peter, Lawrence and Keith , Steven D., and Mark-Antoine Senechal with whom I have shared numerous discussions, and have made my stay here pleasurable.

I would also like to thank some people from my home country, Greece. I would like to thank Georgia and Adreas for their support and encouragement; it has been invaluable help for me. I would also like to thank Stamati who helped me to understand a lot about myself. I am grateful for the encouragement and financial support from my parents, Ioannis and Anastasia, without which I could not

had finished my studies. I also appreciated the encouragement from my brother Saranto and Giota.

Last but not least, I would like to thank Katerina for her support and encouragement and for helping me to put things in perspective.

Glasgow December 1998

Declaration

In this thesis Chapters 1 and 2 are introductions to lattice QED with Scalars and Fermions. Chapter 3 describes the Lee-Yang zeros analysis and the Lanczos algorithm. The work in Chapters 4 and 5 was done in collaboration with Dr. W. Franzki and Prof. J. Jersak. Chapters 6 and 7 are my own work. All of the work in this thesis was done in conjunction with my supervisor Dr. I. M. Barbour.

Contents

Abstract

Attempts to construct a theory with dynamical breaking of global chiral symmetries in four dimensions, which could explain or replace the Higgs-Yukawa mechanism of particle mass generation, usually lead to the introduction of a new strong gauge interaction beyond the standard model and its standard extensions. A lattice model with fermions and scalar fields and the compact U(1) gauge group, has been suggested in [1] as a promising candidate for such a prototype field theory on the lattice, and it is called the "$\chi U\phi$ model" or QED with scalars and fermions. The chiral symmetry of this model is broken by the gauge interaction and restored by the light scalar.

We investigate the critical behaviour of the three-dimensional lattice $\chi U\phi_3$ model in the chiral limit. The model consists of a staggered fermion field, a $U(1)$ gauge field (with coupling parameter β) and a complex scalar field (with hopping parameter κ). Two different methods are used: 1) fits of the chiral condensate and the mass of the neutral unconfined composite fermion to an equation of state and 2) finite size scaling investigations of the Lee-Yang zeros of the partition function in the complex fermion mass plane. For strong gauge coupling ($\beta \leq 0.80$) the critical exponents for the chiral phase transition are determined. We find strong indications that the chiral phase transition is in one universality class in this β interval: that of the three-dimensional Gross-Neveu model with two fermions. Thus the continuum limit of the $\chi U\phi_3$ model defines here a nonperturbatively renormalizable gauge theory with dynamical mass generation. At weak gauge coupling and small κ, we explore a region in which the mass in the neutral fermion channel is large but the chiral condensate on finite lattices very small. If it does not vanish in the infinite volume limit, then a continuum limit with massive unconfined fermion might be possible in this region, too.

Calculations of the Lee-Yang zeros of the partition function in the complex fermion mass plane, were performed in [40] in order to help to clarify the position

of the critical point and the critical exponent of the transition of non-compact QED. However, exploratory simulations[39] of this theory on a 6^4 lattice showed that these zeros appeared to depend on the "updating" mass at which the ensemble they are found from is generated. This dependence is incorrect

Although we used a multi-precision package for the calculation of the Lee-Yang zeros, our analysis confirmed the dependence of the Lee-Yang zeros on the "updating" mass on a 6^4 lattice. High statistics simulations on large lattices, are probably necessary in order to verify the absence of the dependence of the edge singularity on the update mass at which the ensemble it is found from is generated.

Chapter 1

Introduction

1.1 Motivation

The search for alternatives to the Higgs mechanism generating the masses of gauge bosons and fermions in the electroweak theory is motivated by a feeling that this mechanism is handmade, and some dynamical explanation might be possible. Attempts to construct a theory with dynamical breaking of global chiral symmetries in four dimensions, which could explain or replace the Higgs-Yukawa mechanism of particle mass generation, usually lead to the introduction of a new strong gauge interaction beyond the standard model and its standard extensions. For example the heavy top quark and the idea of top condensate inspired the strongly coupled topcolor and similar gauge models[19]. Among the requirements such a theory should satisfy, the most general ones are the following two: First, because gauge theories tend to confine charges in a regime where they break chiral symmetries dynamically, the physical states, in particular fermions, must be composite singlets of a new gauge symmetry. Second, as a strong coupling regime is encountered, the models should be non-perturbatively renormalisable in order to be physically sensible in a sufficiently large interval of scales. Even in very simplified models, these are too difficult dynamical problems to get reliably under

control by analytic means only. Therefore, a numerical investigation on the lattice of some prototypes of field theories with the above properties may be instructive. In such an approach, the presumably chiral character of the new gauge interaction and numerous phenomenological aspects have to be left out of consideration.

A promising candidate for such a prototype field theory on the lattice, has been suggested in [1]. It is called the "$\chi U \phi$ model" or QED with scalars and fermions.

However, this model is different from the common mechanisms of fermion mass generation in Quantum Field Theories (QFT) which belong to one of the two generic types: First, the chiral symmetry is broken by the scalar field and the fermion mass is a consequence of the Yukawa coupling, like in the Higgs-Yukawa sector of the standard model. Second, the chiral symmetry is broken by a strong gauge interaction accompanied by confinement of the fermions acquiring mass. No scalar field is involved.

Another interesting investigation within lattice gauge theories, involves Quantum Electrodynamics (QED). QED is a very succesful theory in describing the electromagnetic interactions of electrons, muons etc. to a high precision in perturbation theory. Therefore, the motivation at present is, by including a non-perturbative investigation of the theory, to try to improve the theoretical understanding of the general mathematical properies of QED (see chapter(7)).

1.2 Introduction to Lattice QED with Scalars and Fermions in 4D

The feeling that the Higgs mechanism of generating the masses of gauge bosons and fermions in the electroweak theory is handmade motivated the search for alternative dynamical explanations. A fundamental Higgs field is considered to provide a comfortable description of the spontaneous symmetry breaking allowing

a perturbative approach, but its use might not be really necessary. Therefore, most alternative attempts try to avoid the introduction of a fundamental scalar field. The obligatory Goldstone bosons, which should exist, are interpreted as composite states, formed by some strong dynamics beyond the standard model.

However, one should distinguish between a fundamental scalar field whose self-interaction triggers the symmetry breaking already on the tree level, as in the conventional Higgs mechanism, and such a field playing some different important role in the dynamical symmetry breaking occuring only beyond the perturbative expansion. In this second role, a fundamental scalar field is acceptable provided its particle excitations are massive or confined.

It should be pointed out that the experience accumulated on the lattice with strongly coupled vectorlike gauge theories with matter fields **suggests** the existence of still another alternative of dynamically generated spontaneous chiral symmetry breaking (SχSB). This mechanism[1] assumes some new confining gauge field A of a compact gauge group G, and makes use of a fundamental scalar field ϕ which is coupled to this gauge field and, consequently, confined. The scalar field, however, does not generate the SχSB; in fact, it is crucial that ϕ acts against it. The SχSB is generated dynamically by the interaction between the gauge field A and some fermion fields χ, making the gauge-invariant condensate $< \chi\bar{\chi} >$ nonzero in a analogy to the SχSB in Quantum Chromodynamics (QCD).

A special attention should be paid in the role of the scalar field. Its role is twofold. First, it shields the G charge of the fermion χ, so that composite G neutral physical fermion states of the form:

$$F = \phi^{\dagger}\chi$$

can exist asymptotically in spite of the confinement of the G charge. This is why this mechanism is called the shielded gauge mechanism (SGM).

Second, to make the model applicable in (the) continuum physics the lattice constant has to be made small and thus approach a phase transition of second

order. The scalar field has the tendency to suppress the SχSB and induces for very strong gauge coupling a new second order phase transition, at which the chiral symmetry is smoothly restored.

However, one should be more specific about the continuum physics of such a model; if e.g., the broken global symmetry is SU(2) with one fermion field doublet χ coupled to A, one can find a massive fermion doublet $F = \phi^\dagger\chi$ and three Goldstone bosons π, all being gauge invariant with respect to G. Because of confinement due to the new gauge interaction there are no physical states corresponding to the field ϕ, but bosonic gauge-invariant states consisting of χ, ϕ, and A, e.g., of the type $\phi^\dagger\phi$ and $\bar{\chi}\chi$, should be expected, some of them possibly looking like the Higgs boson. The situation is then quite similar to the standard model with the standard gauge fields switched off, symmetry breaking present, and one degenerate weak isospin fermion doublet heavy. The other fermions, not coupling to A, are massless. If the standard $SU(2)\otimes U(1)$ gauge fields are switched on, the broken global SU(2) changes into the local one, and the ϕ's lead to massive vector bosons. The Higgs mechanism has been replaced by the SGM but, of course, the fermion spectrum is quite nonrealistic, except possible speculations about a very heavy fourth family with small mass differences in weak isospin doublets. A more realistic application is suggested by ideas ascribing the top quark a special role in the symmetry breaking. In fact, the mechanism described, might be related to the top quark condensate models based on new strong gauge interactions at some energies beyond the electroweak scale, as suggested by various authors[9]. The problem is that these models are chiral gauge theories which still cannot be simulated on the lattice. Thus for this kind of physical application of the SGM it is assumed that the dynamics of strongly coupled chiral gauge theories with scalars is similar to the vectorlike lattice models.

Except for being non-chiral, the lattice $\chi U\phi$ model with the compact U(1) gauge group is a prototype of a lattice model with such properties. It is a vector-

like U(1) gauge theory which contains the staggered fermion field χ and the scalar field ϕ, both of unit charge. A Yukawa coupling between these matter fields is prohibited by the gauge symmetry. The global U(1) chiral symmetry, present when the bare mass m_0 of the fermion field χ vanishes, is broken dynamically at strong gauge coupling by the gauge interaction. Whereas both χ and ϕ constituents are confined, the massive physical fermion $F = \phi^\dagger\chi$ with shielded charge appears. The Dynamical Mass Generation(DMG) occurs naturally at strong coupling due to the gauge interaction, i.e., without the help of the charged scalar field. The scalar suppresses the symmetry breaking when it gets lighter and induces a phase transition to the chiral symmetric phase. If the theory is renormalisable, a continuum theory with massive fermion F, as well as a massless Goldstone boson ("pion" π) would be obtained. When the global U(1) chiral symmetry, modelling the SU(2) symmetry of the standard model, is gauged, this π boson is eaten by the corresponding massive gauge boson. This is what is achieved in standard approaches by the Higgs-Yukawa mechanism.

The question is, whether this model is non-perturbatively renormalizable at strong gauge coupling so that the lattice cutoff can be removed. If so, the resulting theory might be applicable in the continuum and constitute a possible alternative to the Higgs mechanism [1].

We investigate such a lattice model in **three dimensions** with a vectorlike U(1) gauge symmetry, which is called the $\chi U\phi_3$ **model** or **QED with scalars and fermions in three dimensions**.

The same model has also been investigated in two and four dimensions. In two dimensions it seems to be in the universality class of the Gross-Neveu model [10] at least for strong gauge coupling, and so is renormalizable. Thus the shielded gauge-charge mechanism of dynamical mass generation suggested in [1] works in two dimensions and its long range behaviour is equivalent to the four fermion theory. In four dimensions there is also a strong coupling region in which the

model behaves in a very similar manner to the corresponding four-fermion theory, the Nambu–Jona-Lasinio model with a massive fermion whose mass scales at the critical point [37]. Here both models belong to the same universality class and have the same renormalizability properties. But for intermediate coupling there evidently exists a special point. It is a tricritical point at which, together with the composite fermion F, scaling of a particular scalar state was found. This composite scalar can be interpreted as a gauge ball mixing with a $\phi^\dagger$-ϕ state. Thus the gauge degrees of freedom play an important dynamical role and the model belongs to a new universality class of models with dynamical mass generation and whose renormalizability is of much interest [12, 13].

1.3 Lattice Discretization in 4D

The great feature of the lattice method is that it provides a non-perturbative regularisation for QFT, enabling systematic calculation without the aid of Feynman diagrams.

There are many different ways of discretizing a given continuum action for the lattice. It is important for universality that they do not lead to different continuum theories in the limit of the lattice spacing going to zero. In addition it is desirable to retain the symmetries of the continuum action in the lattice discretization.

1.3.1 Gauge and Scalar Fields on the Lattice

As we have already mentioned we consider the $\chi U \phi$ model with U(1) gauge symmetry. The U(1) gauge action in the continuum ($S_G^{(cont.)}$) is given by:

$$S_G^{(cont.)} = \frac{1}{4} \int d^4x \, F_{\mu\nu} F^{\mu\nu} \tag{1.1}$$

where:

$$F_{\mu\nu} = \partial_\mu A_\nu(x) - \partial_\nu A_\mu(x) \tag{1.2}$$

is the gauge invariant field strength tensor, and $A_\mu(x)$ is a four vector potential.

In lattice QED the gauge field is represented by the group element connecting neighbouring lattice sites:

$$U_\mu(x) = \exp\left(ieA_\mu(x)a\right) \tag{1.3}$$

where a is the lattice spacing, e turns out to be the coupling constant in the continuum limit and $A_\mu(x)$ is a field defined on the link which turns out to be the gauge potential field in the continuum limit. Our choice of lattice gauge action is dictated by the requirement of local gauge invariance under the transformation:

$$U_\mu(x) \rightarrow \Omega(x)U_\mu(x)\Omega^{-1}(x+\hat{\mu}) \tag{1.4}$$

where $\Omega \in U(1)$ and is defined independently on each lattice site.

Eqn.(1.3) can also be writen as :

$$U_\mu(x) = \exp(i\theta_\mu(x)) \tag{1.5}$$

where $\theta_\mu(x)$ is restricted to the **compact** domain $[0, 2\pi]$.

The simplest possible gauge invariant action is defined in terms of the elementary plaquette variable $U^P_{\mu\nu}(x)$ which is the trace of a directed product of gauge links around a closed loop joining a sequence of nearest neighbour sites:

$$U^P_{\mu\nu}(x) = U_\mu(x)\, U_\nu(x+\hat{\mu})\, U^\dagger_\mu(x+\hat{\nu})\, U^\dagger_\nu(x). \tag{1.6}$$

Inserting the expression (1.3) into (1.6) we find:

$$U^P_{\mu\nu}(x) = \exp\left(iea^2 F^L_{\mu\nu}(x)\right) \tag{1.7}$$

where $F^L_{\mu\nu}(x)$ is a discretized version of the continuum field strength tensor:

$$F^L_{\mu\nu}(x) = \frac{1}{2}[(A_\nu(x+\hat{\mu}) - A_\nu(x)) - (A_\mu(x+\hat{\nu}) - A_\mu(x))]. \tag{1.8}$$

It now follows from (1.7) that for small lattice spacing:

$$\frac{1}{e^2}\sum_{x,\mu;\,\nu>\mu}\left[1 - \frac{1}{2}\left(U^P_{\mu\nu}(x) + (U^P_{\mu\nu})^\dagger(x)\right)\right] \approx \frac{1}{4}\sum_{x\,,\mu\,\nu} a^4 F^L_{\mu\nu}(x)F^L_{\mu\nu}(x) \tag{1.9}$$

where the sum appearing on the left hand side extends over the contributions coming from all distinct plaquettes on the lattice. Therefore, the lattice action for the gauge potential in the compact form can be written as:

$$S_G = \frac{1}{e^2} \sum_P \left[1 - \frac{1}{2} \left((U^P_{\mu\nu})(x) + (U^P_{\mu\nu})^\dagger(x) \right) \right]. \tag{1.10}$$

We have also mentioned earlier that we consider the $\chi U \phi$ model with a complex scalar field ϕ. The action of the complex scalar field, in the lattice formulation, is introduced as:

$$S_\phi = \sum_x \left[(\phi^\dagger_x \phi_x) + \lambda[(\phi^\dagger_x \phi_x) - 1]^2 - \kappa \sum_{\mu=\pm 1}^{\pm 4} (\phi^\dagger_x U_{x,\mu} \phi_{x+\mu} + \phi^\dagger_{x+\mu} U^\dagger_{x,\mu} \phi_x) \right] \tag{1.11}$$

where κ is the gauge-scalar coupling (or hopping parameter) and the λ term determines the quartic selfinteraction of the scalar field. The action is symmetric under the reflection of κ, so that it is sufficient to consider $\kappa \geq 0$. For $\lambda = \infty$ the modulus of the scalar field is frozen at the value one. We consider the scalar field in the fixed length limit,i.e.:

$$(\phi^\dagger_x \phi_x) = 1. \tag{1.12}$$

Therefore, in this limit, the action of the complex scalar field reads (omitting irrelevant constant) :

$$S_\phi = -\kappa \sum_x \sum_\mu (\phi^\dagger_x U_{x,\mu} \phi_{x+\mu} + \phi^\dagger_{x+\mu} U^\dagger_{x,\mu} \phi_x). \tag{1.13}$$

1.3.2 Fermions on the Lattice

Before introducing the fermion fields on the lattice we recall the Dirac fermionic action:

$$S_F^{(cont.)} = \int d^4x \, \bar{\psi}(x) \left(\gamma_\mu (\partial_\mu + ieA_\mu) + m_o \right) \psi(x) \tag{1.14}$$

with

$$\gamma_\mu \gamma_\nu + \gamma_\nu \gamma_\mu = 2\delta_{\mu\nu} \; ; \; \gamma^\dagger_\mu = \gamma_\mu. \tag{1.15}$$

The fermion fields are associated with lattice sites and the continuum Dirac action is discretized by approximating the partial derivative by an antihermitean lattice derivative defined by:

$$\partial_\mu \psi_\alpha(x) \equiv \frac{1}{2a}\left[\psi_\alpha(x + a\hat{\mu}) - \psi_\alpha(x - a\hat{\mu})\right] \tag{1.16}$$

where ψ_α is a single component of the four component field ψ. The lattice form of the fermion action is:

$$S_F = \sum_{x,y,\alpha,\beta} \bar{\psi}_\alpha(x) M_{\alpha\beta}(x,y) \psi_\beta(y) \tag{1.17}$$

where in the interacting case the fermion Dirac matrix M is given by:

$$M_{\alpha\beta}(x,y) = \sum_\mu \frac{1}{2a}(\gamma_\mu)_{\alpha\beta}\left[U_\mu(x)\delta_{y,x+a\hat{\mu}} - U_\mu^\dagger(x)\delta_{y,x-a\hat{\mu}}\right] + m_0 \delta_{yx}\delta_{\alpha\beta} \tag{1.18}$$

so the dimensionless two point function is given by:

$$\left\langle \hat{\psi}_\alpha(x), \hat{\bar{\psi}}_\beta(y) \right\rangle = [M_{\alpha\beta}(x,y)]^{-1}. \tag{1.19}$$

After Fourier transforming to momentum space and taking the continuum limit we obtain the following expression for the physical correlation function:

$$\left\langle \psi_\alpha(x)\bar{\psi}_\beta(y) \right\rangle = \lim_{a\to 0} \int_{-\pi/a}^{\pi/a} \frac{d^4p}{(2\pi)^4} \frac{\left[-i\sum_\mu \gamma_\mu \tilde{p}_\mu + m_0\right]_{\alpha\beta}}{\tilde{p}_\mu^2 + {m_0}^2} e^{ip(x-y)} \tag{1.20}$$

where:

$$\tilde{p}_\mu = \frac{1}{a}\sin(p_\mu a). \tag{1.21}$$

The poles of eqn(1.20) correspond to physical particles. On the other hand the zeros of the sine function (eqn.(1.21)) at the edges of the first Brillouin zone destroy the correct continuum limit – they give rise to fermion species doubling [8]. Thus there exist sixteen regions of integration in eqn.(1.20) where $\tilde{p}$ takes a finite value in the limit $a \to 0$. Of these, fifteen regions involve high momentum excitations of the order of $\frac{\pi}{a}$ (and $\frac{-\pi}{a}$), which give rise to a momentum distribution

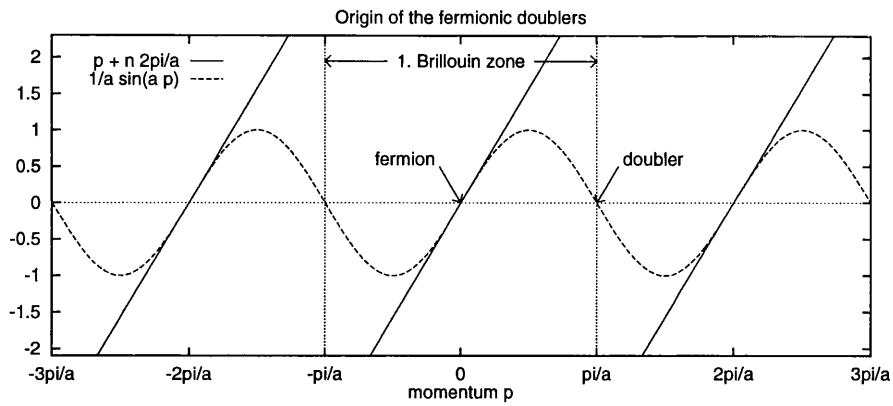

Figure 1.1: The origin of the fermionic doublers is clear from this plot of the inverse fermion propagator for the case of a massless free fermion.

function having the form resembling that of a single particle propagator. Hence, in the continuum limit, the Green function (1.20) receives contributions from sixteen fermion-like excitations in momentum space, of which fifteen are pure lattice artefacts having no continuum analog. In d space-time dimensions the number would be 2^d; i.e. it doubles for each additional dimension.

In other words, the inverse propagator for a massless free fermion is given by:

$$S^{-1}(p) = i \sum_{\mu} \gamma_\mu \frac{1}{a} \sin(p_\mu a) \; ; \; -\pi/a < p_\mu \leq \pi/a \tag{1.22}$$

where the periodicity of the sine function means that we have not one, but sixteen poles in every Brillouin zone. This is illustrated in Fig.(1.1). Nielsen and Ninomiya [5, 6, 7] showed that the fermion doubling problem cannot be eliminated without breaking the chiral symmetry in the limit $m_0 \to 0$.

1.3.3 Kogut-Susskind Fermions

One of the schemes dealing with fermion doubling is the Wilson fermions, whereby an irrelevant term is added to the action (1.17) which vanishes in the naive continuum limit. Wilson fermions have the disadvantage that the irrelevant term

explicitly breaks the chiral symmetry (even for $m_0 \to 0$) of the original lattice action. Since we are interested in the chiral phase transition, we will use Kogut-Susskind fermions which preserve a non-trivial piece of the full chiral symmetry.

The Kogut-Suskind scheme deals with the fermion doubling problem by reducing the Brillouin zone; i.e. by doubling the effective lattice spacing.

We consider the naive fermion action with spin indices α, β shown explicitly (and where the lattice spacing, $a = 1$, where not explicitly stated) :

$$\begin{aligned} S &= \frac{1}{2}\sum_{x,\mu}\left[\bar{\psi}_\alpha(x)(\gamma_\mu)_{\alpha\beta}\psi_\beta(x+\hat{\mu}) - \bar{\psi}_\alpha(x)(\gamma_\mu)_{\alpha,\beta}\psi_\beta(x-\hat{\mu})\right] \\ &\quad + m_0\sum_x \bar{\psi}_\alpha(x)\delta_{\alpha\beta}\psi_\beta(x). \end{aligned} \tag{1.23}$$

By making a local change of variables we arrive at an action which is diagonal in the Dirac indices thus the different fermion field components are decoupled and we keep only a single field component per site.

In more detail, we perform a local change of the fermionic variables, such as:

$$\psi_\alpha(x) = T_{\alpha\beta}(x)\chi_\beta(x) \;\; ; \;\; \bar{\psi}_\alpha(x) = \bar{\chi}_\beta(x)T^\dagger_{\beta\alpha}(x) \tag{1.24}$$

where in d spacetime dimensions, $T(x)$ are $2^{d/2}\times 2^{d/2}$ unitary matrices, and we can spin diagonalize the previous expression by choosing the matrices $T(x)$ in such a way that:

$$T^\dagger(x)\gamma_\mu T(x+\hat{\mu}) = \eta_\mu(x)\mathbf{1}. \tag{1.25}$$

If we choose:

$$T(x) = \gamma_1^{x_1}\gamma_2^{x_2}\gamma_3^{x_3}\gamma_4^{x_4} \tag{1.26}$$

where (x_1, x_2, x_3, x_4) are the components of the lattice site four-vector x, then the appropriate phases are:

$$\eta_1(x) = \mathbf{1}\,;\; \eta_\mu(x) = (-1)^{x_1+x_2+\ldots x_{\mu-1}}. \tag{1.27}$$

After spin diagonalization and inclusion of gauge interactions the action reads:

$$S_F^{(K.S.)} = \frac{1}{2}\sum_{x,\mu,\alpha}\eta_\mu(x)\left[\bar{\chi}_\alpha(x)U_\mu(x)\chi_\alpha(x+\hat{\mu}) - \bar{\chi}_\alpha(x)U^\dagger_\mu(x-\hat{\mu})\chi_\alpha(x-\hat{\mu})\right]$$

$$+ \quad m_0 \sum_{x,\alpha} \bar{\chi}_\alpha(x)\chi(x). \tag{1.28}$$

By eliminating the Dirac matrix γ_μ we have decoupled the fermion field components thus we can reduce the number of fermion field components to a single one per site. The above action is diagonal in $\chi_\alpha(x)$ and is thus simply four copies of the same action written in terms of a one-component Grassmann variable $\chi_\alpha(x)$ and a space dependent sign $\eta_\mu(x)$.

The remaining four fermion species are interpreted as physical flavours in the continuum limit. Thus the lattice action reduces in the naive continuum limit to a sum of free fermion actions, one for each of the quark flavours:

$$S_f^{(K.S.)} \to \int d^4x \sum_{\alpha,\beta,f} \bar{\psi}^f_\alpha(x) \left(\gamma_\mu \partial_\mu + m\right)_{\alpha\beta} \psi^f_\beta(x) \tag{1.29}$$

where f is the flavour index which ranges from 1 to 4 and α, β are the spinor indices. Note that the staggered formulation has the disadvantage that in d spacetime dimensions it is restricted to a description of $2^{d/2}$ degenerate quark flavours.

The staggered fermion action (Eqn.(1.28)) is local, Hermitian and invariant under the global $U(1)_1$ rotation:

$$\chi(x) \to e^{i\alpha}\chi(x) \; ; \; \bar{\chi}(x) \to \bar{\chi}(x)e^{-i\alpha}. \tag{1.30}$$

In the massless case ($m_0 = 0$) this symmetry becomes extended and we have the additional $U(1)_\epsilon$ symmetry defined by the transformations:

$$\chi(x) \to e^{i\beta\epsilon(x)}\chi(x) \; ; \; \bar{\chi}(x) \to \bar{\chi}(x)e^{i\beta\epsilon(x)} \tag{1.31}$$

where $\epsilon(x) = (-1)^{x_1+x_2+x_3+x_4}$. The $U(1)_\epsilon$ invariance is a continuous remnant of the full chiral symmetry of the naive action and in the continuum limit, the full chiral symmetry of the free theory is restored.

The full $U(1)_\epsilon \otimes U(1)_1$ symmetry can be re-expressed in terms of independent rotations on odd and even lattice sites $U_o(1) \otimes U_e(1)$. In the ($m_0 = 0$) case the

even sites will be rotated by the angle $\alpha + \beta$ while the odd sites will be rotated by $\alpha - \beta$.

1.4 Chiral Symmetry Breaking

A symmetry of the action is said to be spontaneously broken if it is not respected by the ground state. If the transformations leaving the action invariant form a continuus group, then this spontaneous breakdown is accompanied by the appearance of massless particles, the so-called Goldstone bosons. The number of such Goldstone bosons equals the number of generators associated with the broken part of the symmetry group.

In the limit of vanishing quark masses the pions observed in nature are believed to be the Goldstone bosons associated with a spontaneous breakdown of chiral symmetry. We consider the case of an abelian $U(1)$ gauge theory. The continuum fermion action for vanishing fermion mass has the form:

$$S_F^{(cont.)} = \int d^4x\, \bar{\psi}(x) \left(\gamma_\mu(\partial_\mu + ieA_\mu)\right) \psi(x). \tag{1.32}$$

The fields ψ can always be decomposed into left and right handed parts as follows:

$$\psi = \psi_R + \psi_L$$

where

$$\psi_L = \Gamma_L \psi \;\; ; \;\; \psi_R = \Gamma_R \psi \tag{1.33}$$

where the matrices $\Gamma_L = \frac{1+\gamma_5}{2}$ and $\Gamma_R = \frac{1-\gamma_5}{2}$ are chirality projection operators. With

$$\bar{\psi_R} = \bar{\psi}\Gamma_L \;\; ; \;\; \bar{\psi_L} = \bar{\psi}\Gamma_R \tag{1.34}$$

the fermion action becomes:

$$S_F = \int \bar{\psi}_L \gamma_\mu(\partial_\mu + ieA_\mu)\psi_L + \bar{\psi}_R \gamma^\mu(\partial_\mu + ieA_\mu)\psi_R. \tag{1.35}$$

This action is invariant under the following transformations:

$$\psi_L \rightarrow e^{(ia)}\psi_L \ ; \ \bar{\psi_L} \rightarrow e^{(-ia)}\psi_L \tag{1.36}$$

$$\psi_R \rightarrow e^{(i\lambda)}\psi_R \ ; \ \bar{\psi_R} \rightarrow e^{(-i\lambda)}\psi_R \tag{1.37}$$

where a and λ are arbitrary parameters. These transformations are elements of the $U(1)_R \otimes U(1)_L$ chiral group. We consider now the ground state expectation value of $\bar{\psi}_R\psi_L$, i.e., $< \bar{\psi}_R\psi_L >$. $\bar{\psi}_R\psi_L$ transforms as follows under (1.36, 1.37):

$$\bar{\psi}_R\psi_L \rightarrow e^{i\Lambda}\bar{\psi}_R\psi_L \tag{1.38}$$

where $\Lambda = a - \lambda$. If the transformations (1.36, 1.37) are implemented by a unitary operator, and if the ground state is left invariant under the action of this operator, $< \bar{\psi}_R\psi_L >$ must vanish. The same is true for $< \bar{\psi}_L\psi_R >$. This need however not be the case in a quantum theory involving an infinite number of degrees of freedom, where the ground state may not be chirally invariant. Hence, $< \bar{\psi}_R\psi_L >$ may in fact be different from zero, implying that chiral symmetry has been broken spontaneously.

A good quantity for testing the spontaneous breakdown of chiral symmetry is $< \bar{\psi}_R\psi_L >$. Alternatively,

$$< \bar{\psi}\psi > = < \bar{\psi}_R\psi_L > + < \bar{\psi}_L\psi_R > \tag{1.39}$$

is an also good quantity for testing the spontaneous breakdown of chiral symmetry and is the quantity usually studied.

Chiral symmetry breaking has also been studied in the context of four-fermion interaction models where the chiral symmetry breaking is achieved via a short range interaction. In the Nambu-Jona Lasinio model the interaction is attractive and has zero range. If the strength of the four-fermion interaction is above a critical value then a chiral condensate forms and the fermions develop a dynamical mass (due to the interaction) non-perturbatively and a triplet of massless pions

emerge as the Goldstone bosons of the spontaneously broken symmetry operators. Lattice studies of the Gross-Neveu model in three dimensions have demonstrated that the chiral symmetry transition predicted by mean-field theory can be successfully reproduced using lattice Monte-Carlo techniques. The principal feature of four-fermi interaction models is that a short range interaction is sufficient for chiral symmetry breaking.

1.5 The Higgs Mechanism

As we mentioned earlier in this chapter our motivation is to search for alternatives to the Higgs mechanism which generates the masses of gauge bosons and fermions in the electroweak theory. Therefore, we will describe the Higgs mechanism in order to become more obvious that it is handmade and some dynamical explanation might be necessary.

The electroweak interaction is based on an $SU(2)$ group of weak isospin I and a $U(1)$ group of weak hypercharge Y, with the gauge bosons acquiring well defined masses through a mechanism called spontaneous symmetry breaking without spoiling the renormalizability of the theory. This is achieved with the help of an isospin doublet of scalar bosons called Higgs scalars, which generate mass as a result of self interaction.

To be more specific, the weak interactions obey the $SU(2)_L$ symmetry in which the left handed (LH) fermion states transform as members of a doublet. Hence, we can write :

$$I = 1/2 \qquad \begin{pmatrix} \nu_e \\ e^- \end{pmatrix}_L \quad \begin{pmatrix} \nu_\mu \\ \mu^- \end{pmatrix}_L \quad \begin{pmatrix} \nu_\tau \\ \tau^- \end{pmatrix}_L \qquad I_3 = \begin{pmatrix} 1/2 \\ -1/2 \end{pmatrix} \tag{1.40}$$

$$I = 1/2 \qquad \begin{pmatrix} u \\ d' \end{pmatrix}_L \quad \begin{pmatrix} c \\ s' \end{pmatrix}_L \quad \begin{pmatrix} t \\ b' \end{pmatrix}_L \qquad I_3 = \begin{pmatrix} 1/2 \\ -1/2 \end{pmatrix} \tag{1.41}$$

where, I and I_3 represent the weak isospin and the third component of the weak isospin, respectively. All the right handed (RH) fermion states transform as

singlets under $SU(2)_L$. Hence:

$$I = 0 \qquad e_R^-, \qquad \mu_R^-, \qquad \tau_R^-, \qquad u_R, \qquad d_R, \qquad \ldots \tag{1.42}$$

One can now define the weak hypercharge as :

$$Y = 2Q - 2I_3 \tag{1.43}$$

where Q is the electric charge, I_3 is the third component of the weak isospin and Y is the weak hypercharge. Thus, we have :

$$Y = -1 \qquad \begin{pmatrix} \nu_e \\ e^- \end{pmatrix}_L \qquad \begin{pmatrix} \nu_\mu \\ \mu^- \end{pmatrix}_L \qquad \begin{pmatrix} \nu_\tau \\ \tau^- \end{pmatrix}_L \tag{1.44}$$

$$Y = -2 \qquad e_R^- \qquad \mu_R^- \qquad \tau_R^- \tag{1.45}$$

$$Y = 1/3 \qquad \begin{pmatrix} u \\ d' \end{pmatrix}_L \qquad \begin{pmatrix} c \\ s' \end{pmatrix}_L \tag{1.46}$$

$$\begin{aligned} Y &= 4/3 \qquad u_R \qquad c_R \\ Y &= -2/3 \qquad d_R \qquad s_R \,. \end{aligned} \tag{1.47}$$

A local $SU(2)_L$ transformation of the weak isospin has the form :

$$\begin{pmatrix} \nu_e \\ e^- \end{pmatrix}_L = \exp(\, i\,(g/2)\,\boldsymbol{\sigma}\cdot\mathbf{b}(x)) \times \begin{pmatrix} \nu_e \\ e^- \end{pmatrix}_L \tag{1.48}$$

where g is the $SU(2)$ coupling constant, $\boldsymbol{\sigma} = (\sigma_1, \sigma_2, \sigma_3)$ are the Pauli matrices and $\mathbf{b}(x) = (b_1(x), b_2(x), b_3(x))$ are three independent angles. On the other hand, a local $U(1)$ hypercharge, for LH doublets and RH singlets transform respectively as:

$$\begin{pmatrix} \nu_e \\ e^- \end{pmatrix}_L = \exp(\, i\,(g'/2)\,Y_L\, a(x)) \times \begin{pmatrix} \nu_e \\ e^- \end{pmatrix}_L \tag{1.49}$$

$$e'_R = \exp(\, i\,(g'/2)\,Y_R\, a(x)) \times e_R \tag{1.50}$$

where g' is the $U(1)_Y$ coupling constant, $a(x)$ is the phase angle and Y_L , Y_R are the hypercharge values given above.

If we want the theory to be invariant under the previous local transformations, we have to introduce three vector fields W_μ^1 , W_μ^2, W_μ^3 for the $SU(2)_L$ group and one vector field B_μ for the $U(1)$ group. Hence, the covariant derivative has the form :

$$D_\mu = \partial_\mu + ig\,\mathbf{T}\cdot\mathbf{W} + i\,(g'/2)\,Y\,B_\mu. \tag{1.51}$$

For the left handed leptons we know that $\mathbf{T} = \boldsymbol{\sigma}/2$, $Y = -1$ and then $Eqn.(1.51)$ becomes :

$$D_\mu = \partial_\mu + i(g/2)\,\boldsymbol{\sigma}\cdot\mathbf{W} - i\,(g'/2)\,B_\mu. \tag{1.52}$$

On the other hand, for the RH leptons $\mathbf{T} = \mathbf{0}$, $Y = -2$ and the covariant derivative becomes :

$$D_\mu = \partial_\mu - ig'\,B_\mu. \tag{1.53}$$

We can write :

$$\begin{aligned} \boldsymbol{\sigma}\cdot\mathbf{W} &= \sigma_1\,W_\mu^1 + \sigma_2\,W_\mu^2 + \sigma_3\,W_\mu^3 \\ &= \sqrt{2}\,(\sigma_+\,W_\mu^- + \sigma_-\,W_\mu^+) + \sigma_3\,W^3 \end{aligned} \tag{1.54}$$

where,

$$\sigma_+ = \frac{(\sigma_1 + i\sigma_2)}{2} = \begin{pmatrix} 0 & 1 \\ 0 & 0 \end{pmatrix} \tag{1.55}$$

$$\sigma_- = \frac{(\sigma_1 - i\sigma_2)}{2} = \begin{pmatrix} 0 & 0 \\ 1 & 0 \end{pmatrix}$$

and

$$W_\mu^\pm = \frac{W_\mu^1 \pm W_\mu^2}{\sqrt{2}}. \tag{1.56}$$

Substituting *Eqn.*(1.56) into *Eqn.*(1.52) we obtain :

$$\begin{aligned} D_\mu &= \partial_\mu + \left(\frac{g}{\sqrt{2}}\right)(\sigma_+ W^- + \sigma_- W^+) \\ &+ i\left(\frac{g}{2}\right)\sigma_3 W_\mu^3 - i\left(\frac{g'}{2}\right)B_\mu. \end{aligned} \tag{1.57}$$

It is obvious from *Eqs.*(1.57, 1.53) that if we want $SU(2)_L$,$U(1)$ to be invariant under local transformations we end up with three vector fields W_μ^+,W_μ^-, W_μ^3 and one vector field B_μ respectively. The two couplings constants g,g' represent the couplings of the W-bosons, B-boson to fermions respectively.

Although, W_3^μ and B_μ fields do not carry any electric charge, neither describe the photon A_μ field, or the neutral vector boson Z_μ^0. Rather the physical boson fields A_μ and Z_μ^0 are taken as linear combinations of W_μ^3 and B_μ :

$$A_\mu = B_\mu \cos\theta_W + W_\mu^3 \sin\theta_W \tag{1.58}$$

$$Z_\mu^0 = -B_\mu \sin\theta_W + W_\mu^3 \cos\theta_W \tag{1.59}$$

where the angle θ_W is called the weak mixing angle (or Weinberg angle) and is defined as follows:

$$\begin{aligned} \sin\theta_W &= \frac{g'}{\sqrt{g^2+g'^2}}, \\ \cos\theta_W &= \frac{g}{\sqrt{g^2+g'^2}}. \end{aligned} \tag{1.60}$$

It can be shown that:

$$e = g'\cos\theta_W = g\sin\theta_W \tag{1.61}$$

which establishes the relation between the coupling constants g, g', e.

The **deficiency** of this model as it stands, is that the $W^\pm$, Z^0 and A_μ **bosons and the fermions are massless**. The problem is to generate the required masses while preserving the renormalizability of the gauge theory . This is **achieved** by **spontaneous symmetry breaking**, where the gauge symmetry of the Lagranzian remains but is hidden in the ground state by the appearance of a preferred direction in weak isospin space.

The simplest Higgs field that we can choose is a complex doublet:

$$\phi = \begin{pmatrix} \phi_a \\ \phi_b \end{pmatrix} = \frac{1}{\sqrt{2}} \begin{pmatrix} \phi_1 + i\phi_2 \\ \phi_3 + i\phi_4 \end{pmatrix} \tag{1.62}$$

where, $I = \frac{1}{2}$, $Y = 1$, and $(\phi_1, \phi_2, \phi_3, \phi_4)$ are four real scalar fields. We consider the Higgs potential:

$$V = \mu^2 \phi^\dagger \phi + \lambda \, (\phi^\dagger \phi)^2 \tag{1.63}$$

with $\mu^2 < 0$, $\lambda > 0$ and $\phi^\dagger = \frac{1}{\sqrt{2}}(\phi_1 - i\phi_2, \phi_3 - i\phi_4)$. This potential takes its minimum value when:

$$\phi^\dagger \phi = \tfrac{1}{2}(\phi_1^2 + \phi_2^2 + \phi_3^2 + \phi_4^2) = \frac{\mu^2}{2\lambda}. \tag{1.64}$$

We choose:

$$\phi_1 = \phi_2 = \phi_4 = 0, \quad \phi_3^2 = \frac{\mu^2}{2\lambda} \equiv u \tag{1.65}$$

which means that we have chosen:

$$< \phi >_o = \frac{1}{\sqrt{2}} \begin{pmatrix} 0 \\ u \end{pmatrix} \tag{1.66}$$

to be the vacuum expectation value of the Higgs field. Using perturbation theory we can expand the ϕ field around $< \phi >_o$ and obtain :

$$\phi = \frac{1}{\sqrt{2}} \begin{pmatrix} 0 \\ u + h(x) \end{pmatrix} \tag{1.67}$$

where, $h(x)$ has zero vacuum expectation value. It can be noticed that, from the four scalar Higgs fields of *Eqn.*(1.62) we end up with a single field $h(x)$.

Finally using the Higgs field and the spontaneous breaking of the symmetry, the vector bosons $W^\pm, Z^0$ acquire masses whilst the photon field A_μ remains massless. More specifically it can be proved that :

$$M_W = \frac{gu}{2} \tag{1.68}$$

$$M_Z = \frac{gu}{2\cos\theta_W} \tag{1.69}$$

$$\frac{M_W}{M_Z} = \cos\theta_W \tag{1.70}$$

where M_W is the mass of the $W^{\pm}$ and M_Z is the mass of the Z^0. It is obvious that the inequality $M_W \neq M_Z$ is due to the mixing between the W^3_μ and B_μ fields. In the limit $\theta_W = 0$ we see that $M_Z = M_W$. More complicated choices of the Higgs sector lead to different mass relations. The value of u=246Gev is determined experimentally from μ-decay. Finally, it can also be shown that:

$$M_W = \frac{37.3}{\sin\theta_W} GeV, \tag{1.71}$$

which means that we can use this equation to predict the mass of the W-boson if the value of $\sin\theta_W$ is known. The value of $\sin\theta_W$ is known from experiment. The mass of the Z-boson is then also predicted.

The Higgs mechanism also generates the masses of the fermions. The gauge invariant $\mathcal{L}$agrangian of the electroweak sector of the standard model describes massless gauge bosons interacting with massless fermions. The Higgs-fermion couplings give masses to the fermions. We consider the so-called "Yukawa" couplings of the form:

$$-G_Y[(\bar{\psi}_L\phi)\psi_R + \bar{\psi}_R(\phi^\dagger\psi_L)]. \tag{1.72}$$

We now consider the previous Yukawa term for the electron doublet:

$$\mathcal{L}^e_Y = -G_e\left[(\bar{\nu}_e, \bar{e})_L \begin{pmatrix} \phi_a \\ \phi_b \end{pmatrix} + \bar{e}_R(\bar{\phi}_a, \bar{\phi}_b)\begin{pmatrix} \nu_e \\ e \end{pmatrix}_L\right]. \tag{1.73}$$

When we spontaneously break the symmetry and substitute Eqn.(1.67) the previous term becomes:

$$\mathcal{L}^e_Y = -\frac{G_e}{2^{1/2}}(u+h)(\bar{e}_L e_R + \bar{e}_R e_L) \equiv -m_e(\bar{e}e) - \frac{m_e}{u}(\bar{e}eh) \tag{1.74}$$

revealing that the electron's mass and coupling are:

$$m_e = \frac{G_e u}{2^{1/2}}, \tag{1.75}$$

$$g(he\bar{e}) = \frac{m_e}{u} = \frac{gm_e}{2M_W}. \tag{1.76}$$

Since G_e is arbitrary, the actual mass of the elctron is not predicted, but its Higgs coupling is specified and, being proportional to $\frac{m_e}{M_W}$, is very small. The quark masses and couplings are generated in an analogous manner.

Chapter 2

Compact lattice QED with scalars and fermions in 3D

2.1 The Model

2.1.1 Introduction

We investigate a lattice model with a vectorlike U(1) gauge symmetry, which is called [1][18] the $\chi U \phi_3$ model. It consists of a staggered fermion field χ with a global U(1) chiral symmetry, a gauge field $U \in \mathrm{U}(1)$ living on the lattice links of length a and a complex scalar field ϕ with frozen length $|\phi| = 1$ and charge one. It is characterized by the dimensionless gauge coupling parameter β (proportional to the inverse squared coupling constant), the hopping parameter κ of the scalar field and the bare fermion mass am_0. The unconfined fermion is the composite state $F = \phi^\dagger \chi$. In a phase with broken chiral symmetry, it has nonvanishing mass am_F in the chiral limit $am_0 = 0$. The $\chi U \phi_3$ model can be seen either as a generalization of three-dimensional compact QED with a charged scalar field added or as three-dimensional U(1) Higgs model with added fermions.

2.1.2 The $\chi U\phi_3$ model with $U(1)$ gauge symmetry

The $\chi U\phi_3$ model is defined on a 3-dimensional cubic lattice with periodic boundary conditions except for antiperiodic boundary conditions for the fermion field in the "time" direction. The action reads:

$$S_{\chi U\phi} = S_\chi + S_U + S_\phi, \tag{2.1}$$

with:

$$\begin{aligned}
S_\chi &= \frac{1}{2}\sum_x \overline{\chi}_x \sum_{\mu=1}^{3} \eta_{\mu x}(U_{x,\mu}\chi_{x+\mu} - U^\dagger_{x-\mu,\mu}\chi_{x-\mu}) + am_0 \sum_x \overline{\chi}_x\chi_x \ , \\
S_U &= \beta \sum_{x,\mu<\nu} (1 - \mathrm{Re}\, U_{x,\mu\nu}) \ , \\
S_\phi &= -\kappa \sum_x \sum_{\mu=1}^{3} (\phi^\dagger_x U_{x,\mu}\phi_{x+\mu} + \phi^\dagger_{x+\mu}\, U^\dagger_{x,\mu}\, \phi_x \ ).
\end{aligned}$$

χ_x are the Kogut-Susskind fermion fields with $\eta_{\mu x} = (-1)^{x_1+\cdots+x_{\mu-1}}$. The model describes two four-component fermions ($N_f = 2$,) because of doubling . The bare mass am_0 of the fermion is introduced for technical reasons as will be discussed in chapter(3). We are interested in the chiral limit $m_0 = 0$. The a in front of m_0 indicates that we have to distinguish between the chiral limit in the continuum ($m_0 = 0$) and the continuum limit of the lattice model, where $am_0 \to 0$ can also be achieved by $a \to 0$ at nonzero m_0.

$U_{x,\mu}$ represents the compact link variable and $U_{x,\mu\nu}$ is the plaquette product of the link variables $U_{x,\mu}$. The charge of χ, determining its $U(1)$ gauge transformation properties, is one.

The hopping parameter κ vanishes if the square of the bare mass of the scalar field is $+\infty$, and is infinite if the bare mass squared is $-\infty$. The choice of $|\phi| = 1$ is made in order to restrict the number of parameters of the model. Without that choice, symmetries and dimensionality of couplings would allow several other terms in the action.

We stress that the charges of the fundamental fields exclude a direct Yukawa coupling between the fundamental fields.

2.1.3 Limiting cases of the $\chi U \phi_3$ model

The model has some interesting limiting cases:

- For $\kappa = 0$

the scalar field decouples and the model is equivalent to three-dimensional compact QED with fermions. It is known [22, 21, 31, 32] that pure compact QED has no phase transition and, as $\beta \to \infty$, it is confining via a linear potential with an exponentially decreasing string tension. There is an indication that, with fermions, chiral symmetry is broken at large coupling, but at weak coupling results are inconclusive [33]. It has been suggested that, in non-compact QED with fermions (see chapter(7)), the phase diagram is dependent on the number of flavors and that, at weak coupling, chiral symmetry is broken only for a small number (less than about 3.5) of fermions [23, 25, 27, 28]. It is quite **probable** that, at **weak coupling**, both the **compact and non-compact** formulations have quite **similar properties**. If so, then these (uncertain) features suggest that the chiral symmetry is broken in the $\kappa = 0$ limit of the weak coupling region.

- In the weak gauge coupling limit, $\beta = \infty$,

the fermions are free with mass am_0, and S_ϕ reduces to the XY_3 model. It has a phase transition at $\kappa \approx 0.27$.

- At $am_0 = \infty$

the model reduces to the three-dimensional compact U(1) Higgs model.

- For $\beta = 0$

the gauge and scalar fields can be integrated out exactly[16] which means that the $\chi U\phi_3$ model can be rewritten exactly as a lattice four-fermion model. In the path integral:

$$\int \prod_{x,\mu} d\chi_x d\overline{\chi}_x d\phi_x dU_{x,\mu} \exp\{-S_{\chi U\phi_3}\} \tag{2.2}$$

the gauge and scalar fields can be integrated out exactly. This results in:

$$Z = r^N J_1^{N_l} \int \prod_x d\chi_x d\overline{\chi}_x \exp\{-S_{4f}\}, \tag{2.3}$$

where N and N_l are the number of lattice sites and links respectively, and:

$$S_{4f} = -\sum_x \sum_{\mu=1}^{3} [G\overline{\chi}_x\chi_x\overline{\chi}_{x+\mu}\chi_{x+\mu} - \frac{1}{2}\eta_{\mu x}(\overline{\chi}_x\chi_{x+\mu} - \overline{\chi}_{x+\mu}\chi_x)] + \frac{am_0}{r}\sum_x \overline{\chi}_x\chi_x, \tag{2.4}$$

with:

$$r = r(\kappa) = \frac{J_U}{J_1} \tag{2.5}$$

and

$$J_U = \int dU e^{2\kappa ReU} U = I_1(2\kappa), \tag{2.6}$$

$$J_1 = \int dU e^{2\kappa ReU} = I_0(2\kappa) \tag{2.7}$$

where, I_0 and I_1 are modified Bessel functions. The fermion field has been rescaled by $\sqrt{r}$. The parameter r is an analytic function of κ increasing monotonically from $r(0) = 0$ to $r(\infty) = 1$. The action (2.4) obviously describes a lattice version of the four-fermion theory. The four-fermion coupling parameter G is related to κ via r:

$$G := \frac{1 - r^2}{4r^2}. \tag{2.8}$$

From (2.5),(2.6),(2.7) one sees that G is decreasing monotonically with increasing κ; $G = \infty$ at $\kappa = 0$, and $G = 0$ at $\kappa = \infty$.

The action (2.4) describes the lattice Gross-Neveu model. Some caution is necessary, however. There is some uncertainty whether the four-fermion model (2.4) is a lattice version of the Gross-Neveu model or of the Thirring model. The

four-fermion action (2.4) was used in four dimensions for the study of the Nambu–Jona-Lasinio model e.g. in [34, 35], which would correspond to the Gross-Neveu model in three dimensions. Recently in [29, 30] the four-fermion action (2.4) in three dimensions is interpreted as the Thirring model and similar interpretation is implied in [36]. For our number of fermions, $N_f = 2$, the distinction might be unimportant and both models might actually coincide. The Gross-Neveu model has a chiral phase transition and is nonperturbatively renormalisable [15]. The properties of the $N_f = 2$ Thirring model appear to be similar [36, 29, 30]. For our purposes the important property of the three-dimensional four-fermion model obtained in the $\beta = 0$ limit of the $\chi U \phi_3$ model is its renormalisability, which presumably holds for both interpretations.

2.2 Observables

2.2.1 Chiral Condensate and Fermion Mass

Because we are interested in the chiral properties of the model we concentrate on the chiral condensate, the fermion mass and the Lee-Yang Zeros (which will be described in chapter(3)). Our aim is to localize the chiral phase transition.

The chiral condensate can be evaluated using stochastic estimators. This procedure avoids the full inversion of the fermionic matrix, M, which can be computationally intensive. (We will refer to the fermionic matrix, in detail, in the next chapter). Instead the traces appearing in the expressions for expectation values of the observables are approximated by unbiased estimators. These are obtained by introducing N_η vectors of complex Gaussian random numbers $\eta^{(\mu)}$ with $(\mu = 1, 2, ..., N_\eta)$ of dimension equal to the dimension of M. The components of $\eta^{(\mu)}$ are distributed according to $e^{-(\eta^{(\mu)}, \eta^{(\mu)})} = e^{-\sum_x (\eta_x^{(\mu)\dagger} \eta_x^{(\mu)})}$ so that the diagonal matrix element with respect to the random vector is an unbiased estimator for

the trace:

$$Tr\left\{M^{-1}\right\} = \lim_{N_\eta \to \infty} \frac{1}{N_\eta} \sum_{\mu=1}^{N_\eta} \left(\eta^{(\mu)}, M^{-1}\eta^{(\mu)}\right). \tag{2.9}$$

The chiral condensate now is defined by:

$$\langle \overline{\chi}\chi \rangle = \left\langle \mathrm{Tr}\, M^{-1} \right\rangle \tag{2.10}$$

where M is the fermionic matrix. The trace is measured with the gaussian estimator.

The physical fermion of the $\chi U \phi_3$ model is the gauge invariant composite fermion $F = \phi^\dagger \chi$. Its mass am_F is measured in momentum space [37]. Considering the gauge invariant fermionic field

$$F_x := \phi_x^\dagger \chi_x, \bar{F} = \phi_x \bar{\chi}_x \tag{2.11}$$

the corresponding fermion propagator:

$$G_F(t) = \frac{2^3}{V} \sum_{\vec{x}} \sum_{\vec{y}} < F_{\vec{x},t} \bar{F}_{\vec{y},0} > \tag{2.12}$$

is determined numerically ([37] and references therein). The numerical data for $G_F(t)$ are then fitted to an ansatz[37] and the mass am_F of the gauge-invariant fermion is calculated. The calculations of the chiral condensate and of the physical fermion mass were made in [20].

2.3 Equation of State

A standard way to analyse the critical exponents of a chiral phase transition is via the use of an equation of state (EOS). Normally data close to the phase transition can be well described by such an ansatz. In this model for fixed β this equation reads:

$$am_0 = \langle \overline{\chi}\chi \rangle^\delta F\left((\kappa - \kappa_c)\langle \overline{\chi}\chi \rangle^{-1/\beta_\chi}\right), \quad F(x) = Rx + S. \tag{2.13}$$

Here $\langle\overline{\chi}\chi\rangle$ is the infinite volume value of the chiral condensate for given am_0, κ and β. β_χ and δ are the exponents defined in analogy to a magnetic transition. The index χ is added to distinguish the exponent and the coupling. The scaling function F is used in its linear approximation and R and S are constants. This equation is applied in the region for which $\kappa \approx \kappa_c$ and where we might expect the scaling deviations to be small.

In order to clarify what we mean by a magnetic transition we consider the continuous phase transition of iron, from paramagnetic form to ferromagnetic at temperature T_c (Curie Temperature). At $T > T_c$ iron is paramagnetic. That is, the material is not magnetised in the absence of an applied magnetic field, and if a weak field $\mathbf{B}$ is applied, the material's magnetic moment per unit volume $\mathbf{m}$ is proportional to the applied field: $\mathbf{m} \simeq \mu\mathbf{B}$ with μ a positive constant. In the ferromagnetic state ($T < T_c$), the material is magnetised even when no field is applied, and when an external field $\mathbf{B}$ is applied this magnetisation swings almost instantaneously to align with $\mathbf{B}$. Consequently, $\mathbf{m}$ is no longer linearly related to $\mathbf{B}$. The magnitude of the magnetisation $\mathbf{m}_0(T)$ at $\mathbf{B} = 0$ vanishes as one approaches T_c from below. Therefore, as one heats a sample of iron, through T_c, in zero applied field, nothing very dramatic happens at T_c. The iron's magnetisation steadily decreases as T_c is approached, vanishing entirely at T_c and for all higher temperatures. What changes discontinuously at T_c is the rate of change of $\mathbf{m}_0$ rather than $\mathbf{m}_0$ itself. This is the essence of a continuous phase change: the properties of the system do not change discontinuously at T_c, but at least, one of their rates of change, does.

In a magnetic system now, m_0 tends to zero as

$$m_0 \sim (T_c - T)^{\beta_x},$$

where β_x is a critical exponent of the system. At T_c itself, m becomes proportional to a power of B:

$$m \sim B^{\frac{1}{\delta}}$$

where δ is another critical exponent of the system. Thus, at T_c, m_0 responds sensitively and highly non-linearly to small fields B. a is another critical exponent which describes how the specific heat diverges with temperature as the critical temperature is approached. Finally, γ is the critical exponent which describes how the magnetic susceptibility varies with the temperature as the critical temperature is approached.

We now assume, as we did for the chiral condensate, the corresponding scaling equation for the fermion mass:

$$am_0 = (am_F)^{1/\tilde{\nu}} G\left((\kappa - \kappa_c)(am_F)^{-1/\nu}\right) \ , \quad G(x) = Ax + B \, . \tag{2.14}$$

The exponent ν is the correlation length critical exponent in the chiral plane ($am_0 = 0$). $\tilde{\nu}$ is an analogous exponent obtained if one approaches the critical point from outside the chiral plane. The two exponents have to be distinguished. At fixed β in the chiral plane ($am_0 = 0$) the fermion mass scales with ν: $am_F \propto (\kappa - \kappa_c)^{\nu}|_{am_0=0}$, whereas for all other straight paths into the critical point (for example $\kappa = \kappa_c$) it scales with am_0 as: $am_F \propto (am_0)^{\tilde{\nu}}|_{\kappa-\kappa_c \propto am_0}$. This is indicated in figure(2.1) in the plane $\beta = const.$

Figure(2.1) also illustrates that for $\kappa < \kappa_c$ the chiral condensate changes sign and makes a jump if one crosses the line $am_0 = 0$. This means that it is a line of first order phase transitions. For $\kappa > \kappa_c$ the line becomes a line of second order phase transitions on which the fermion mass gets critical. In between there is a critical point ($\kappa = \kappa_c$).

It can be shown that the critical exponents we described earlier can be written in terms of just two numbers: ν and η, where ν is the correlation length critical exponent and η is a critical exponent which describes the variation at the critical temperature of the connected two-point correlation function $G_c(x)$ with the separation x of the two points, as $x \to \infty$. Using this, one can show, that the following scaling laws hold:

$$2\beta + \gamma = 2 - \alpha, \tag{2.15}$$

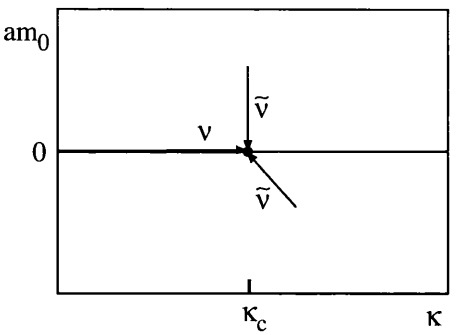

Figure 2.1: First order chiral phase transition line (bold line) and the critical point in a plane $\beta = const.$ The fermion mass am_F scales with exponent ν in the direction tangential to the transition line and with exponent $\tilde{\nu}$ in any other direction.

$$2\beta\delta - \gamma = 2 - \alpha, \tag{2.16}$$

$$\gamma = \nu(2 - \eta) \tag{2.17}$$

$$\nu d = 2 - \alpha \tag{2.18}$$

where d is the space-time dimension. Using now eqns.(2.15)(2.16)(2.18) we see that only two of the four exponents defined by the equations of state are independent. The corresponding scaling relations are:

$$\delta = \frac{1}{d\tilde{\nu} - 1} \quad \text{and} \quad \beta_\chi = \nu\left(d - \frac{1}{\tilde{\nu}}\right) . \tag{2.19}$$

2.4 Phase Structure of compact QED with scalars and fermions in three dimensions

We investigated the phase diagram and the critical behaviour of the $\chi U\phi$ model in three dimensions. We have found that in the chiral limit $m_0 = 0$ the $\chi U\phi_3$model

has three regions in the $\beta - \kappa$ plane with different properties with respect to the chiral symmetry. They are indicated in Fig.(2.2). The region at strong gauge coupling (small β) and small κ is the Nambu phase where the chiral symmetry is broken and the neutral fermion F is massive. At large κ chiral symmetry is restored and the fermion F is massless. This phase is labelled the Higgs phase because of its properties in the weak coupling limit. The third is the X region at large β and small κ. It is conceivable that this region is analytically connected with either the Nambu or Higgs phase but it may well be a separate phase. In this region the mass measured in the fermion channel is large, but the chiral condensate is very small (within our numerical accuracy consistent with zero).

The main result of our investigation is the determination of the critical behaviour at strong gauge coupling. We found strong indications that the chiral phase transition between the Nambu and Higgs phases is in one universality class for all $\beta \leq 0.80$ and possibly for all $\beta \leq 1.25$. It is the class of the three-dimensional Gross-Neveu model which is known to be (nonpertubatively) renormalizable [15]. That model is the $\beta = 0$ limit of the $\chi U \phi_3$model [16]. This universality means that the continuum limit of the $\chi U \phi_3$ model defines a nonperturbatively renormalisable gauge theory in which the fermion mass is generated dynamically by the shielded gauge-charge mechanism. However, it also means that in this β region the gauge field is auxiliary and the $\chi U \phi_3$ model does not represent a new class of field theories.

The chiral properties of the region X are elusive and we made only an exploratory investigation. But we point out that, provided the chiral symmetry is broken there, the phase transition between the region X and the Higgs phase gives rise to another possible construction for a continuum theory containing an unconfined fermion with dynamically generated mass. It could continue to be in the universality class of the three-dimensional Gross-Neveu model. But experience [12, 13] with the four-dimensional model in the vicinity of the tricritical point

suggests that at larger β the gauge degrees of freedom are dynamical and a new universality class may be present. This interesting possibility, and the possible existence of a tricritical point in three dimensions, deserves further study.

Our investigation was mainly based on two methods: firstly, via fits to an equation of state and, secondly, via a finite size scaling investigation of the Lee-Yang zeros in the complex fermion mass plane (see chapter(3)). As first pointed out by Lee and Yang [45, 46], the determination of the finite size scaling behaviour of the complex zeros of a partition function could be a direct method for the determination of the critical properties of the associated theory. We investigated these zeros of the canonical partition function in the complex bare fermion mass plane. These zeros control the fermion condensate and its associated susceptibilities [11, 14], physical quantities which are often measured directly on the lattice and used, via finite size scaling, to determine the critical behaviour.

As we described earlier, the investigation of a phase transition via fits to an equation of state is quite reliable because the finite size effects we find close to the phase transition are usually small. Therefore we expect a simple finite size scaling, described by the empirical formula we mentioned earlier. Then the observables were extrapolated to the infinite volume and a simultaneous fit to the fermion mass am_F and the chiral condensate $\langle\overline{\chi}\chi\rangle$ was performed.

In the region X, the chiral condensate is very small. A small condensate suggests that the Lee-Yang zeros cannot be near to the physical region. Nevertheless, it was of interest to investigate if the closest zeros can be determined with sufficient accuracy to ascertain their finite size scaling (and hence that of the condensate).

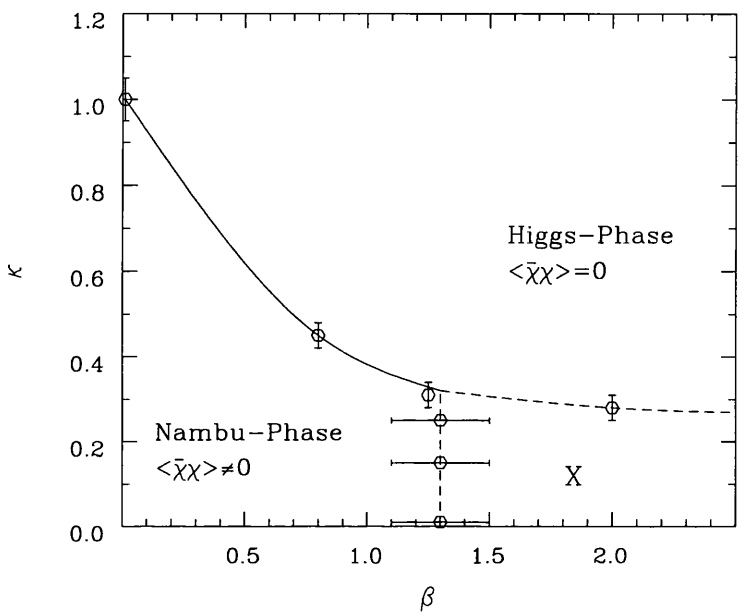

Figure 2.2: Phase diagram of the $\chi U\phi_3$ model for $m_0 = 0$. For $\beta \leq 0.80$ a clear phase transition between the Nambu and Higgs phases can be observed. Whether the region X at large β and small κ forms a third phase or belongs to one of the other phases, separated from it only by a crossover, is discussed in chapter5. All phase transitions seem to be 2^{nd} order.

Chapter 3

Zeros of the Grand Canonical Partition Function

3.1 Motivation

As we have already mentioned in the introduction, the lattice approach to quantum field theories is a mathematically well defined way to extract results in the non perturbative regime. Being a regularization scheme, the lattice formulation has to be connected with the continuum limit, which is supposed to describe the real theory, through a renormalization procedure. The equivalence can be meaningful only when the effects of the discretisation of space-time become negligible, i.e.: when the system is scale invariant. This is known to happen in the vicinity of a continuous phase transition.

Therefore the knowledge of the phase diagram of the corresponding statistical mechanical system is crucial in order to establish the existence of the theory in the continuum and to make predictions about its physical properties. It is a well known result of statistical mechanics that, if one knows the grand canonical partition function (GCPF) of a system then one can, in principle, calculate all thermodynamic quantities.

The critical behaviour of a statistical system can be investigated using several different approaches; one of the most direct is the study of the Lee-Yang zeros, i.e.: the zeros of the analytical continuation of the GCPF for complex values of the critical parameter. The thermodynamical functions can be reconstructed from the Lee-Yang zeros and the critical properties of the theory in the continuum can be inferred from the dependence of the thermodynamical functions on the volume.

3.2 Lee-Yang Theorem

Phase transitions are manifested in nature by the occurence of singularities in thermodynamic(s) functions, such as the pressure in a liquid-gas system, or the magnetization in a ferromagnet. How is it possible that such singularities arise from the GCPF, which seems to be analytic function of its arguments? The answer lies in the fact that a macroscopic body is close to the idealized thermodynamic limit-the limit of infinite volume with particle density held fixed. As this limit is approached, the GCPF can develop singularities, because the limit function of a sequence of analytic functions need not be analytic.

By studying the zeros of the GCPF we can visualize its properties and learn much about the occurrence of singularities in the thermodynamic limit.

Lee and Yang[45, 46], first, showed that a knowledge of the distribution of the zeros of the GCPF can yield much information on the phase structure of the system under investigation. They studied a simple statistical system of a lattice gas with attractive interactions (Ising ferromagnetic system). The Lee-Yang circle theorem states that for this particular system the roots of the GCPF lie on a circle in the activity plane (e^{-2h} where h is the magnetic field).

Consider a (quantum mechanical) system consisting of particles in volume V, interacting with one another through a pairwise potential[47]. A finite volume can accommodate a maximum number of particles n_{max}. When n exceeds n_{max} so

that two of them touch, the free energy will become infinite and the GCPF will vanish.

The grand canonical partition function (GCPF) comprises a sum of terms

$$Z(z,V) = 1 + c_1(V)z + c_2(V)z^2 + ... + c_{n_{max}}(V)z^{n_{max}} \tag{3.1}$$

corresponding to canonical partition functions and the coefficients c_n reflect the relative probability that the system will be in a state with n particles. If the expansion coefficients are to be interpreted as probabilities then in order to be physical they must be real and positive. Since all the expansion coefficients, c_n, are positive the polynomial can have no real positive roots. We can however observe negative roots which are unphysical and, of course, complex roots. Yang and Lee showed that phase transitions are controlled by the distribution of roots of the GCPF in the complex z plane. A phase transition occurs whenever a root approaches the real axis in the limit $V \to \infty$.

Consider the parametric form of the equation of state in the infinite volume limit:

$$\begin{aligned} \frac{P}{kT} &= \lim_{V\to\infty} V^{-1} \ln Z(z,V) \\ \frac{1}{v} &= \lim_{V\to\infty} V^{-1} z \frac{\partial}{\partial z} \ln Z(z,V) \end{aligned} \tag{3.2}$$

where v is the specific volume. Then the Lee-Yang theorems can be stated as follows:

- **THEOREM 1** The following limit exists for all $z > 0$

$$F_\infty(z) \equiv \lim_{V\to\infty} \frac{1}{V} \ln Z(z,V) \tag{3.3}$$

  and this function is a continuous non-decreasing function of z.

- **THEOREM 2**

  Suppose **R** is a region in the complex z plane that includes a segment of the positive real axis and contains no roots of the GCPF then in this region

$V^{-1} \log Z(z, V)$ will converge uniformly to its limit as $V \to \infty$ and this limit is analytic for all z in **R**.

A thermodynamic phase is defined by those values of z contained in any single region **R** of theorem(2). As a result of the second theorem it follows that in any region **R** the order of the partial derivative and the limit in Eqn.(3.2) can be interchanged so that in any single phase:

$$\begin{aligned} \frac{P(z)}{kT} &= F_\infty(z) \\ \frac{1}{v(z)} &= z\frac{\partial}{\partial z}F_\infty(z). \end{aligned} \tag{3.4}$$

If region **R** includes the entire positive z axis then the system always exists in a single phase. However, if a zero of the GCPF approaches a point, z_o, on the real positive z axis, then the system will have two phases : one in the region $z < z_o$ and one in the region $z > z_o$. P(z) must be continuous according to theorem(1) but a discontinuity in $\partial P/\partial z$ would correspond to a first order phase transition while a discontinuity in $\partial^2 P/\partial z^2$ would indicate a second order phase transition.

Of course in practical lattice calculations we are not close to the thermodynamic limit $V \to \infty$. At finite volume the GCPF has a finite number of complex zeros lying outside a region surrounding the real axis. At increasing finite volume the sequence of the real parts of the zero lying nearest to the real axis (critical zeros) converges to the critical point. The finite volume scaling behaviour of the lowest zero can be used to determine the order of the phase transition as we will explain later in this chapter. We have to notice that in a physically meaningful system which has positive GCPF expansion coefficients we do not expect any of the zeros to lie on the positive real axis and the coefficients will all be positive once the statistical average is complete.

3.3 The GCPF of the $\chi U\phi_3$ model

The GCPF for the $\chi U\phi_3$ model with staggered fermions may be written as a function of the bare fermion mass:

$$Z(\beta,\kappa,m_0)=\int\int\int[d\chi][d\overline{\chi}][d\phi][d\phi^\dagger][dU]e^{-S_{\chi U\phi_3}} \tag{3.5}$$

where $S_{\chi U\phi_3}$ is given by(2.1). (Note that in the remaining of this chapter we have taken the lattice spacing a=1 so that all dimensionful quantities are to be understood in units of the (inverse) lattice spacing.) The fermion fields can be integrated out using the standard Gaussian integration technique:

$$\begin{aligned} Z(\beta,\kappa,m_0) &= \int\int[d\phi][d\phi^\dagger][dU]e^{-(S_{U\phi})}\int[d\overline{\chi}][d\chi]e^{-S_\chi} \\ &= \int\int[d\phi][d\phi^\dagger][dU]e^{-(S_{U\phi})}\det M[m_0,U[\beta,\kappa]] \end{aligned} \tag{3.6}$$

where $S_{U\phi}=S_U+S_\phi$ and $M[m_0,U[\beta,\kappa]]$ is the fermionic matrix:

$$M_{x,y}[m_0,U[\beta,\kappa]]=m_0\delta_{x,y}+\frac{1}{2}\sum_{\nu=\hat{x}+\hat{y}+\hat{t}}[U_\nu(x)\eta_\nu(x)\delta_{y,x+\nu}-U_\nu^\dagger(x-\nu)\eta_\nu(x)\delta_{y,x-\nu}]. \tag{3.7}$$

The fermionic matrix M can be decomposed for a finite lattice as the sum of a hermitean term diagonal in mass which we denote m_0I and an anti-hermitian term which corresponds to the nearest-neighbour interaction between even and odd sites denoted by $\mathcal{H}$. These are $V\times V$ matrices. In matrix block form it can be written as:

$$M[m_0,U[\beta,\kappa]]=m_0I_V+\mathcal{H}=\begin{pmatrix} m_0I_{\frac{V}{2}} & \tilde{M}i \\ -\tilde{M}^\dagger i & m_0I_{\frac{V}{2}}\end{pmatrix} \tag{3.8}$$

where the subscripts of the square unit matrices denote their size and the $\frac{V}{2}\times\frac{V}{2}$ block matrix $\tilde{M}$ is the even-to-odd site interaction. The matrix $\tilde{M}$ is hermitean. Hence, the fermionic determinant can be written as:

$$det(M[m_0,U[\beta,\kappa]]) = det(m_0^2+\tilde{M}^\dagger\tilde{M})=\prod_{i=1}^{\frac{V}{2}}(m_0+i\lambda_i)(m_0-i\lambda_i) \tag{3.9}$$

$$= \prod_{i=1}^{\frac{V}{2}} (m_0^2 + \lambda_i^2)$$

where $\imath\lambda_i$ are the eigenvalues of $\mathcal{H}$.

This characteristic form of M allows one to write its determinant as a polynomial in the fermion mass for each configuration of the gauge fields (at fixedβ, κ):

$$\det(M[m_0, U[\beta, \kappa]]) = \sum_{n=0}^{V} \hat{C_n}[U[\beta, \kappa]] m_0^n. \tag{3.10}$$

In this formulation, the polynomial has degree equal to the volume of the system. Its even coefficients are positive, and the odd ones are identically zero; hence, equation(3.10) becomes:

$$\det(M[m_0, U[\beta, \kappa]]) = \sum_{n=0}^{\frac{V}{2}} C_n[U[\beta, \kappa]] m_0^{2n} \tag{3.11}$$

where $C_n = \hat{C_{2n}}$.

At fixed β, κ the GCPF is proportional to the expectation value of the fermionic determinant:

$$< \det(M[m_0, U[\beta, \kappa]]) >_{P[U,\phi]}$$

averaged over configurations which are generated with a probability weight proportional to $\exp -(S_U + S_\phi)$. Therefore we can express equation(3.6) in the form of a polynomial in the bare fermion mass:

$$Z(\beta, \kappa, m_0) =< \sum_{n=0}^{\frac{V}{2}} C_n m_0^{2n} >= \sum_{n=0}^{\frac{V}{2}} < C_n > m_0^{2n}. \tag{3.12}$$

The zeros of this polynomial are the Lee-Yang zeros in the complex fermion mass plane, introduced in the previous section.

3.4 The expansion of the GCPF

The lattice approach to the computation of the bare fermion mass dependence of the GCPF amounts to the determination of the coefficients in (3.12). In general,

the functional integration over the gauge and scalar fields in (3.6) can be performed numerically using a Hybrid Monte Carlo ([1] and references therein) scheme for the generation of statistically independent gauge configurations from the correct probability distribution.

3.4.1 Introduction of the "updating" mass

One of the main problems arising in the measurement of the expectation value of the fermionic determinant is, that there may be little overlap between the probability distribution of the pure gauge fields with the effective support of the operator (3.11) and this spoils the convergence of the averaging procedure.

The problem can be faced by shifting the probability distribution of the gauge fields by introducing an "updating" mass $\hat{m}_0$ [3]. This procedure corresponds to the measurement of a new operator that can be analytically related to the old fermionic determinant. The support of the new operator overlaps with the shifted probability distribution, at least for m_0 belonging to a neighborhood of $\hat{m}_0$.

Hence, since we have the freedom to define the GCPF up to a constant multiplicative factor, we may write:

$$Z(\beta,\kappa,m_0) = \frac{\int dU d\phi \det M[m_0,U] e^{S_{U\phi}}}{\int dU d\phi \det M[\hat{m}_0,U] e^{S_{U\phi}}} \tag{3.13}$$

or

$$Z(\beta,\kappa,m_0) = \frac{\int dU d\phi \frac{\det M[m_0,U]}{\det M[\hat{m}_0,U]} \det M[\hat{m}_0,U] e^{S_{U\phi}}}{\int dU d\phi \det M[\hat{m}_0,U] e^{S_{U\phi}}} \tag{3.14}$$

or

$$Z(\beta,\kappa,m_0) = \int [d\phi][dU] \frac{\det M[m_0,U]}{\det M[\hat{m}_0,U]} P[U,\phi,\hat{m}_0] \tag{3.15}$$

where

$$P[U,\phi,\hat{m}_0] = \frac{\det M[\hat{m}_0,U] e^{-(S_U+S_\phi)}}{\int [d\phi'][dU'] \det M[\hat{m}_0,U'] e^{-(S_{U'}+S_{\phi'})}}. \tag{3.16}$$

The GCPF is now expressed as the vacuum expectation value of the determinant ratio $\frac{\det M[m_0,U]}{\det M[\hat{m}_0,U]}$, averaged over configurations which are generated with the

probability weight $P[U, \phi, \hat{m}_0]$, i.e :

$$Z(\beta, \kappa, m_0) = \langle \frac{\det M[m_0, U]}{\det M[\hat{m}_0, U]} \rangle_{P[U,\phi,\hat{m}_0]}. \tag{3.17}$$

The role of the "updating" mass $\hat{m}_0$ is now clear: by considering a particular region of the configuration space (critical region) we will tune $\hat{m}_0$ to be as near as possible as the expected value of the lowest zero. We will then perform measurements on the ratio $\frac{\det M[m_0,U]}{\det M[\hat{m}_0,U]}$ (which is now close to unity) and obtain reliable results for all values of am_0 which are close to $\hat{m}_0$.

Obviously, this procedure should not change the zeros of the GCPF. At every set of (β, κ) values the configurations for the gauge fields are generated, following the new distribution (3.16), with a HMC ([1] and references therein) code. For a single configuration a modified Lanczos algorithm [42], without reorthogonalisation, gives the eigenvalues λ_i of the massless fermionic matrix $M[m_0 = 0]$, which are pure imaginary. The coefficients are then computed from the eigenvalues and then averaged over the configurations: they are the fundamental quantities for the determination of the zeros of the polynomial.

3.4.2 Shifted expansion of the GCPF

As we saw earlier in this chapter we can write the fermionic determinant in terms of its eigenvalues as:

$$\det(M[am_0, U]) = \prod_{i=1}^{\frac{V}{2}} (m_0^2 + \lambda_i^2). \tag{3.18}$$

Introducing now a second arbitrary (and apparently irrelevant) mass parameter $\bar{m}$, which is called the "mass shift"[3], we can write a shifted expansion of the femionic determinant:

$$\det(M[am_0, U]) = \prod_{i=1}^{\frac{V}{2}} (m_0^2 - \bar{m}^2 + \bar{\lambda}_i^2) \tag{3.19}$$

where we just substituted $\bar{\lambda}_i^2 = (\lambda_i^2 + \bar{m}^2)$. The reasons for introducing $\bar{m}$ will become clear in the next sections.

We can now express the determinant ratio as:

$$\begin{aligned} \frac{\det(M[am_0, U])}{\det(M[\hat{m_0}, U])} &= \sum_{n=0}^{\frac{V}{2}} \exp(x_n) \frac{(m_0^2 - \bar{m}^2)^n}{\det(M[\hat{m_0}, U])} \\ &= \sum_{n=0}^{\frac{V}{2}} \exp(c_n)(m_0^2 - \bar{m}^2)^n \end{aligned} \tag{3.20}$$

where

$$c_n \equiv x_n - \ln \det(M[\hat{m_0}, U]). \tag{3.21}$$

The series coefficients $\exp(c_n)$ have been expressed in exponential form in order to stress the fact that they vary by many orders of magnitude.

From Eqs.(3.17) and (3.20) the GCPF becomes a finite polynomial in mass:

$$Z(\beta, \kappa, m_0) = \sum_{n=0}^{\frac{V}{2}} < \exp(c_n) >_{P[\hat{m_0}, \beta, \kappa]} (m_0^2 - \bar{m}^2)^n = \sum_{n=0}^{\frac{V}{2}} \exp(\overline{C}_n)(m_0^2 - \bar{m}^2)^n \tag{3.22}$$

where the logarithm of the averaged coefficients $\overline{C}_n$ is defined to be:

$$\exp(\overline{C}_n) \equiv < \exp(c_n) >_{P[\hat{m_0}, \beta, \kappa]} . \tag{3.23}$$

Recalling equation(3.9) we note that for real $\bar{m}^2$, the coefficients in equation(3.20) are real positive numbers. The coefficients are thus identified with products of real positive eigenvalues λ^2 shifted by the real positive quantity $\bar{m}^2$.

3.4.3 Determination of the coefficients of the polynomial

We can now describe the method that has been used[3] to extract the coefficients of the polynomial (3.22). We are looking for real positive coefficients of the determinant ratio $\det(M[m_0])/\det(M[\hat{m_0}])$ expressed as a polynomial in $(m_0^2 - \bar{m}^2)$. The first step is the Lanczos tridiagonalisation of the hermitian matrix $\tilde{M}^2$ through a

similarity transformation:

$$X^{\dagger}\tilde{M}^2X = T_{V/2}, \tag{3.24}$$

where T is a $\frac{V}{2} \times \frac{V}{2}$ real tridiagonal matrix:

$$T_{\frac{V}{2}} = \begin{pmatrix} \alpha_1 & \beta_1 & & & \\ \beta_1 & \alpha_2 & \beta_2 & & \\ & \beta_2 & \alpha_3 & & \\ & & & \ddots & \beta_{N-1} \\ & & & \beta_{N-1} & \alpha_N \end{pmatrix} \tag{3.25}$$

and X is a series of column vectors $(x_1, x_2, ..., x_N)$. These are the Lanczos vectors which are orthogonal: $x_i^{\dagger}x_j = \delta_{ij}$ and recalling Eqn.(3.24) we have:

$$\tilde{M}^2X = XT \tag{3.26}$$

or

$$\tilde{M}^2x_1 = a_1x_1 + \beta_1x_2, \tag{3.27}$$

$$\tilde{M}^2x_i = \beta_{i-1}x_{i-1} + a_ix_i + \beta_ix_{i+1} \quad , 2 \leq i \leq N-1, \tag{3.28}$$

$$\tilde{M}^2x_N = \beta_{N-1}x_{N-1} + a_Nx_N. \tag{3.29}$$

These are the Lanczos equations which can be used recursively to calculate all the a_i, β_i and x_i. We choose x_1 to be a unit vector. We then take the scalar product of x_1 with the first Lanczos equation and we can obtain a_1 from:

$$a_1 = x_1^{\dagger}\tilde{M}^2x_1 \tag{3.30}$$

where a_1 is asuumed to be real because $\tilde{M}^2$ is hermitian. We then calculate:

$$\beta_1x_2 = \tilde{M}^2x_1 - a_1x_1 \tag{3.31}$$

and using $x_2x_2^{\dagger} = 1$ we obtain β_1 and x_2. However, we need to check that x_2 is orthogonal to x_1:

$$x_1^{\dagger}\beta_1x_2 = x_1^{\dagger}a_1x_1 - x_1^{\dagger}\tilde{M}^2x_1, \tag{3.32}$$

$$\beta_1 x_1^\dagger x_2 = a_1 - a_1 = 0. \tag{3.33}$$

We continue in a similar way with all the other equations in turn:

$$a_i = x_i^\dagger \tilde{M}^2 x_i, \tag{3.34}$$

$$\beta_i x_{i+1} = \tilde{M}^2 x_i - \beta_{i-1} x_{i-1} - a_i x_i \quad , 2 \leq i \leq N-1. \tag{3.35}$$

We calculate the final a from the last equation in order to complete the calculation:

$$a_n = x_N^\dagger \tilde{M}^2 x_N. \tag{3.36}$$

Finally we can check that the last equation is automatically satisfied because we can show that:

$$u = \tilde{M}^2 x_N - \beta_{N-1} - \beta_{N-1} x_{N-1} - a_N x_N \tag{3.37}$$

is orthogonal to all the Lanczos vectors and must therefore be zero. In fact a good check on the accuracy of the calculation is that:

$$\beta_N = |u| \tag{3.38}$$

is small.

We can now calculate the denominator $\det(M[\hat{m}_0])$. The fermionic determinant is invariant under similarity transformations and we can write:

$$\det(M[\hat{m}_0]) = \det(\tilde{M}^2 + \hat{m}_0^2) = \det(T_{\frac{V}{2}} + \hat{m}_0^2). \tag{3.39}$$

By omitting the last p rows and columns of $T_{\frac{V}{2}}$ we introduce a new $p \times p$ matrix T_p. Then the Laplace expansion of the determinant gives rise to the following recursion:

$$\det(T_p + \hat{m}_0^2) = (\alpha_p + \hat{m}_0^2)\det(T_{p-1} + \hat{m}_0^2) - \beta_{p-1}^2 \det(T_{p-2} + \hat{m}_0^2). \tag{3.40}$$

Since we are dealing with variations of several orders of magnitude, it is essential to express the above recursion in exponential form. By defining $E_p = \ln \det(T_p + \hat{m}_0^2)$

equation(3.40) becomes:

$$E_p = E_{p-1} + \ln\left[(\alpha_p + \hat{m}_0^2) - \beta_{p-1}^2 \exp(E_{p-2} - E_{p-1})\right] \tag{3.41}$$

with initial conditions:

$$E_0 = 0,\ E_1 = \ln(\alpha_1 + \hat{m}_0^2). \tag{3.42}$$

We can now obtain $\ln\det(M[\hat{m}_0])$ after $\frac{V}{2}$ iterations of equation(3.41).

Our task now is to calculate $\det(M[m_0])$ as a power series in $(m_0^2 - \bar{m}^2)$. The first steps are identical to those above; writing the determinant in terms of the matrix $T_{\frac{V}{2}}$:

$$\det(M[m_0]) = \det(T_{\frac{V}{2}} + m_0^2 - \bar{m}^2) \tag{3.43}$$

we have, analogously to equation(3.40), the recursion:

$$\begin{aligned} \det[T_p + (m_0^2 - \bar{m}^2)] &= [\alpha_p + ((m_0^2 - \bar{m}^2)]\det[T_{p-1} + (m_0^2 - \bar{m}^2)] \\ &- \beta_{p-1}^2 \det[T_{p-2} + (m_0^2 - \bar{m}^2)]. \end{aligned} \tag{3.44}$$

Each minor determinant is then expressed as a polynomial in $(m_0^2 - \bar{m}^2)$:

$$\det[T_p + (m_0^2 - \bar{m}^2)] = \sum_{n=0}^{p} exp(x_n^{(p)})(m_0^2 - \bar{m}^2)^n. \tag{3.45}$$

When $p = V/2$ we recover the final expansion of interest; i.e. equation(3.20), with $\exp(x_n^{V/2}) \equiv \exp(x_n)$. This time the recursion of equation(3.44) imposes a recursion on the x_n^p 's:

$$x_n^{(p)} = x_n^{(p-1)} + \ln[\alpha_p + exp(x_{n-1}^{(p-1)} - x_n^{(p-1)}) - \beta_{p-1}^2 exp(x_n^{(p-2)} - x_n^{(p-1)})] \tag{3.46}$$

with initial conditions:

$$\begin{aligned} x_0^{(1)} &= log(\alpha_1), & x_1^1 &= 0, \\ x_0^{(2)} &= log(\alpha_1\alpha_2 - \beta_1^2), & x_1^{(2)} &= log(\alpha_1 + \alpha_2), \quad x_2^{(2)} = 0, \end{aligned} \tag{3.47}$$

from which the coefficients $exp(x_n)$ are obtained after $\frac{V}{2}$ iterations. Note that the coefficients $exp(x_n)$ depend on the mass parameter $\bar{m}$ as will be described in detail

later in this chapter. Having now calculated the coefficients x_n and $\ln\det(M[\hat{m}_0])$, the coefficients c_n can be obtained through:

$$c_n \equiv x_n - \ln\det(M[\hat{m}_0]). \tag{3.48}$$

For each given configuration we have now obtained the coefficients c_n but we need to average them over our ensemble of thermalised configurations in order to obtain $\overline{C}_n$'s from equation(3.23). This is also done in exponential form through the recursion:

$$\overline{C}_{(k)} = c_{(k)} + \ln(\frac{1+(k-1)\exp(c_{(k-1)} - c_{(k)})}{k}), \tag{3.49}$$

where k runs over configurations. We have dropped the subscript n of the coefficients c_n and $\overline{C}_n$ and the initial condition is:

$$\overline{C}_1 = c_1. \tag{3.50}$$

Having obtained the averaged coefficients $\exp\overline{C}_n$, we normalize the polynomial so that $\exp\overline{C}_0 = 1$. Clearly, this does not affect the roots.

This method is efficient when applied to small lattices but it meets difficulties for large lattices. The problem is that Lanczos algorithm is characterized by a rapid accumulation of rounding errors. As a result the last vector x_i obtained after each iteration loses its orthogonality with the earliest Lanczos vectors. The problem is resolved by re-orthogonalising the Lanczos vectors: we project each new Lanczos vector $[x_i \rightarrow x_i - x_j(x_j^\dagger x_i)]$ to make it orthogonal with an earlier vector x_j. If we assume that all the previous vectors are approximately orthogonal then x_i can be reorthogonalised against all previous ones in turn and will then be orthogonal to all of them:

$$x_i \rightarrow x_i - \sum_{j<i} x_j(x_j^\dagger x_i) + \sum_{k<j<i} x_j(x_j^\dagger x_k)(x_k^\dagger x_i).... \tag{3.51}$$

However, this is a memory intensive operation and thus is not applicable to large lattices.

Fortunately we can avoid the reorthogonalisation of the Lanczos vectors by using a method which consists in allowing the previous algorithm to proceed beyond the $\frac{V}{2}^{th}$ iteration and end up with a tridiagonal matrix $\tilde{T}$ from which all the eigenvalues of the fermionic matrix can be found[42].

In more detail, we perform the Lanczos algorithm without reorthogonalisation and allow it to proceed beyond the N^{th} iteration. We calculate the new Lanczos vectors, α's and β's. The α's and β's now form a $\tilde{N} \times \tilde{N}$ tridiagonal matrix $\tilde{T}$ with $\tilde{N}$ eigenvalues $\tilde{\lambda}_r$ from which we can sort out the true eigenvalues λ_i of M.

Empirically, we see that if $\tilde{N}$ is sufficiently large then all eigenvalues of M will converge as eigenvalues of $\tilde{T}$. However, $\tilde{T}$ will also have spurious eigenvalues which are not eigenvalues of M. The spurious eigenvalues of $\tilde{T}$ can be recognised by comparing them with the eigenvalues of the tridiagonal matrix $\hat{T}$, formed from just the first $\tilde{N} - 1$ iterations. The real eigenvalues of M will be eigenvalues of $\hat{T}$ as well as $\tilde{T}$. However, $\hat{T}$ will have different spurious eigenvalues than $\tilde{T}$. This happens because the last component of their eigenvectors are large and they are therefore greatly affected by removing the last alpha and beta.

Our aim now is to calculate the eigenvalues of the matrix $\tilde{T}$ using the method of the Sturm sequences. The whole method is based on the following theorem: If V is any hermitian $N \times N$ matrix and D_i is the minor determinant of $V - I\lambda$ formed from the first i rows and columns only, then the number of eigenvalues of V less than λ is equal to the number of sign changes in the sequence $D_0, D_1, D_2, ...D_N$ (where we consider $D_0 = 1$ and regard any $D_i = 0$ as positive).

In our case we have the tridiagonal matrix $\tilde{T}$ and we can generate the D_i's by a recurrence relation:

$$\begin{aligned} D_i &= (\alpha_i - \lambda)D_{i-1} - \beta_{i-1}^2 D_{i-2} \\ D_0 &= 1, \\ D_1 &= \alpha_1 - \lambda. \end{aligned} \tag{3.52}$$

or instead we can just calculate the ratios:

$$r_i = \frac{D_i}{D_{i-1}} \tag{3.53}$$

which satisfy

$$r_1 = a_1 - \lambda,\ r_i = \alpha_i - \lambda - \frac{\beta_{i-1}^2}{r_{i-1}}. \tag{3.54}$$

This is the way one can calculate the number of eigenvalues less than a given λ and locate the k^{th} eigenvalue λ_k by a series of bisections. We can start from an interval $[\lambda_{min}, \lambda_{max}]$ known to contain the eigenvalue. Hence, by repeatedly halving the interval and calculating the number of eigenvalues less than the mid-point, to determine whether λ_k is in the lower or upper half, we may home in on the k^{th} eigenvalue until its value is known to within machine precision.

In order to decide whether this is a spurious or a true eigenvalue we need only to calculate the Sturms sequence twice for each eigenvalue on the reduced tridiagonal form $\hat{T}$, to determine whether or not it has moved outside a given interval $[\lambda_k - \delta,\ \lambda_k + \delta]$.

In practice a more convenient technique is to observe the final ratios r_N of determinants for each bisection at the lower and higher limits i.e.: $r_N(\lambda-\delta), r_N(\lambda+\delta)$. If these terms have the same sign this indicates that the interval contained (is) an eigenvalue of $\hat{T}$ as well as $\tilde{T}$. Hence, the size of the smallest interval during the bisection sequence, for which this is the case, can be taken as a measure of the shift of the eigenvalue and this is usually accurate anough to enable the identification of spurious eigenvalues.

We then define the coefficients $r_k^{(n)}$ through the expansion:

$$\det(M[am_0, U]) = \prod_{i=1}^{\frac{V}{2}}(m_0^2 - \bar{m}^2 + \bar{\lambda}_i^2) = \sum_{k=0}^{n} r_k^{(n)}(m_0^2 - \bar{m}^2)^k \tag{3.55}$$

where we just substituted $\bar{\lambda}_i^2 = (\lambda_i^2 + \bar{m}^2)$.

This gives rise to the iteration:

$$r_k^{(n+1)} = r_k^{(n)}\bar{\lambda}_{n+1}^2 + r_{k-1}^n \tag{3.56}$$

with initial conditions:

$$r_0^{(1)} = \bar{\lambda}_1^2,\ r_1^{(1)} = 1. \tag{3.57}$$

After $\frac{V}{2}$ of these iterations one finally obtains the coefficients $\exp(c_n) = r_n^{(\frac{V}{2})}$. This is the way we calculated the coefficients $\exp(c_n)$ and it is obvious that they depend on the mass parameter $\bar{m}$. Note that the coefficients $\exp(c_n)$ in eqns.(3.45,3.46) also depend on the mass parameter $\bar{m}$. This dependence is expected since we want to evaluate the zeros in m_0 near $\bar{m}$ for different choices of $\bar{m}$. However, the same zeros should appear for adjacent choices of $\bar{m}$ if they are the true zeros of the polynomials.

3.5 Extraction of the zeros from the polynomial

As we have already mentioned on a lattice with N sites, the GCPF is a polynomial of order $N/2$ in m_0^2, and the range of its coefficients is large[3]. It is known that standard root finders suffer from several problems when we have this kind of data[14]. One of the most important problems is that, unless the starting point is very near a complex zero, the root finder is not expected to converge. This is a typical problem when one has to deal with huge variation in the values of the coefficients of the polynomials. Moreover, once one finds a zero, the usual deflation algorithm lowers the precision at each step. After several deflations the results become unreliable.

The "mass shift"($\bar{m}$) method, that was described in the previous section, attempts to solve some of the problems previously cited. We want, for different choices of $\bar{m}$, to evaluate the zeros in m_0 near $\bar{m}$ by using a standard rootfinder. The same zeros should appear for adjacent choices of $\bar{m}$ if they are the true zeros of the polynomials. We have to notice that $\bar{m}$ works as a starting point for a Taylor expansion of the GCPF in $m_0^2 - \bar{m}^2$. If $m_0^2 - \bar{m}^2$ is small enough the last terms in the polynomial give negligible contributions. For a given $\bar{m}$ it is not

possible to determine accurately all the zeros of the GCPF but only those which are in the neighbourhood of $\bar{m}$.

The zeros were found by using two standard root finding algorithms on the equivalent sets of polynomials generated as in equation(3.22) :

$$\sum_{n=0}^{\frac{V}{2}} A_n^i (m_0^2 - \bar{m}_i^2)^n \tag{3.58}$$

for a set of $\bar{m}_i$ in the region where we expect the lowest zeros to occur. These zeros in the bare mass we label as y_i in the following chapters.

We have to notice that we used two rootfinders to determine the zeros of the GCPF: one based on Muller's algorithm[14] and a second one based on Newton-Aberth algorithm[44]. With both of these rootfinders we could handle complex coefficients of the polynomials when complex values of $\bar{m}$ were introduced. The agreement beetween the two rootfinders, based on different algorithms, was very good. In our calculations we used, for lattices up to $8^3 - 10^3$ the Newton-Aberth rootfinder, because it appeared to be a lot $(2 - 3$ times) faster. For simulations on larger lattices the other rootfinder was used.

One has to notice that, both our rootfinders could handle the problems associated with deflation and slow convergence. However, they still suffered from the fact that if one looks for zeros further away from a given $\bar{m}$, more and more coefficients of the polynomial control the position of the zero. Thus the value of the GCPF Z will be sensitive to delicate cancellations among higher powers in the polynomial expansion. In this way spurious zeros may appear. Only the zeros that reproduce themselves as $\bar{m}^2$ is varied were taken as genuine zeros of the GCPF.

The errors in the Lee-Yang zeros were estimated by a Jacknife method. The coefficents for each lattice size were averaged to produce 6 subsets of averaged coefficients, each taking into account 5/6 of the measurements. These 6 different sets of coefficients give 6 different results for the Lee-Yang zeros from which the

variance was calculated.

Finally we would like to note that, in the calculation of the Lee-Yang zeros of the Non-Compact QED GCPF polynomial we also used a multi-precision package MPFun[43] which was implemented in the Newton-Aberth rootfinder. Knowing that we had to deal with a huge variation in the values of the coefficients of the polynomials, this package allowed us to to consider approximately known coefficients. We could use an input precision, d_n, which defined the polynomial neighbourhood of the GCPF polynomial, i.e, the set of all the polynomials with coefficients having d_n common digits with the corresponding coefficients of the GCPF polynomial. For example, we could choose 15 common digits (as in the standard machine precision) up to 500 common digits.

3.6 Chiral Condensate and Lee-Yang Zeros

The Lee-Yang zeros in the strong coupling region of the $\chi U\phi_3$ model are purely imaginary (as we will describe in the next chapter) and evenly spaced along the imaginary axis. Therefore, we can parametrize these zeros as:

$$zeros_n = \pm i(a + nb) \tag{3.59}$$

where a and b are constants and $n = 0, 1, 2.....$ Using the distribution(3.59) it is possible to calculate the chiral condensate $< \bar{\psi}\psi >$ in the infinite volume limit. For the $\chi U\phi_3$ model:

$$lnZ = \sum_{n=0}^{\frac{V}{2}} ln(m_0^2 + (a + nb)^2) \tag{3.60}$$

or

$$lnZ = V \int_0^{\frac{1}{2}} ln(m_0^2 + (a + Vbx)^2)dx \tag{3.61}$$

where $V = L^3$ is the volume of the lattice and $x = \frac{n}{V}$.

Hence:

$$< \bar{\psi}\psi >= \frac{1}{V}\frac{\partial}{\partial m_0} lnZ \tag{3.62}$$

or

$$< \bar{\psi}\psi >= \frac{2}{Vb}\left[\arctan(\frac{Vbx+a}{m_0})\right]_{\frac{a}{m_0}}^{\frac{\frac{Vb}{2}+a}{m_0}}. \tag{3.63}$$

For a first order phase transition in the infinite volume limit at $m_0 = 0$ a, b should scale with some positive power of the inverse volume V.

We now introduce :

$$a = \frac{a'}{V},$$
$$b = \frac{b'}{V}$$

and in the infinite volume limit ($V \to \infty$) equation(3.63) becomes:

$$< \overline{\psi}\psi >= \frac{2}{b'}\arctan(\frac{b'}{2m_0}), \tag{3.64}$$

where in the chiral limit ($m_0 = 0$) we obtain:

$$< \overline{\psi}\psi > \to \frac{\pi}{b'}. \tag{3.65}$$

Hence, for a first order phase transition, in the infinite volume($V \to \infty$) and chiral ($m_0 = 0$) limit, b should scale as

$$b \to V^{-1}. \tag{3.66}$$

3.7 Scaling exponents and the order of the transition

Although, the complete set of the zeros is needed in order to reconstruct the thermodynamical functions of the model, the critical properties of the system are determined by the zeros lying closest to the real axis.

The zero with the smallest imaginary part we label y_1. It is also called the edge singularity. With increasing finite volume it converges to the critical point.

For a continuous phase transition, the position of the zeros closest to the real axis in the complex plane, is ruled by the scaling law:

$$y_i(\beta, \kappa, L) - y_R(\beta, \kappa, \infty) = A_i L^{-1/s}, \tag{3.67}$$

where the A_i's are complex numbers. The exponent $s = s(\beta, \kappa)$ describes the finite size scaling of the correlation length. For the $\chi U \phi_3$ model (and for the non-compact QED in 4D which will be described in chapter(7))

$$y_R(\beta, \kappa, \infty) = 0 \tag{3.68}$$

in the strong coupling region and we ignore it in the following. We do not exlude that it could be possible to have $y_R(\beta, \kappa, \infty) \neq 0$ in the weak coupling region of the $\chi U \phi_3$ model. However, our data (up to 12^3 lattices) show that $y_R(\beta, \kappa, \infty) \to 0$ as the lattice volume increases.

It immediately follows that the real and the imaginary parts of the zeros should scale independently with the same exponent. In particular, for the zero y_1 closest to the chiral phase transition (at $m_0 = 0$)

$$\mathrm{Im}\, y_1(\beta, \kappa, L) = A_I L^{-1/s}, \tag{3.69}$$

with a similar scaling behaviour for $\mathrm{Re}\, y_1(\beta, \kappa, L)$ via A_R. In practice the real part of the zero is much smaller than its imaginary part or is identically zero. So Eqn.(3.69) usually provides a more reliable measure of the exponent than the scaling of the real part.

Although the above scaling law was originally established for the case of a continuous phase transition, it can also be extended to that of a first order phase transition. Since there is no divergent correlation length, the exponent is determined only by the actual dimension of the system. In this case, for a three-dimensional model we expect $s = \frac{1}{3}$.

At the critical point ($\kappa = \kappa_c$) we expect s to be equal to $\tilde{\nu}$, because the fermion correlation length should be the relevant one. In the symmetric phase ($\kappa > \kappa_c$)

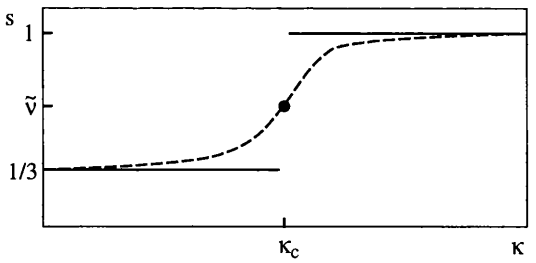

Figure 3.1: Schematic plot of the exponent s in infinite volume (full lines and dot) and the effective s in finite volume (dashed line).

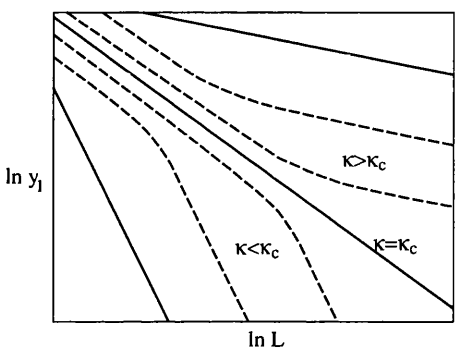

Figure 3.2: Expected finite size scaling of the zero y_1 with lattice size.

we expect scaling with $s = 1$, because $am_F \propto am_0$. This behaviour is indicated in Fig.(3.1) by the full lines and the dot.

In practice it is important to understand the scaling deviations on a finite lattice. The expected behaviour is shown schematically in Fig.(3.2). Far away from the critical point we expect linear scaling in the log-log plot with $s = 1/3$ in the broken phase, and $s = 1$ in the symmetric phase. At the critical point we expect linear scaling and the exponent should be $s = \tilde{\nu}$. These expectations are indicated by the full lines. Close to the phase transition, we expect a crossover. For small lattice sizes the exponent should be close to $\tilde{\nu}$ and then change to $1/3$ and 1, respectively, if the lattice size is increased and the true scaling shows up.

This is indicated in Fig.(3.2) by the dashed lines. For a set of lattice sizes this defines an effective s which smoothly goes through $\tilde{\nu}$ at the critical point. Such an effective s is represented in Fig.(3.1) by a dashed line.

Therefore, in order that the critical exponent can be determined, we must either know the position of the critical point accurately or have many simulations on large lattices so that the scaling deviations can be measured accurately. In practice the limited knowledge of the position of the critical point leads to the largest uncertainty in the determination of $\tilde{\nu}$ by this method.

Chapter 4

Strong Coupling Calculations

4.1 Motivation

As we have already mentioned in the introduction, strongly coupled lattice [1] gauge theories are interesting candidates for new mass generating mechanisms because they tend to break chiral symmetry dynamically. The question is, whether these models are nonperturbatively renormalizable at strong gauge coupling so that the lattice cutoff can be removed. If so, the resulting theory might be applicable in the continuum and constitute a possible alternative to the Higgs mechanism [1].

4.2 Universality at Strong Coupling

At strong gauge coupling we can clearly see the chiral phase transition and we investigate the scaling behaviour and the universality along this line. The Lee-Yang zeros, the chiral condensate and the fermion mass are determined for various values of κ at $\beta = 0.00$ and 0.80. Investigating the universality along this line means that we are looking at the scaling of the data at $\beta = 0$ as a reference and compare it with the scaling found at $\beta = 0.80$. At $\beta = 0$ the scalar and gauge

fields can be integrated out exactly and we end up with a lattice version of the GN_3 model[16]. This model is known to have a chiral phase transition at which it is non-perturbatively renormalizable [15].

4.2.1 Equation of State

The critical exponents of the chiral phase transition are determined by using the EOS for am_F and $\langle\overline{\chi}\chi\rangle$[18][20]. The conclusions seem to depend, to some extent, on the choice of ansatz for the extrapolation of am_F and $\langle\overline{\chi}\chi\rangle$ to infinite volume, although, simulations on lattices up to 24^3 were performed. For the extrapolation three approaches were tried[20]:

$$am_F(L) = am_F(\infty) + A\frac{1}{L^2}, \tag{4.1}$$

$$am_F(L) = am_F(\infty) + A\frac{1}{L}, \tag{4.2}$$

$$am_F(L) = am_F(\infty) + A\frac{1}{L}\exp(-am_F(\infty)\,L). \tag{4.3}$$

Each has two free parameters: $am_F(\infty)$ and A. Fig.(4.1) shows, for example, the data for am_F at $\beta = 0.80$ and $am_0 = 0.01$ plotted against $1/L^2$.

In table (4.1)[20] one can see the comparison of the χ^2's per degree of freedom using the data on 16^3, 20^3 and 24^3 lattices, at the values of β and κ at which there is good statistics. It turned out that the results for these lattice sizes are not conclusive as to which extrapolation formula should be used, because, for each ansatz, all χ^2 per degree of freedom are usually below 1.

The fit with eq.(4.1) was adopted for the extrapolations because it is significantly preferred if compared with the 12^3 data. However, data from the 12^3 lattice was not included. Such an extrapolation is indicated in Fig.(4.1) by the dotted lines.

For the chiral condensate the finite size effects are in general smaller and with opposite sign. Again, consideration of the 12^3 lattices favoured a fit ansatz analogous to eq.(4.1).

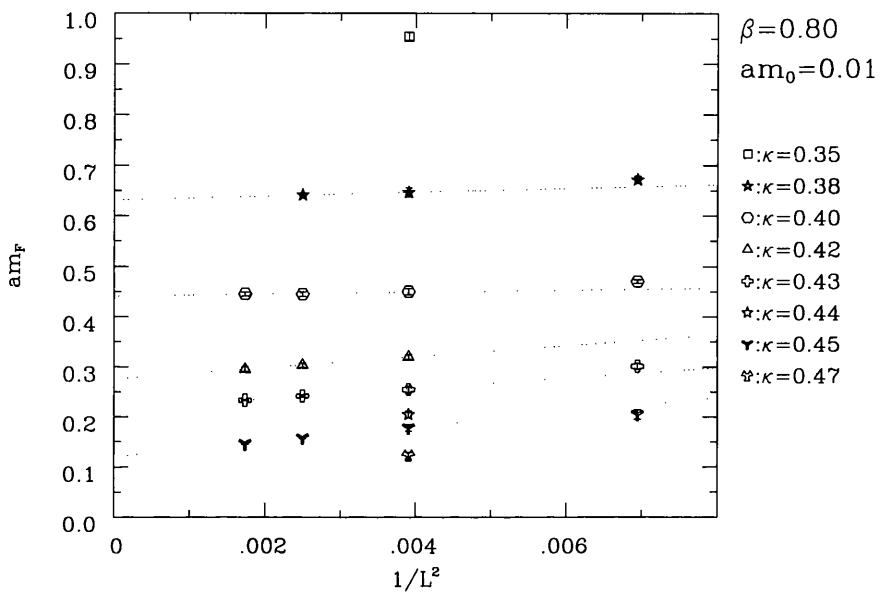

Figure 4.1: Data for am_F at $\beta = 0.80$ and $am_0 = 0.01$ plotted against $1/L^2$. The dotted lines are a fit with eq.(4.1) to the data with $L \geq 16$.

			Fit 1		Fit 2		Fit 3	
β	κ	am_0	am_F	χ^2	am_F	χ^2	am_F	χ^2
0.00	0.95	0.01	0.269(3)	0.30	0.256(7)	0.53	0.278(2)	0.01
0.00	1.00	0.01	0.194(4)	0.22	0.180(9)	0.45	0.202(2)	0.01
0.00	1.05	0.01	0.132(5)	0.23	0.111(10)	0.04	0.142(3)	0.62
0.00	0.95	0.02	0.337(3)	0.41	0.327(6)	0.22	0.343(1)	2.07
0.80	0.40	0.01	0.441(8)	0.12	0.437(2)	0.15	0.445(3)	0.03
0.80	0.42	0.01	0.276(8)	0.01	0.247(16)	0.08	0.295(4)	0.31
0.80	0.43	0.01	0.215(5)	0.07	0.191(9)	0.01	0.230(2)	1.33
0.80	0.45	0.01	0.122(2)	0.01	0.087(1)	0.14	0.137(3)	0.36

Table 4.1: Results of the fits to the finite size behaviour at different couplings and masses on 16^3, 20^3, 24^3 lattices. The extrapolated infinite volume mass $am_F = am_F(\infty)$ and the χ^2 per degree of freedom for the three fits are given: with eq.(4.1) (Fit 1), eq.(4.2) (Fit 2) and eq.(4.3) (Fit 3).

am_F:

β	κ_c	ν	$\tilde{\nu}$	A	B	χ^2
0.00	0.987(33)	0.91(22)	0.43(8)	1.1(3)	0.38(8)	0.72
0.80	0.425(5)	0.78(14)	0.40(5)	3.6(6)	0.33(5)	0.82

$\langle\overline{\chi}\chi\rangle$:

β	κ_c	β_χ	δ	R	S	χ^2
0.00	0.983(12)	0.56(5)	3.1(3)	1.3(2)	1.1(3)	0.84
0.80	0.429(7)	0.56(10)	3.0(5)	4.4(12)	2.4(13)	0.58

Table 4.2: Results of fits at $\beta = 0.00$ and 0.80 using the equations of state. The upper table shows the results of the fit of am_F based on eq.(2.14), the lower table those of $\langle\overline{\chi}\chi\rangle$ based on eq.(2.13).

Therefore the ansatz of eq.(4.1) was used to extrapolate all the data for am_F and $\langle\overline{\chi}\chi\rangle$, obtained on 16^3 and larger lattices, to infinite volume. It is very important to notice that the results presented in the following change somewhat *quantitatively*, but not *qualitatively*, if a different extrapolation formula is used.

The data at different κ and am_0, extrapolated to the infinite volume, were analyzed by means of the EOS. Only the data at $am_0 = 0.01$ and $am_0 = 0.02$ were included. The chosen κ range was $0.80 \ldots 1.05$ for $\beta = 0.00$ and $0.38 \ldots 0.47$ for $\beta = 0.80$[20].

First the data for am_F and $\langle\overline{\chi}\chi\rangle$ were analysed independently and fitted to their corresponding EOS (2.14) and (2.13). The results are shown in table (4.2)[20]. As can be seen, for both β's the critical κ values κ_c are identical within the error bars.

As a next step a simultaneous fit with one common κ_c for am_F and $\langle\overline{\chi}\chi\rangle$ (table 4.3)[20] was performed. A very good fit to all the data was obtained.

Then the scaling relations were checked (2.19). Calculating β and δ with ν

β	κ_c	ν	$\tilde{\nu}$	β_χ	δ	χ^2
0.00	0.983(12)	0.88(8)	0.42(3)	0.56(5)	3.1(3)	0.71
0.80	0.425(4)	0.78(11)	0.40(4)	0.47(5)	3.4(3)	0.71

Table 4.3: Results of fits of am_F and $\langle\overline{\chi}\chi\rangle$ at $\beta = 0.00$ and 0.80, using both equations of state with a common κ_c.

β	κ_c	ν	$\tilde{\nu}$	χ^2	β_χ	δ
0.00	0.981(6)	0.79(2)	0.437(5)	2.2	0.56(4)	3.2(2)
0.80	0.425(2)	0.75(2)	0.431(6)	2.3	0.51(4)	3.4(2)

Table 4.4: Results of the fits using the equations of state at $\beta = 0.00$ and 0.80 with one κ_c and the scaling relations (2.19) at $\beta = 0.00$ and 0.80.

and $\tilde{\nu}$ gives $\beta_\chi = 0.54(20)$ and $\delta = 3.8(15)$ for $\beta = 0.00$ and $\beta_\chi = 0.39(25)$ and $\delta = 5(3)$ for $\beta = 0.80$. The agreement with the fit is quite good. Note that in (2.19), $d\tilde{\nu} = 3\tilde{\nu}$ is close to 1 and hence the statistical errors are increased.

A third fit was also tried in which the validity of the scaling relations was assumed (2.19). The result is shown in Figs.(4.2) and (4.3) and summarized in table(4.4)[20]. As one can see, the quality of the fit is still good and χ^2 are reasonable. The figures also show the prediction of the fit for the fermion mass and chiral condensate at $am_0 = 0.04$ and 0.06. Only small deviations are visible. It is therefore concluded that (2.19) is consistent with the data.

The values of the exponents ν, $\tilde{\nu}$, and β_χ in table (4.2) and table (4.3) agree with those in table (4.4). Thus all three fitting procedures gave consistent results at each β.

The most important observation is that the exponents obtained at $\beta = 0.00$

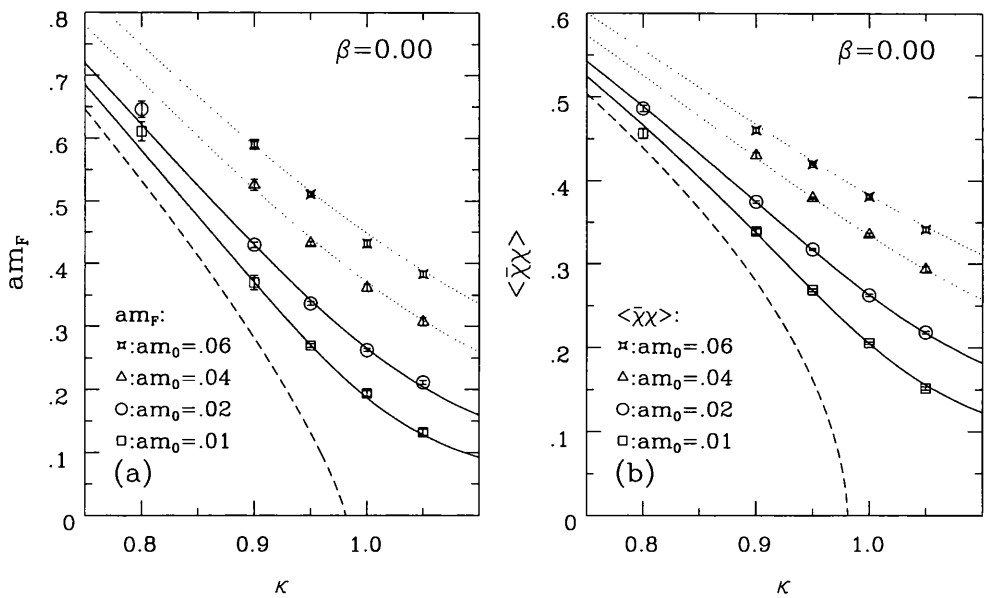

Figure 4.2: (a) Fermion mass and (b) chiral condensate for $\beta = 0.00$. The data are the extrapolation into the infinite volume. The fit assumes the validity of the scaling relations and is described in the text. The parameters are given in table (4.4). The dashed line shows the extrapolation into the chiral limit.

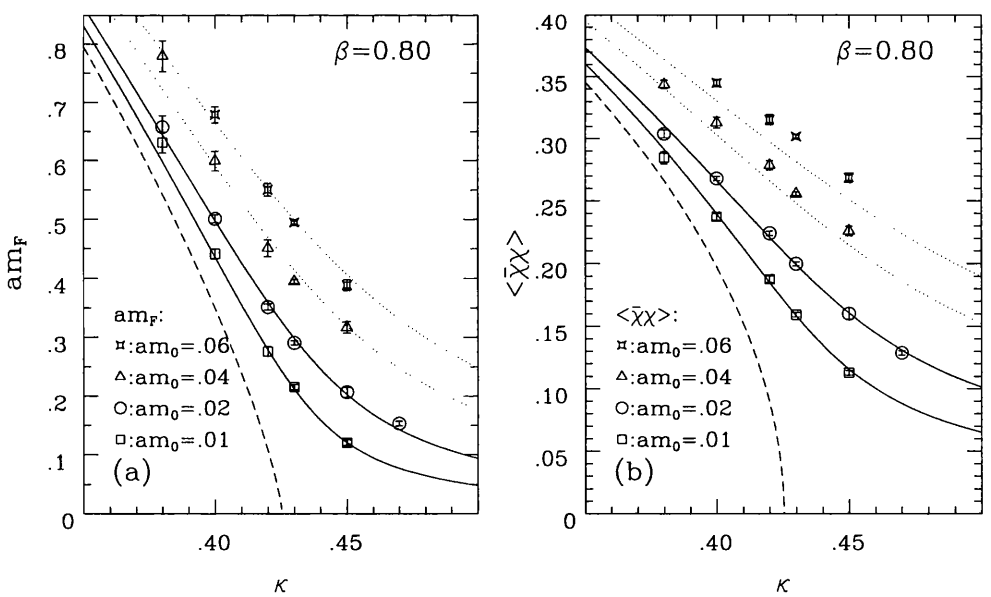

Figure 4.3: (a) Fermion mass and (b) chiral condensate for $\beta = 0.80$.

β	κ_c	ν	$\tilde{\nu}$	χ^2	β_χ	δ
0.00	0.968(9)	0.76(3)	0.426(8)	0.89	0.50(6)	3.6(3)
0.80	0.419(3)	0.66(4)	0.409(10)	0.64	0.37(6)	4.4(6)

Table 4.5: Results of fits, when eq.(4.2) is used for the extrapolation to infinite volume. As in table (4.4), the equations of state with common κ_c and the scaling relations (2.19) are used.

and $\beta = 0.80$ agree within errors which is a strong signal that the chiral phase transition is in one universality class at these β's and probably also for those in between. The difference in the exponents of the last fit, which is somewhat larger than the pure statistical errors may for example be the result of small scaling deviations.

To estimate the uncertainty due to the choice of the extrapolation formula, the above procedures were repeated using the extrapolation (4.2). The results are given in table(4.5). The χ^2's are even smaller and the exponents differ by a little more than one standard deviation. Although the agreement for the two β's is less good, it is still compatible with universality if one takes into account that the error bars only reflect the statistical errors and not the uncertainty due to scaling deviations.

4.2.2 The Finite Size Scaling of the Lee-Yang Zeros

The Lee-Yang zeros were found to be purely imaginary for all κ values in the strong coupling region. For small κ they are equally spaced, consistent with a strong first order transition in the condensate as the bare mass am_0 goes through zero.

Figs.(4.4)[20] and (4.5) show the finite size scaling behaviour of the edge sin-

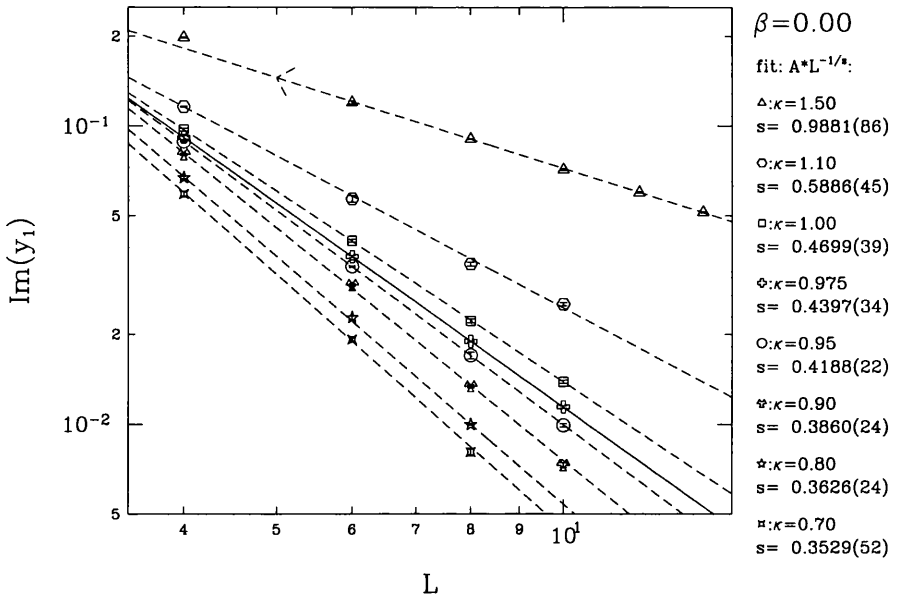

Figure 4.4: Imaginary part of zero y_1 as function of the lattice size for different κ at $\beta = 0.00$. The different straight lines should help to investigate the linearity and claim only for $\kappa = 0.975 \approx \kappa_c$ (full line) to describe the data well.

gularity at various κ for $\beta = 0.00$ and 0.80, respectively. Our data confirm the expectations presented in chapter3 and Fig.(3.2). Close to the critical point we see the expected crossover: for small lattices the exponent is close to $\tilde{\nu}$ and shifts for increasing lattice size to the exponent 1/3 or 1.

At small κ the exponent s is consistent with a first order phase transition, $s \gtrsim \frac{1}{3}$. At large κ is $s \lesssim 1$. Close to the critical point, determined in the previous section and given in table (4.4), the data scale linearly on the log-log plot allowing determination of $\tilde{\nu}$.

At the κ points closest to κ_c we expect $s \simeq \tilde{\nu}$. At $\beta = 0.00$ we find at $\kappa = 0.975 \simeq \kappa_c = 0.981(6)$ the exponent $s = 0.440(4)$ in excellent agreement with $\tilde{\nu} = 0.437(5)$, as determined in the previous section. For $\beta = 0.80$ we did the simulations at $\kappa = 0.43$ slightly larger than the $\kappa_c = 0.425(2)$ obtained from the

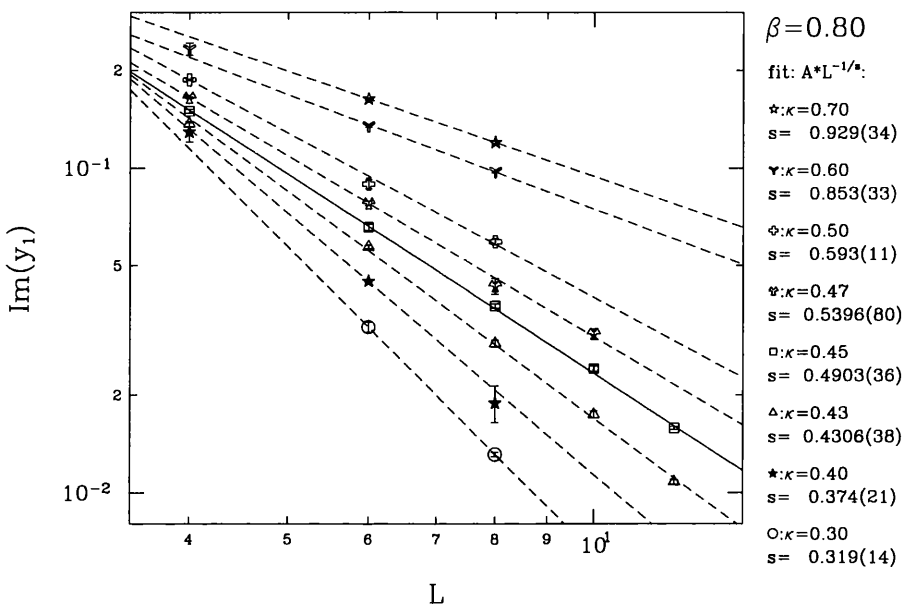

Figure 4.5: Imaginary part of zero y_1 as function of the lattice size for different κ at $\beta = 0.80$.

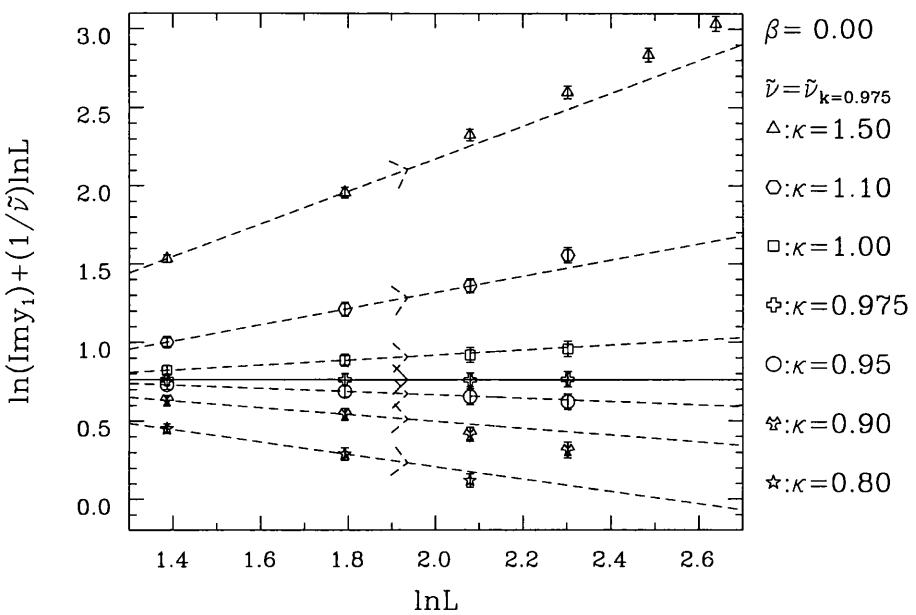

Figure 4.6: $\ln[Im(y_1)] + 1/\tilde{\nu} \ln L$ with $\tilde{\nu} = 0.440$ as a function of the lattice size for different κ's at $\beta = 0.00$. The dashed straight lines are linear extrapolations to the data points at the lowest two values of L.

EOS. We found $s = 0.431(4)$, in good agreement with $\tilde{\nu} = 0.431(6)$ from the EOS.

If one analyses these plots without the knowledge of the critical point determined with the EOS, the critical point can also be determined by looking for linearity of $\ln[Im(y_1)]$ as a function of $\ln L$. For this purpose we show in Figs.(4.6) and (4.7) the quantity $\ln[Im(y_1)] + 1/\tilde{\nu} \ln L$. The addition of the second term makes the plots approximately horizontal and so allows us to enhance the vertical scale making the error bars clearer. In the figures we have used $\tilde{\nu} = 0.440(3)$ and 0.490(4), respectively. The dashed lines are a linear extrapolation of the data points at the two lowest L-values. They provide a guide as to the linearity of the data.

Figs.(4.6) and (4.7) suggest a larger κ_c and $s(\kappa_c)$ than those obtained from the EOS analysis. For example, at $\beta = 0.80$, Fig.(4.7) would suggest $\kappa = 0.45$ as the

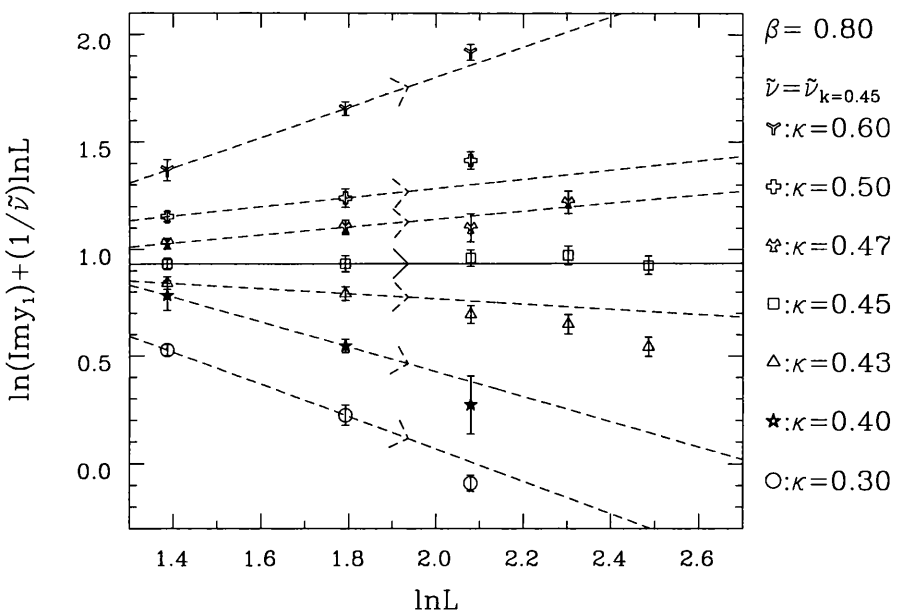

Figure 4.7: As in the previous figure but at $\beta = 0.80$ with $\tilde{\nu} = 0.490$.

point closest to κ_c, with $\tilde{\nu} \simeq s(0.45) = 0.490(4)$. However, the difference between the two methods of analysis is about 10% which is the same size as the statistical error.

All in all, this demonstrates the reliability of the methods we have used. Both (very different) methods agree rather well and their combination is very useful.

4.2.3 Density of the Lee-Yang Zeros

The Lee-Yang zeros, in the strong coupling region, and near the physical mass region ($m \geq 0$ and real) are imaginary. This suggests that any phase transition will only occur at zero fermion mass.

As discussed in chapter(3), in the infinite volume limit and in the chiral limit, the Lee-Yang zeros control the fermion condensate, which is given by $\rho(0)$, the density of zeros at the origin. For large enough lattices, this unrenormalised density corresponds to the slope of the straight line fit of the lowest zeros, at fixed

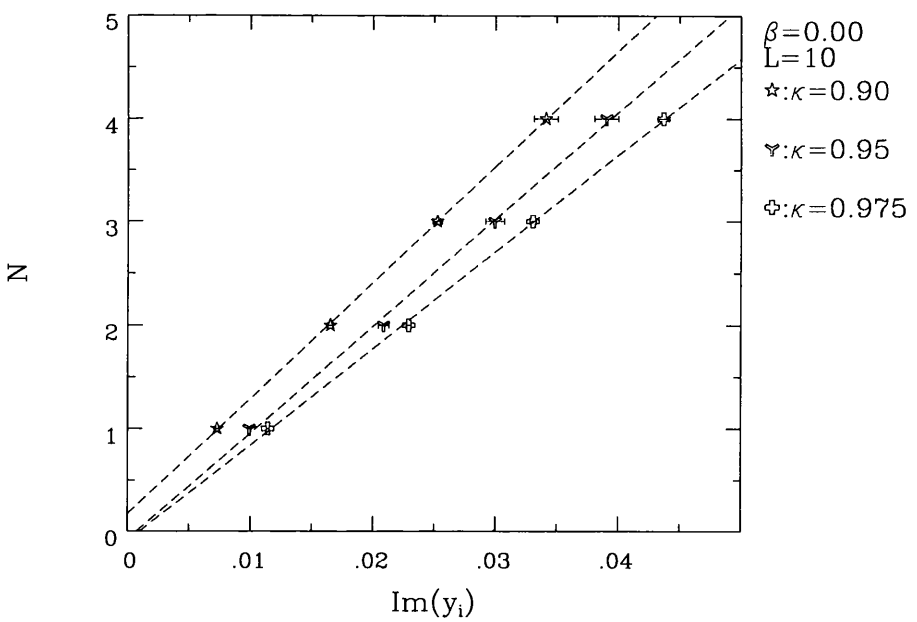

Figure 4.8: The lowest zeros on the 10^3 lattice plotted in sequence for $\beta = 0.00$.

(β, κ). It is given by:

$$\rho(N) = \frac{dN}{dy} \tag{4.4}$$

where N is the index of the zeros.

Figure(4.8) shows the lowest zeros plotted in sequence on the 10^3 lattice for $\beta = 0.00$ and different values of κ. Hence, we estimate the transition to occur at $\kappa_c \approx 0.95$.

We also investigate the separations between the second and third, and the third and fourth zero for $\kappa = 0.95$. The separations scale with respect to the 10^3 lattice as V^α with $\alpha > -1$, indicating a transition different than first order (recall eqn.(3.66)), as expected.

The value of κ_c determined using the densities of the Lee-Yang zeros is very close to the value obtained using the EOS and the value obtained from the finite size scaling of the Lee-Yang zeros. The difference might be due to the fact that larger volumes need to be simulated.

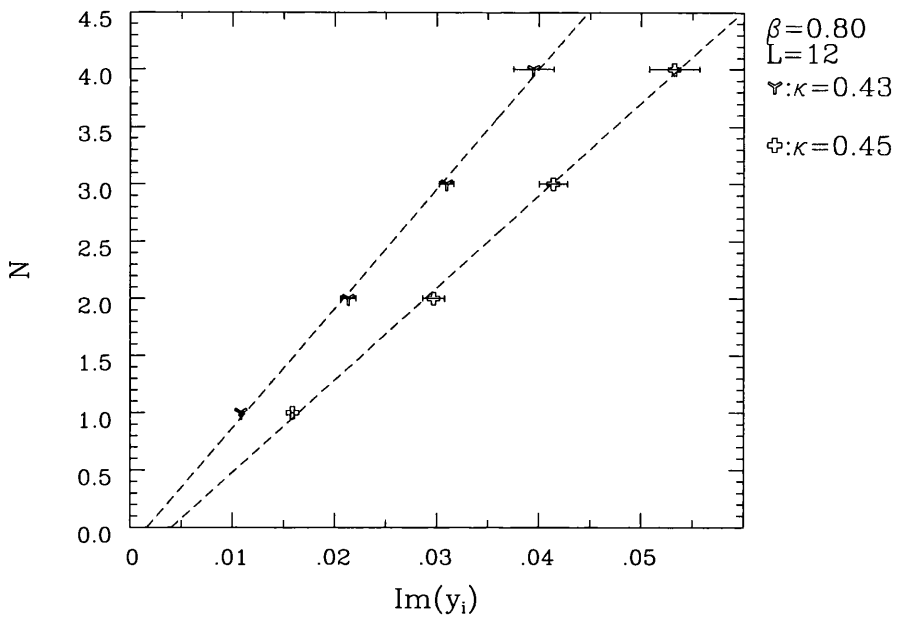

Figure 4.9: The lowest zeros on the 12^3 lattice plotted in sequence for $\beta = 0.80$.

Figure(4.9) shows the lowest zeros plotted in sequence on the 12^3 lattice for $\beta = 0.80$ and different values of κ. This time we estimate the transition to occur at $\kappa_c \approx 0.43$. Investigating again the separations between the second and third, and the third and fourth zero for $\kappa = 0.43$ we find that the seperations scale with respect to the 12^3 lattice as V^α with $\alpha > -1$, indicating a transition different than first order (recall eqn.(3.66)), as expected.

This value of κ_c is consistent with the value obtained using the EOS and is very close to the value obtained from the finite size scaling of the Lee-Yang zeros. Again the difference might be due to the fact that larger volumes need to be simulated.

4.3 Summary of the Strong Coupling Simulations

Our data are a good indication that the chiral phase transition of the $\chi U\phi_3$ model is in the same universality class at $\beta = 0.00$ and $\beta = 0.80$. Assuming this universality we combine the results for exponents at both β values and determine the exponents of this chiral phase transition to be $\nu = 0.75(10)$ and $\tilde{\nu} = 0.43(2)$. The errors take into account the uncertainties discussed above. These values of ν and $\tilde{\nu}$ correspond to $\beta_\chi = 0.51(11)$ and $\delta = 3.45(71)$. We note that the position of the critical point at $\beta = 0$, as well as the results for δ and β are compatible [18] with those obtained for the $N_f = 2$ case in [30] ($\beta_\chi = 0.57(2)$ and $\delta = 2.75(9)$). In that work the same action (2.4) has been simulated, though in a somewhat different representation by means of auxiliary fields than the $\beta = 0$ limit of the $\chi U\phi_3$ model.

The universality might be expected at small β because of the convergence of the strong coupling expansion. But our data are (to our knowledge) the first indication that this is true for a large β interval.

This result indicates that the $\chi U\phi_3$ model belongs to the same universality class as the three-dimensional Gross-Neveu model which is known to be (non-pertubatively) renormalizable [15]. Hence the $\chi U\phi_3$ model is renormalisable and it is a nontrivial example in three dimensions for the shielded gauge-charge mechanism of fermion mass generation proposed in [1].

The universality on the other hand also means that, with respect to the three-dimensional Gross-Neveu model, nothing substantially new happens at small and intermediate β and no new physics arises on scales much below the cutoff. The scalar field shields the fermion χ giving rise to the fermion F equivalent to the fermion of the four-fermion theory. We find no indication that composite states consisting only of fundamental scalars or gauge fields, which would not fit into

the Gross-Neveu model, scale at the chiral phase transition.

Chapter 5

Intermediate-Weak Coupling Calculations

5.1 Motivation

As we saw in the previous chapter the bosonic fields appear to be auxiliary at strong gauge coupling, as they are in a rigorous sense [16] at $\beta = 0$. However, as indicated by the results in four dimensions [12, 13], this may change as the gauge coupling gets weaker. Our aim is to perform an explorative study and see how far the methods applied succesfully at strong coupling can be of use also at weaker coupling.

5.2 Intermediate Coupling Simulations

We have already presented our data for $\beta = 0.00$ and $\beta = 0.80$ indicating that the chiral phase transition of the $\chi U \phi_3$ model is in the same universality class at these two β values. We also noticed in the previous chapter that the Lee-Yang zeros were imaginary for both these β values. Our aim now is to investigate at which value of the gauge coupling the Lee-Yang zeros become complex and what

their behaviour is. Therefore, we performed our simulations with increasing β coupling at $\kappa = 0.33$. We noticed that the Lee-Yang Zeros became complex for $\beta = 1.25$ and $\kappa = 0.33$ on a 4^3 lattice. The Lee-Yang zeros were determined for various values of κ at $\beta = 1.25$ in order to see any chiral phase transition at this β value and investigate if the critical exponent of the finite size scaling of the edge singularity is the same as for $\beta = 0.0$ and $\beta = 0.80$.

5.2.1 The Finite Size Scaling of the Lee-Yang Zeros

The Lee-Yang Zeros were complex (with a very small real part) at $\beta = 1.25$ and $\kappa = 0.33$ on a 4^3 lattice but they became imaginary for larger lattices ($6^3 - 8^3$). We noticed this behaviour of the Lee-Yang Zeros for almost all the κ values at $\beta = 1.25$ at which we performed our simulations. Fig.(5.1) show the finite size scaling behaviour of the edge singularity at various κ for $\beta = 1.25$. Our data confirm again the expectations presented in chapter(3) and Fig.(3.2). Close to the critical point we see the expected crossover: for small lattices the exponent is close to $\tilde{\nu}$ and shifts for increasing lattice size to the exponent $1/3$ or 1.

Therefore, we analysed our plot without any previous knowledge of the critical point. As we have already mentioned in the previous chapter the critical point can be determined by looking for linearity of $\ln[Im(y_1)]$ as a function of $\ln L$.

For this purpose we show in Fig.(5.2) the quantity $\ln[Im(y_1)] + 1/\tilde{\nu} \ln L$. The addition of the second term makes the plots approximately horizontal and so allows us to enhance the vertical scale making the error bars clearer. In the figure we have used $\tilde{\nu} = 0.490(7)$. The dashed lines are a linear extrapolation of the data points at the two lowest L-values. They provide a guide as to the linearity of the data.

Figs.(5.1) and (5.2) would suggest $\kappa = 0.31$ as the point closest to κ_c with $\tilde{\nu} \simeq s(0.31) = 0.490(7)$. This value of $\tilde{\nu}$ agrees very well with the value obtained from the finite size scaling of the edge singularity at $\beta = 0.80$ and $\kappa = 0.45$ and

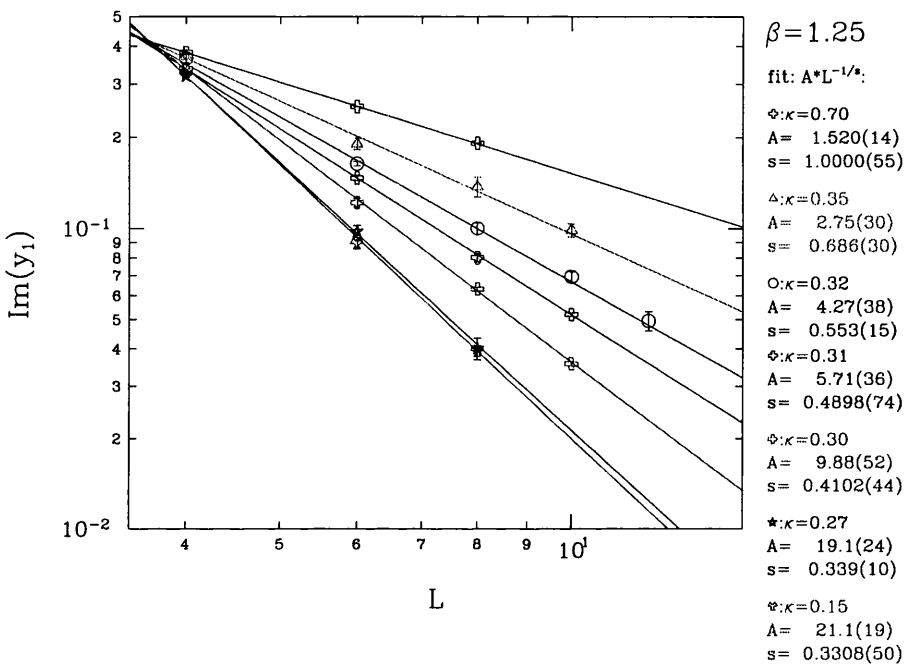

Figure 5.1: Imaginary part of zero y_1 as function of the lattice size for different κ at $\beta = 1.25$. The different straight lines should help to investigate the linearity.

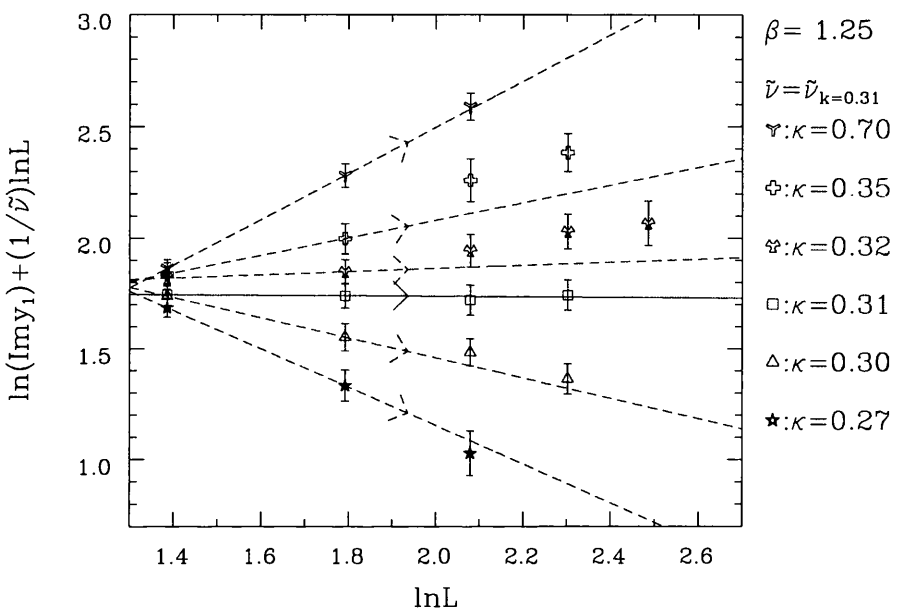

Figure 5.2: $\ln[Im(y_1)] + 1/\tilde{\nu} \ln L$ with $\tilde{\nu} = 0.49$ as a function of the lattice size for different κ's at $\beta = 1.25$. The dashed straight lines are linear extrapolations to the data points at the lowest two values of L.

is close to the value of $\tilde{\nu}$ obtained at $\beta = 0.00$ and $\kappa = 0.975$. Hence, at $\beta = 1.25$, the analysis using the finite size scaling of the edge singularity suggest a value of $\tilde{\nu}$ close to the one at $\beta = 0.00$ and $\beta = 0.80$ indicating that the chiral phase transition might be in the same universality class at these three β values.

We have to notice that the Lee-Yang zeros at $\beta = 1.25$ and various κ's (on a 4^3 lattice) were determined using the information about the behaviour of the edge singularity at intermediate coupling, described in the following chapter.

5.3 Weak Coupling Simulations

5.3.1 Condensate and fermion mass

To investigate the chiral properties of the weak coupling region the chiral condensate and the fermion mass have been used[18] [20].

Fig.(5.3) shows the fermion mass and condensate at $\kappa = 0.25$ as a function of β, at three values of the bare fermion mass. The neutral fermion mass decreases for increasing β but then stabilizes with $am_F > 1$. So it is clearly nonzero at all β and again only weakly dependent on the bare fermion mass. The condensate is large at small β (the Nambu phase) but rapidly decreases with β and becomes very small (zero?) in the chiral limit for $\beta > \beta_X \simeq 1.3$. Thus here a new, weakly coupled region is encountered.

In order to see how this region is related to the Higgs phase at large κ, the fermion mass and condensate are shown in Fig.(5.4) at $\beta = 2.0$ and three values of the bare fermion mass. For nonvanishing bare mass, where the simulations have been performed, the mass of the neutral fermion is large for $\kappa < \kappa_X \simeq 0.27$ whereas it is small for larger κ. It is only very weakly dependent on the bare fermion mass and therefore we expect this behaviour to persist in the chiral limit. For $\kappa > \kappa_X$ its small nonzero value probably vanishes in the infinite lattice size limit.

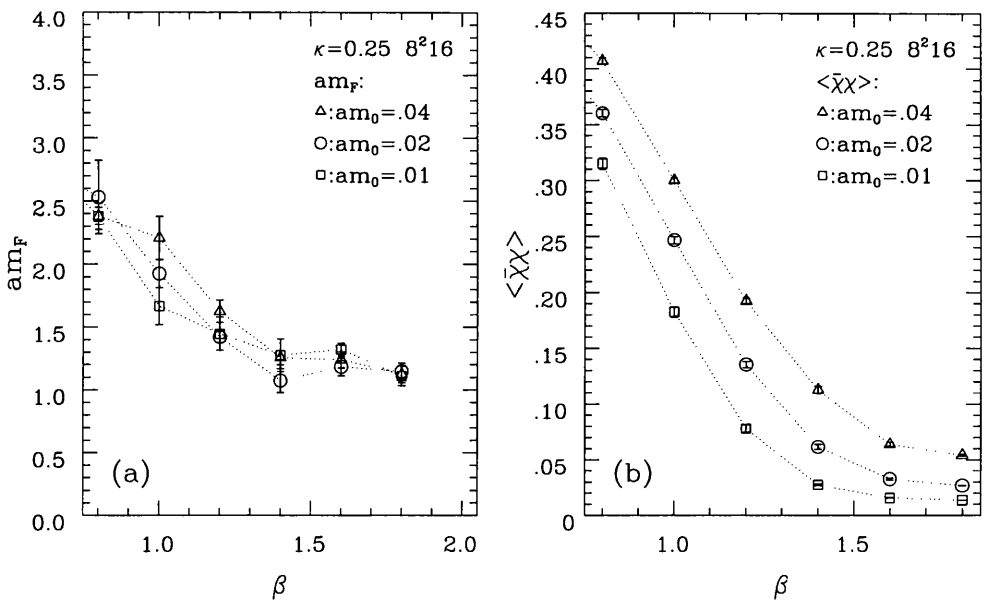

Figure 5.3: (a) fermion mass and (b) chiral condensate for different small am_0 as function of β at $\kappa = 0.25$ on the $8^2 16$ lattice.

The condensate, as expected, does depend strongly on the bare mass am_0 but does show a crossover behaviour at $\kappa = \kappa_X$ with $\langle\overline{\chi}\chi\rangle(am_0)_{\kappa<\kappa_X} < \langle\overline{\chi}\chi\rangle(am_0)_{\kappa>\kappa_X}$. However, at large κ we believe that we are in the Higgs phase where the condensate is zero in the chiral limit. It is therefore conceivable that, in this limit, it is zero at $\beta = 2.0$ for all κ. It is very surprising, however, that, at fixed bare fermion mass and lattice size, the condensate tends to slightly increase with increasing κ, quite in contrast from its behaviour in the strong coupling region. Of course, this can change in the infinite volume and chiral limit.

Fig.(5.5a) confirms the weak dependence of the fermion mass am_F on the bare mass. At $\kappa = 0.22$ below κ_X, the fermion mass is large and stays clearly nonzero at $am_0 \to 0$. Above κ_X, at $\kappa = 0.34$, the fermion mass is too small for the lattice size used and might vanish in the infinite volume limit.

Fig.(5.5b) shows that, at $\beta = 2.0$ and κ just below or above κ_X, the condensate

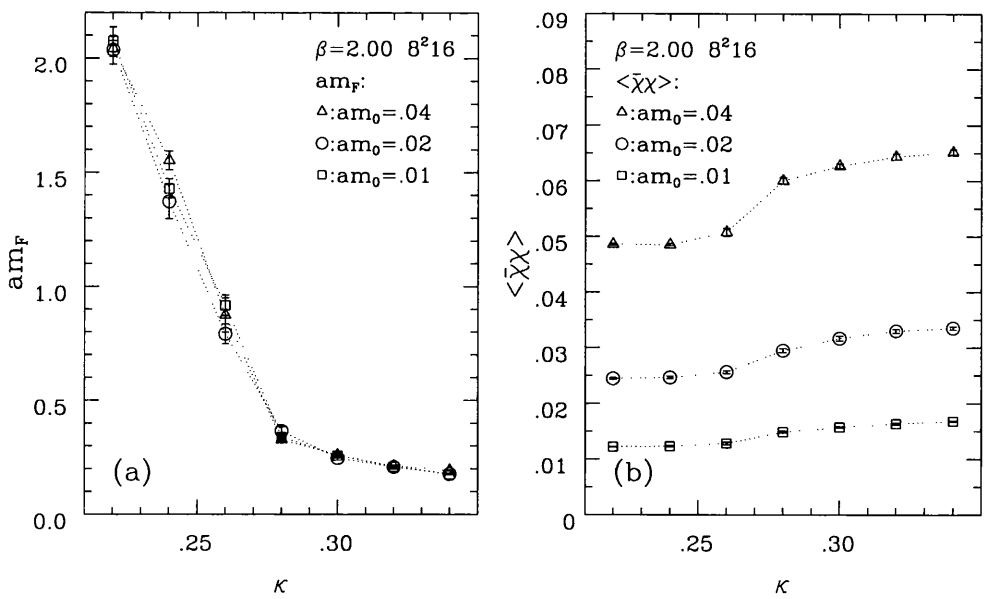

Figure 5.4: (a) fermion mass and (b) chiral condensate for different small am_0 as function of κ at $\beta = 2.00$ on the $8^2 16$ lattice.

extrapolates linearly in am_0 to a very small value or zero. As we shall see later in this chapter, this is due to the Lee-Yang edge singularity in this region being relatively distant from the real axis.

A naive extrapolation to the chiral limit would thus classify the region at small κ ($\kappa < \kappa_X$) and large β ($\beta > \beta_X$) as a phase with zero chiral condensate and nonvanishing fermion mass. But the condensate could also remain very small but nonvanishing. Because of this uncertainty we label this region X. Its boundaries β_X and κ_X may slightly depend on κ and β, respectively.

It would be surprising if in the region X the fermion mass was different from zero with unbroken chiral symmetry. There are essentially two scenarios avoiding such a paradox:

1) Chiral symmetry breaking persists at small κ also for $\beta > \beta_X$. χ is light, because the chiral condensate is very small, though nonzero. F is a bound state of

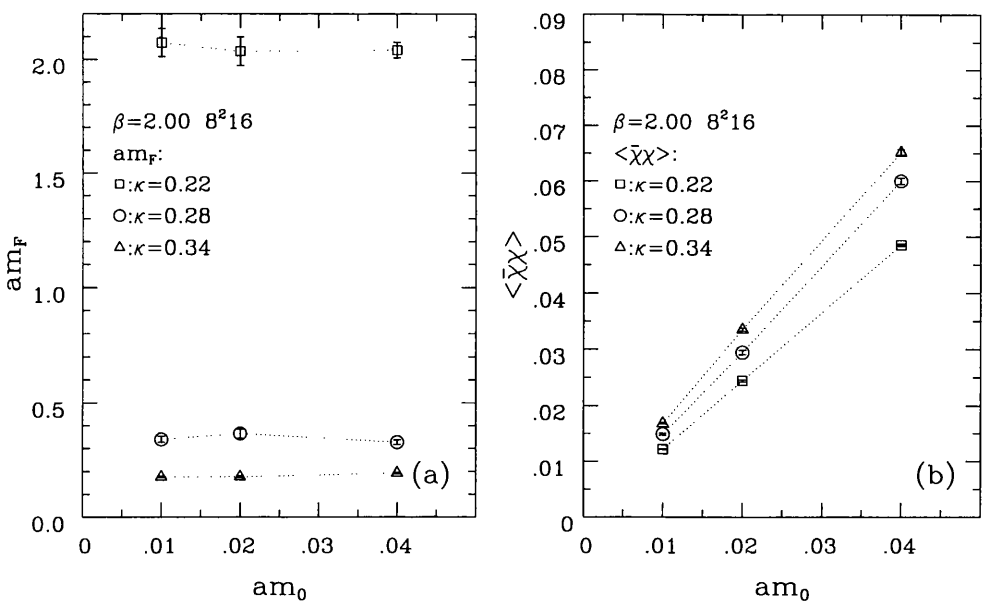

Figure 5.5: (a) Fermion mass and (b) chiral condensate for different κ as function of am_0 at $\beta = 2.00$ on the $8^2 16$ lattice.

ϕ and χ. The binding might be quite loose, presumably by a weak linear confining potential, which one expects in pure U(1) in 3d [21, 31, 32]. F is heavy essentially because ϕ is heavy. The transition at $\beta = \beta_X$ is probably a cross-over, but a genuine phase transition is not excluded.

In this scenario the region X must be separated by a chiral phase transition at $\kappa_X(\beta)$ from the Higgs phase. As the data around κ_X do not indicate any metastability, it would be a higher order transition and a continuum limit should be possible. Thus an interesting continuum limit with a massive unconfined fermion might exist.

2) Chiral symmetry is restored at $\beta = \beta_X$ and the chiral condensate thus vanishes identically and χ is massless in X. The F channel gets a contribution from the two-particle state ϕ and χ. This contribution appears as a massive state because ϕ is heavy. This state presumably cannot be a bound state in the chiral

limit because of the old argument of Banks and Casher [24]: a fermion on a closed orbit must be able to flip its helicity, i.e. existence of the bound state implies chiral symmetry breaking. We cannot distinguish between a bound state F and a two-particle state $\phi + \chi$ looking at the F channel only (as we did). X could be connected to the Higgs phase, where we expect the same spectrum.

Which of these scenarios is true might be investigated in the limit case $\kappa = 0$, i.e. in the three-dimensional compact QED. The results in the non-compact case [23, 25, 27, 28] might be applicable at weak coupling also to the compact one. As the number of fermions in our case is below the critical number $\simeq 3.5$ of fermions in the noncompact model, the more interesting scenario 1) seems to be preferred.

5.3.2 The Lee-Yang zeros at Weak Coupling

In an attempt to clarify the situation at weak coupling we investigate the Lee-Yang zeros in the region X[18][17]. The edge singularity y_1 has a nonzero real part in this region. The zeros must appear in conjugate pairs. We define the edge singularity in this region to be the zero with smallest positive imaginary part and count each pair only once.

The finite size scaling of the lowest zeros is shown in Figs.(5.6) (5.7)[20],(5.8), for $\beta = 2.00$ and $\kappa = 0.00$, $\kappa = 0.15$, $\kappa = 0.27$, respectively. All these three points are points in the the region X.

The real part of the low lying zeros is clearly nonvanishing. Then the first two zeros have within the numerical precision identical imaginary part but their real parts differ by a factor of about 3.5. The first two zeros have imaginary parts so close as to be indistinguishable within statistical error. We have assumed continuity in the behaviour of their real parts as a function of lattice size when plotting Figs.(5.6),(5.7), (5.8).

These imaginary parts scale linearly in the log-log plot with an exponent $s \approx 0.7$. Their real part has somewhat larger errors but scales within the numerical

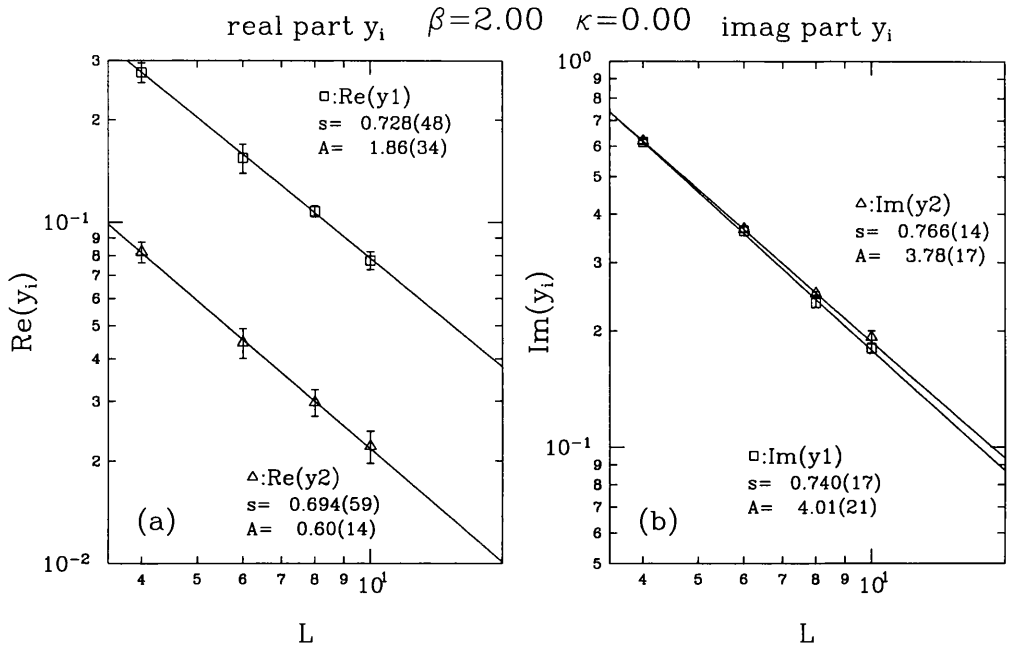

Figure 5.6: (a) Real and (b) imaginary part of the first two Lee Yang zeros (sorted by their positive imaginary part) for $\beta = 2.00$, $\kappa = 0.00$ as function of lattice size.

precision with the same exponent. This pattern for the edge singularity is found throughout the region X as can be easily seen in Fig(5.9) for the imaginary part.

Figs.(5.10),(5.11,5.12), show the Lee-Yang zeros for $\beta = 2.00$ and $\kappa = 0.00$, $\kappa = 0.27$, respectively, in the complex fermion mass plane. One can notice here the indistinguishable imaginary parts of the complex zeros, specially for the edge singularity.

Fig.(5.13) shows the behaviour of the imaginary part of the edge as a function of lattice size at $\kappa = 0$ for various β. There is a crossover between $\beta = 1.25$ and $\beta = 1.88$, i. e. from the Nambu phase, where the imaginary part of the edge zero is small and the transition first order, to a region where the imaginary part is large (with nonzero real part). No scaling deviations can be observed for $\beta \geq 1.88$. In the region X the critical exponent has a very weak dependence on β and increases only very slowly on further increase of κ.

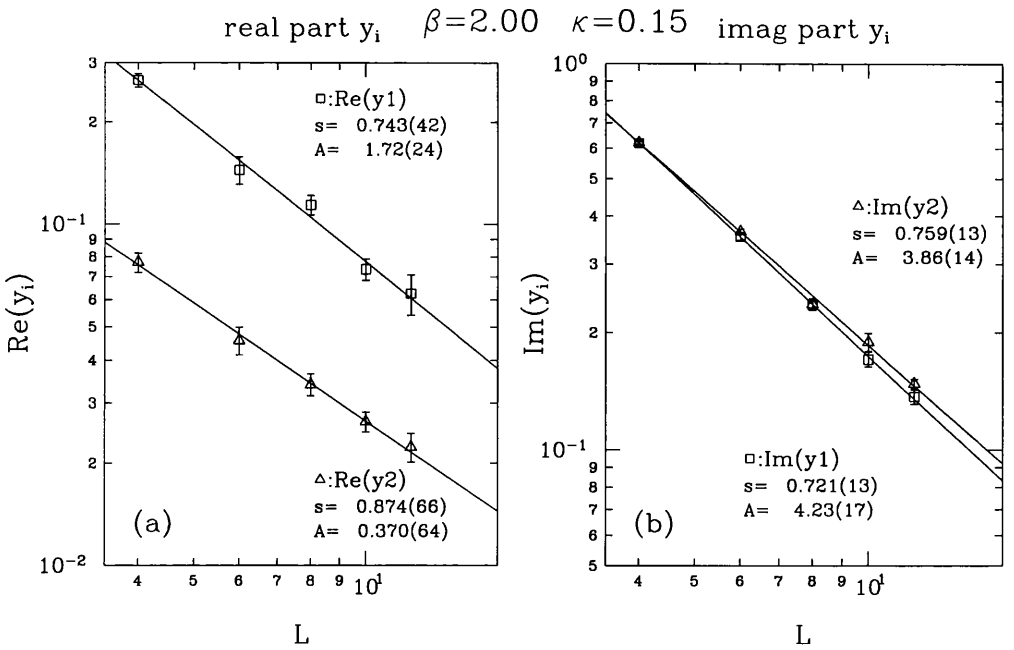

Figure 5.7: (a) Real and (b) imaginary part of the first two Lee Yang zeros (sorted by their positive imaginary part) for $\beta = 2.00$, $\kappa = 0.15$ as function of lattice size.

If the scaling in the region X is different from that in the other regions, the most naive expectation would be that the exponent s is universal. This is compatible with our data at $\beta \approx 2$ but not at $\beta = 5$. Further simulations on larger lattice are necessary to confirm this difference.

It is to our knowledge the first model in which scaling of the real part of the edge singularity to zero has been observed.

Summarizing, the region X can be distinguished from the Nambu and Higgs phase by the edge singularity having a real part (on a finite lattice) and a scaling which cannot be described by either an exponent $s = 1/3$ or $s = 1$. If the exponent s is different from those in Nambu and Higgs phases then the region X is presumably a new phase.

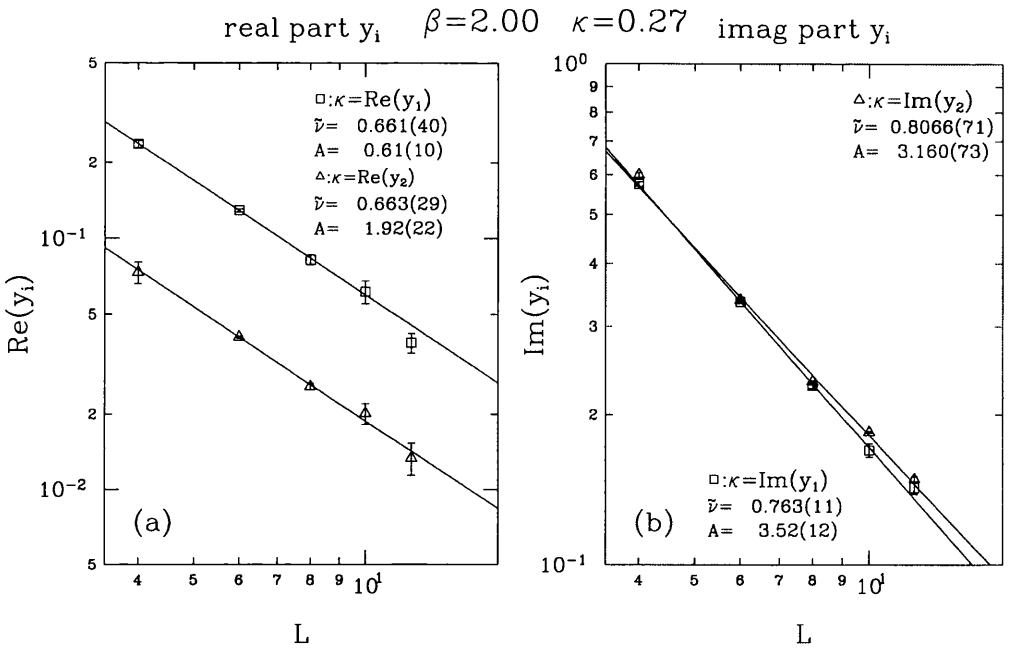

Figure 5.8: (a) Real and (b) imaginary part of the first two Lee Yang zeros (sorted by their positive imaginary part) for $\beta = 2.00$, $\kappa = 0.27$ as function of lattice size.

5.4 Summary of the Intermediate and Weak Coupling Simulations

Our investigations, at weak coupling, showed that there is a region at small κ, where the chiral condensate is zero within our numerical accuracy but the neutral fermion mass is large, called the X region. This region can analytically be connected with either the Nambu or Higgs phase but it may well be a separate phase. If chiral symmetry is not broken in this region, then the mass observed in the fermion channel is presumably the energy of a two-particle state. Otherwise this region might be an interesting example of dynamical mass generation of unconfined fermions. If the continuum limit is taken at the Higgs phase transition, the gauge fields should play an important dynamical role and the model would not fall into the universality class of the three-dimensional Gross-Neveu model. A

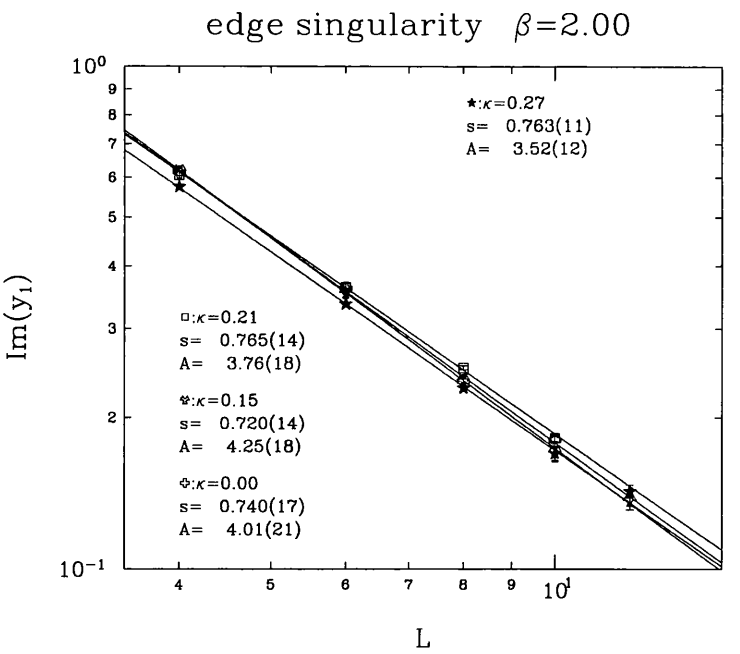

Figure 5.9: (a)Imaginary part of the first Lee Yang zero (sorted by their positive imaginary part) for $\beta = 2.00$ and different κ's as function of lattice size.

further investigation of this possibility is highly desirable.

Our investigations at intermediate coupling, using only the Lee-Yang Zeros, showed that there are indications that the chiral phase transition is in one universality class for all $\beta \leq 1.25$: that of the three-dimensional Gross-Neveu model. An analysis of the Lee-Yang Zeros using larger lattices would be necessary in order to clarify the chiral properties at intermediate coupling.

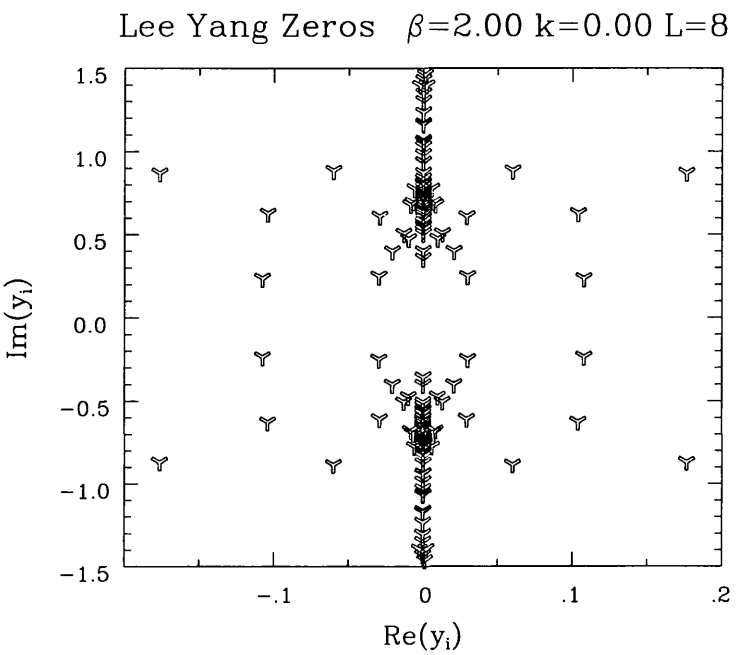

Figure 5.10: Lee Yang zeros for $\beta = 2.00$ and $\kappa = 0.00$ in the complex fermion mass plane for $V = 8^3$.

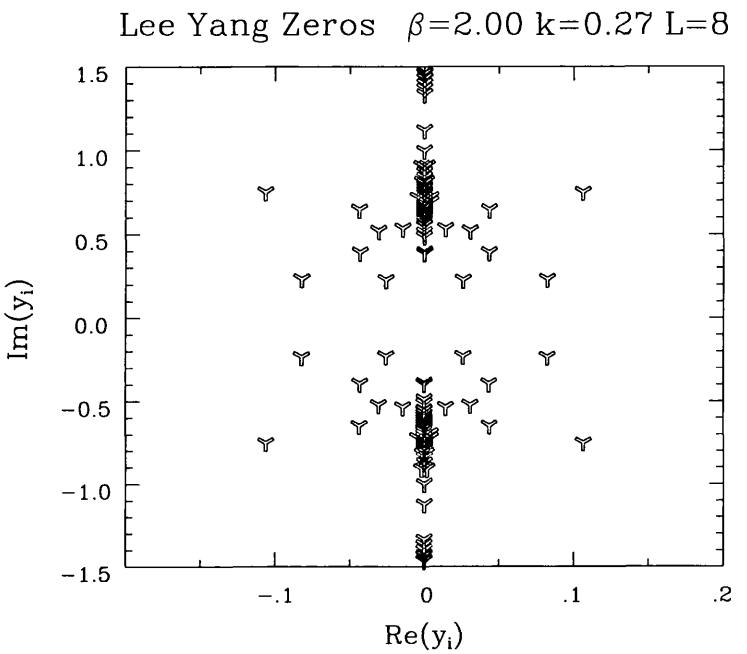

Figure 5.11: Lee Yang zeros for $\beta = 2.00$ and $\kappa = 0.27$ in the complex fermion mass plane for $V = 8^3$.

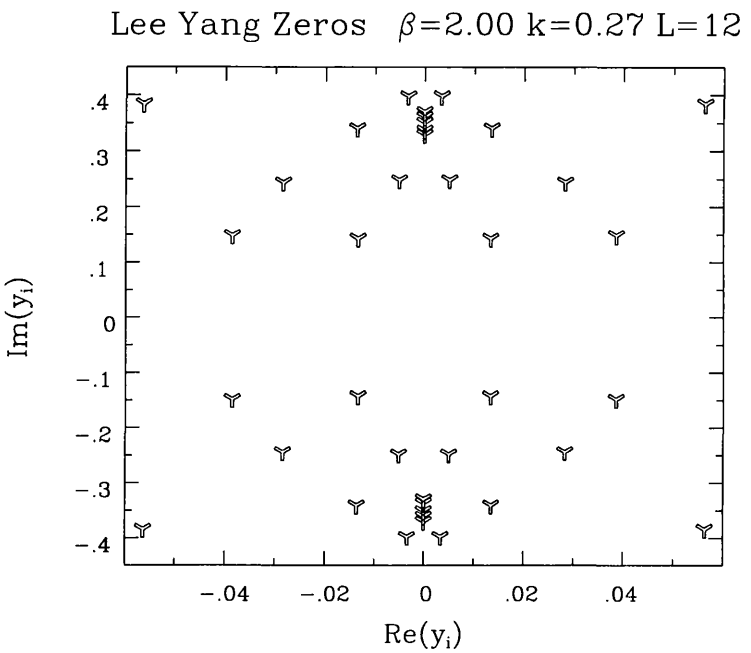

Figure 5.12: Lee Yang zeros for $\beta = 2.00$ and $\kappa = 0.27$ in the complex fermion mass plane for $V = 12^3$.

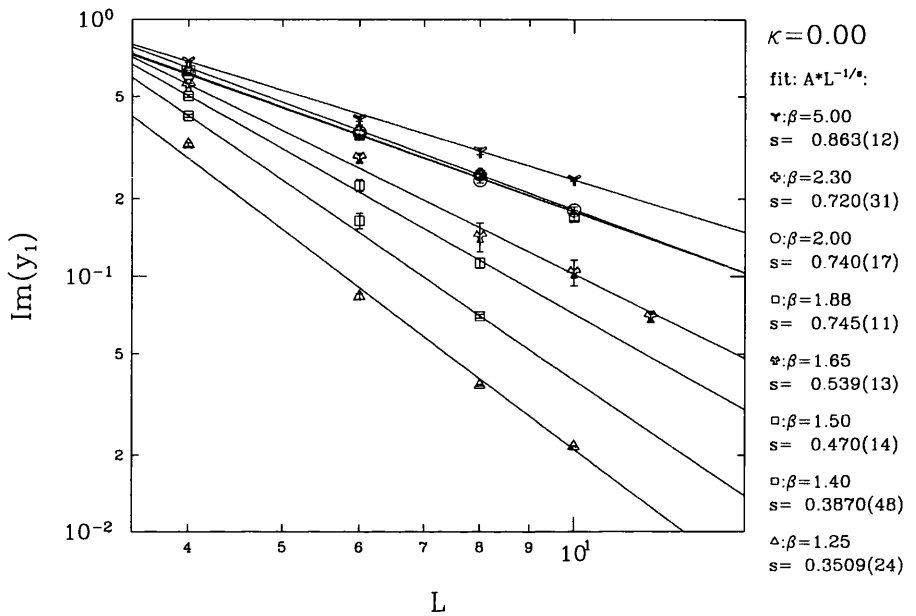

Figure 5.13: Imaginary part of zero y_1 as function of the lattice size for different β at $\kappa = 0$.

Chapter 6

Accurate determination of the Lee-Yang Zeros

6.1 Motivation

As mentioned earlier, in the region X, the chiral condensate is very small, which suggests that the Lee-Yang zeros cannot be near to the physical region. It is of interest to investigate if the closest zeros can be determined with sufficient accuracy to ascertain their finite size scaling behaviour (and hence that of the condensate) in the weak coupling region.

However, we also investigated how accurate the closest zeros are determined in the strong and intermediate coupling.

It appears that the closest zeros in the weak and strong coupling region are determined with **very good** accuracy, and therefore we can ascertain their finite size scaling behaviour as described in chapters(4, 5).

The behaviour of the edge singularity in the intermediate coupling region is desribed later in this chapter.

6.2 The Lee-Yang zeros at Weak Coupling

As mentioned in chapter(5) the Lee-Yang zeros in the weak coupling region are moving in the complex plane. We have defined the edge singularity, in this region, to be the zero with the smallest positive imaginary part and count each pair only once. The real part of the low lying zeros is clearly nonvanishing and the first two zeros have imaginary parts so close as to be indistinguishable within statistical error. Our aim is to investigate any (unexpected) dependence of the edge singularity on the number of measurements(N), the thermalisation of the system from a cold(hot) start, the number of iterations used to thermalize the system(T), the "updating" mass $a\hat{m}_0$ and the units of Monte Carlo Time(I) used between configurations for each measurement of the coefficients for fixed (β, κ).

As can been seen from table(6.2)) for $\beta = 2.00$ and $\kappa = 0.00$ (on a 4^3 lattice) the edge singularity seems to behave very well and no significant dependence on any of the previous parameters was found. However, one has to notice again that the imaginary parts of the first two zeros are so close as (see table(6.2)) to be indistinguishable within statistical error.

In order to see a more clear picture of the behaviour of the edge singularity we monitored the imaginary and the real part of it with the number of measuremenents for $a\hat{m}_0 = 0.02$.

Figs.(6.1,6.2) show the imaginary and the real part of the edge singularity with the number of measurements, respectively, when we thermalised the system with 1000 iterations from a hot start and the measurements of the coefficients were made on configurations separated by 2 units of Monte Carlo Time. It is obvious that the real and the imaginary part of the edge singularity are stable after about 2000 measurements.

As can be seen from tables(6.2,6.3) we also investigated the behaviour of the edge singularity for $\beta = 0.00$ and $\kappa = 0.27$ on a 4^3 and 8^3 lattice. It is obvious that there is no significant dependence of the edge singularity on the "updating"

β	κ	$a\hat{m}_0$	*Start*	N	T	I	*First Zero*	*Second Zero*
2.00	0.00	0.100	Hot	10,000	1,000	2	(0.260,0.6239)	(0.077,0.6197)
2.00	0.00	0.100	Cold	10,000	1,000	2	(0.244,0.6269)	(0.070,0.6317)
2.00	0.00	0.020	Hot	10,000	1,000	2	(0.264,0.6226)	(0.073,0.6296)
2.00	0.00	0.020	Hot	10,000	3,000	2	(0.262,0.6291)	(0.078,0.6134)
2.00	0.00	0.020	Hot	15,000	1,000	2	(0.255,0.6216)	(0.071,0.6308)
2.00	0.00	0.020	Hot	10,000	10,000	2	(0.262,0.6348)	(0.078,0.6340)
2.00	0.00	0.020	Hot	2,000	10,000	10	(0.228,0.6356)	(0.065,0.6533)
2.00	0.00	0.020	Cold	10,000	1,000	2	(0.256,0.6060)	(0.063,0.6247)
2.00	0.00	0.005	Hot	10,000	1,000	2	(0.248,0.6167)	(0.067,0.6242)
2.00	0.00	0.005	Hot	10,000	3,000	2	(0.249,0.6230)	(0.069,0.6309)
2.00	0.00	0.005	Hot	15,000	1,000	2	(0.244,0.6142)	(0.062,0.6294)
2.00	0.00	0.005	Hot	10,000	10,000	2	(0.258,0.6242)	(0.074,0.6211)
2.00	0.00	0.005	Hot	2,000	10,000	10	(0.257,0.6086)	(0.067,0.6252)
2.00	0.00	0.005	Cold	10,000	1,000	2	(0.241,0.6313)	(0.066,0.6399)

Table 6.1: Results of the behaviour of the edge singularity with the number of measurements(N), the thermalisation of the system from a cold(hot) start, the number of iterations used to thermalize the system(T), the "updating" mass $a\hat{m}_0$ and the units of Monte Carlo Time(I) used between configurations for each measurement of the coefficients for $\beta = 2.00$ and $\kappa = 0.00$, on a 4^3 lattice.

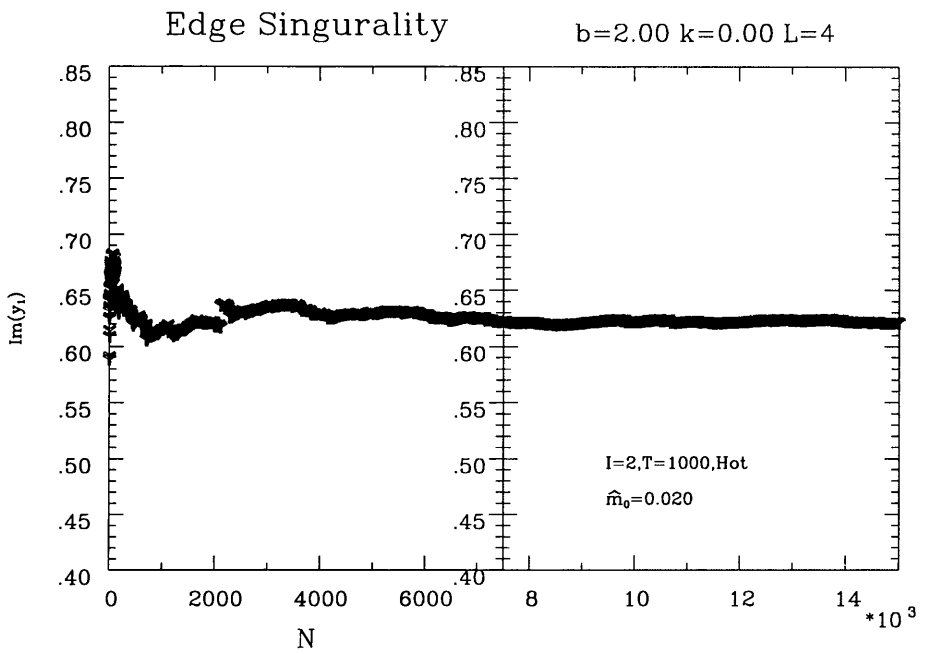

Figure 6.1: Imaginary part of zero y_1 as function of the number of measurements(N) for $\beta = 2.00$ and $\kappa = 0.00$ on a 4^3 lattice.

β	κ	$a\hat{m}_0$	*Start*	*N*	*T*	*I*	*First Zero*	*Second Zero*
2.00	0.27	0.020	Cold	20,000	1,000	2	(0.231,0.5724)	(0.072,0.5948)
2.00	0.27	0.005	Cold	20,000	1,000	2	(0.232,0.5671)	(0.071,0.5940)

Table 6.2: Results of the behaviour of the edge singularity with the number of measurements(N), the thermalisation of the system from a cold(hot) start, the number of iterations used to thermalize the system(T), the "updating" mass $a\hat{m}_0$ and the units of Monte Carlo Time(I) used between configurations for each measurement of the coefficients for $\beta = 2.00$ and $\kappa = 0.27$, on a 4^3 lattice.

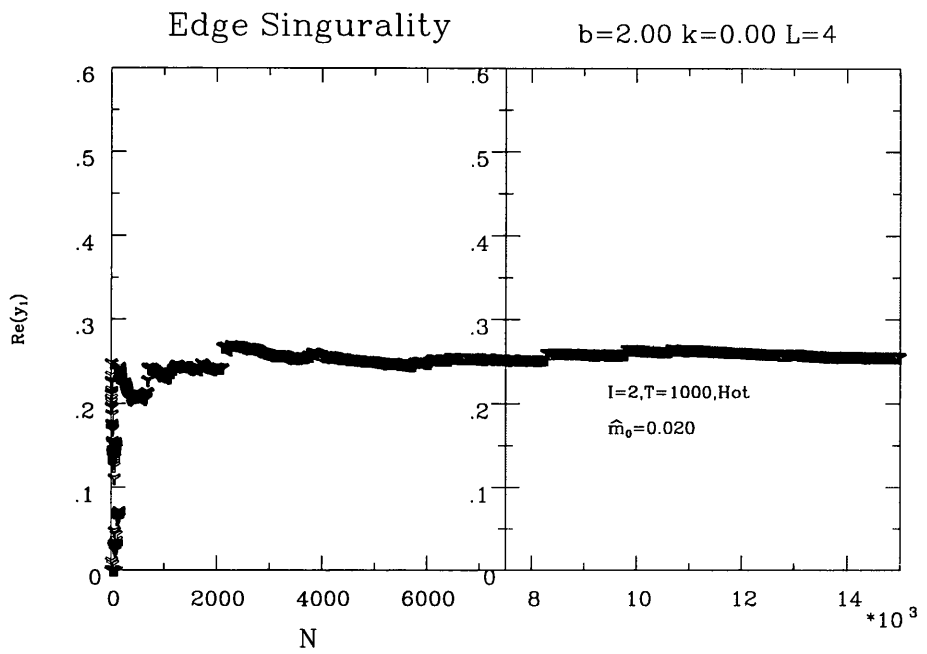

Figure 6.2: Real part of zero y_1 as function of the number of measurements(N) for $\beta = 2.00$ and $\kappa = 0.00$ on a 4^3 lattice.

β	κ	$a\hat{m}_0$	*Start*	*N*	*T*	*I*	*First Zero*	*Second Zero*
2.00	0.27	0.040	Cold	12,000	1,000	2	(0.026,0.2298)	(0.080,0.2341)
2.00	0.27	0.020	Cold	12,000	1,000	2	(0.026,0.2288)	(0.080,0.2334)

Table 6.3: Results of the behaviour of the edge singularity with the number of measurements(N), the thermalisation of the system from a cold(hot) start, the number of iterations used to thermalize the system(T), the "updating" mass $a\hat{m}_0$ and the units of Monte Carlo Time(I) used between configurations for each measurement of the coefficients for $\beta = 2.00$ and $\kappa = 0.27$, on a 8^3 lattice.

mass $a\hat{m}_0$, as expected.

We have to notice that the errors of the Lee-Yang zeros (calculated with the jackknife method described in chapter(3)) were about (or less than) 5% and are not shown for simplicity.

6.3 The Lee-Yang zeros at Strong Coupling

We also investigated the behaviour of the edge singularity in the strong coupling region and specially at $(\beta = 0.80, \kappa = 0.00)$ on a 4^3 lattice. The Lee-Yang zeros were found to be imaginary at this value of the gauge coupling.

In table(6.4) one can notice that there is no significant dependence of the edge singularity on any of the parameters investigated at $(\beta = 0.80, \kappa = 0.00)$.

Again we can see a more clear picture of the behaviour of the edge singularity, when the imaginary part of it is monitored with the number of measuremenents for $a\hat{m}_0 = 0.02$.

Fig.(6.3) shows dependence of the imaginary part of the edge singularity on the number of measurements, respectively, when we thermalised the system with 1000 iterations from a hot start and the measurements of the coefficients were made on configurations separated by 2 units of Monte Carlo Time. One can notice that the imaginary part of the edge singularity is stable after about 500 measurements.

Again the errors of the Lee-Yang zeros (calculated with the jackknife method described in chapter(3)) were about (or less than) 5% and are not shown for simplicity.

6.4 The Lee-Yang zeros at Intermediate Coupling

As we recall from chapter(5), intermediate coupling is where the Lee-Yang

β	κ	$a\hat{m}_0$	*Start*	N	T	I	*First Zero*
0.80	0.00	0.020	Hot	10,000	1,000	2	(0.000,0.0937)
0.80	0.00	0.020	Hot	10,000	3,000	2	(0.000,0.0922)
0.80	0.00	0.020	Hot	15,000	1,000	2	(0.000,0.0932)
0.80	0.00	0.020	Hot	10,000	10,000	2	(0.000,0.0931)
0.80	0.00	0.020	Hot	2,000	10,000	10	(0.000,0.0918)
0.80	0.00	0.020	Hot	1,000	10,000	20	(0.000,0.0922)
0.80	0.00	0.020	Cold	10,000	1,000	2	(0.000,0.0956)
0.80	0.00	0.005	Hot	10,000	1,000	2	(0.000,0.0964)
0.80	0.00	0.005	Hot	10,000	3,000	2	(0.000,0.0948)
0.80	0.00	0.005	Hot	15,000	1,000	2	(0.000,0.0967)
0.80	0.00	0.005	Hot	10,000	10,000	2	(0.000,0.0984)
0.80	0.00	0.005	Hot	2,000	10,000	10	(0.000,0.0933)
0.80	0.00	0.005	Hot	1,000	10,000	20	(0.000,0.0949)
0.80	0.00	0.005	Cold	10,000	1,000	2	(0.000,0.0936)

Table 6.4: Results of the behaviour of the edge singularity with the number of measurements(N), the thermalisation of the system from a cold(hot) start, the number of iterations used to thermalize the system(T), the "updating" mass $a\hat{m}_0$ and the units of Monte Carlo Time(I) used between configurations for each measurement of the coefficients for $\beta = 0.80$ and $\kappa = 0.00$, on a 4^3 lattice.

β	κ	$a\hat{m}_0$	*Start*	N	T	I	*First Zero*
1.25	0.00	0.100	Hot	10,000	1,000	2	(0.063,0.3136)
1.25	0.00	0.100	Cold	10,000	1,000	2	(0.070,0.3101)
1.25	0.00	0.020	Hot	10,000	1,000	2	(0.000,0.2844)
1.25	0.00	0.020	Hot	10,000	3,000	2	(0.077,0.3000)
1.25	0.00	0.020	Hot	2,000	1,000	10	(0.079,0.3131)
1.25	0.00	0.020	Cold	10,000	1,000	2	(0.074,0.3169)
1.25	0.00	0.005	Hot	10,000	1,000	2	(0.000,0.2665)
1.25	0.00	0.005	Hot	10,000	3,000	2	(0.079,0.3068)
1.25	0.00	0.005	Hot	2,000	1,000	10	(0.079,0.2846)
1.25	0.00	0.005	Cold	10,000	1,000	2	(0.054,0.2997)

Table 6.5: Results of the behaviour of the edge singularity with the number of measurements(N), the thermalisation of the system from a cold(hot) start, the number of iterations used to thermalize the system(T), the "updating" mass $a\hat{m}_0$ and the units of Monte Carlo Time(I) used between configurations for each measurement of the coefficients for $\beta = 1.25$ and $\kappa = 0.00$, on a 4^3 lattice.

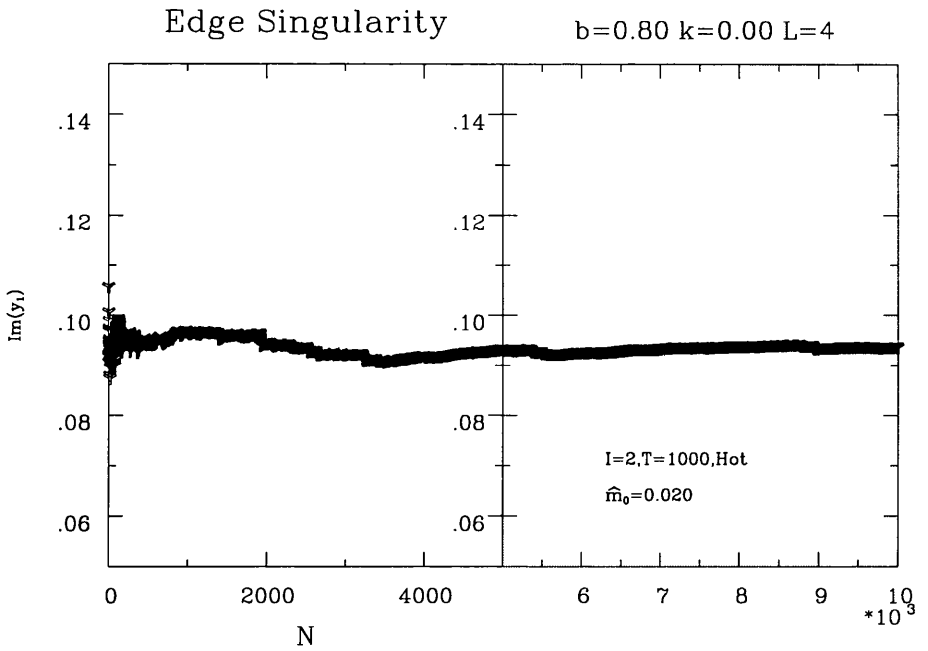

Figure 6.3: Imaginary part of zero y_1 as function of the number of measurements(N) for $\beta = 0.80$ and $\kappa = 0.00$ on a 4^3 lattice.

zeros start moving in the complex fermion mass plane. At $\beta = 1.25$ and $\kappa = 0.33$ we saw the edge singularity becoming complex on a 4^3 lattice. However, the real part of the edge singularity was very small and became zero when the lattice volume was increased.

In table(6.5) one can see the behaviour of the edge singularity with the number of measurements(N), the thermalisation of the system from a cold(hot) start, the number of iterations used to thermalize the system(T), the "updating" mass $a\hat{m}_0$ and the units of Monte Carlo Time(I) used between configurations for each measurement of the coefficients for $\beta = 1.25$ and $\kappa = 0.00$ on a 4^3 lattice.

These results show that the real part of the edge singularity, has a strong dependence on the "updating" mass $a\hat{m}_0$ when we thermalised the system with 1000 iterations from a hot start and the measurements of the coefficients were made on configurations separated by 2 units of Monte Carlo Time. However, this

β	κ	$a\hat{m}_0$	*Start*	N	T	I	*First Zero*
1.25	0.00	0.050	Cold	5,000	1,000	2	(0.000,0.0378)
1.25	0.00	0.020	Cold	12,000	1,000	2	(0.000,0.0379)
1.25	0.00	0.005	Cold	4,000	1,000	2	(0.000,0.0398)
1.25	0.00	0.020	Hot	6,000	1,000	2	(0.000,0.0382)

Table 6.6: Results of the behaviour of the edge singularity with the number of measurements(N), the thermalisation of the system from a cold(hot) start, and the "updating" mass $a\hat{m}_0$ for $\beta = 0.80$ and $\kappa = 0.00$, on a 8^3 lattice.

dependency of the edge singularity on the "updating" mass no longer exists if a cold start is used.

We also notice that if we increase the number of iterations when we thermalise the system from a hot start or the units of Monte Carlo Time between measurements of the coefficients, the dependency of the edge singularity on the "updating" mass does no longer exists.

In order to have a more clear picture of the behaviour of the edge singularity at $\beta = 1.25$ and $\kappa = 0.00$ we investigated the behaviour of it on a 8^3 lattice. We first noticed that the Lee-Yang zeros were imaginary. As can be seen in table(6.6) the edge singularity has **no significant dependence** on any of the parameters investigated at $(\beta = 0.80, \kappa = 0.00)$ **on a** 8^3 **lattice.**

The errors of the Lee-Yang zeros (calculated with the jackknife method described in chapter(3)) were about (or less than) 10% and are not shown for simplicity.

6.5 Summary

Our aim was to investigate if the closest zeros can be determined with sufficient accuracy to ascertain their finite size scaling behaviour (and hence that of the condensate) in the weak coupling where the chiral condensate is very small. However, we also investigated if the edge singularity can be determined with sufficient accuracy in the strong and intermediate coupling region.

Our investigation showed that the edge singularity can be determined with **sufficient accuracy** in the **weak** and **strong** coupling region and therefore, **we can ascertain its finite size scaling behaviour** as described in **chapters**$(4, 5)$.

In the intermediate coupling region we found an interesting behaviour of the edge singularity. In this region the edge singularity has a very small real part. It appears that the real part of the edge singularity at $\beta = 1.25$ and $\kappa = 0.00$, on a 4^3 lattice, depends on the "updating" mass when we thermalised the system from a hot start. However, when the number of iterations or the units of Monte Carlo Time were increased or the system was thermalised from a cold start, this dependence no longer existed. On the other hand, simulations on 8^3 lattice at $(\beta = 1.25, \kappa = 0.0)$ showed **no dependence of the edge singularity on the "updating" mass**, indicating that the previous dependence was due to the simulations being performed on a small lattice (4^3).

Therefore, our investigation showed that the edge singularity can be determined with **sufficient accuracy** in the **weak**, **intermediate** and **strong** coupling region and therefore, **we can ascertain its finite size scaling behaviour** in all the regions of the phase diagram, shown in Fig.(2.2).

Chapter 7

Partition Function Zeros in Non-Compact QED with fermions in 4D

7.1 Introduction to Non-Compact QED with Fermions in 4D

Quantum Electrodynamics (QED) is a very succesful type of quantum field theory in describing the electromagnetic interactions of electrons, muons etc. to a high precision in perturbation theory. It is a part of the standard electroweak model, which describes all phenomena of both electromagnetic and weak interactions in the presently known energy range up to about 100 GeV. Therefore, the non-perturbative lattice study of QED is not motivated by some unexplained phenomena or by lack of theoretical tools for the extraction of numerical predictions from the basic equations of the theory. The motivation at present is to try to improve the theoretical understanding of the general methematical properies of this type of quantum field theories.

It appears that QED suffers from the existence of the so-called Landau pole in the perturbative behaviour of the renormalised coupling constant as a function of the cut-off. The Callan-Symanzik β-function is defined as:

$$\beta(a) = -\Lambda \left(\frac{\partial a}{\partial \Lambda} \right)_{e, m_R} . \tag{7.1}$$

a is the renormalised fine structure constant, Λ is the cut-off, and the derivative is taken at fixed bare coupling e and renormalised mass m_R. The lowest orders in perturbation theory (up to three loops) in QED with one fermion species in the $\overline{MS}$ renormalisation scheme are given by:

$$\beta(a) \equiv a \sum_{\nu=1}^{\infty} \beta_\nu a^\nu, \tag{7.2}$$

$$\beta_1 = \frac{2}{3\pi}, \ \beta_2 = \frac{1}{2\pi^2}, \ \beta_3 = -\frac{31}{144\pi^3}. \tag{7.3}$$

The dependence of a on the cut-off is obtained from the differential equation:

$$\frac{da}{d \log \Lambda} = -\beta(a). \tag{7.4}$$

For simplicity we first consider only the one-loop approximation to the β-function (proportional to β_1). In this case the solution with $a_0 \equiv \frac{e^2}{4\pi}$ is:

$$a \left(\frac{\Lambda}{m_R} \right) = \frac{a_0}{1 + a_0 \beta_1 \log(\Lambda / m_R)}. \tag{7.5}$$

Therefore, in this approximation, the infinite cut-off limit of a is zero for any bare coupling a_0. The continuum theory is consistent only for vanishing renormalised coupling. In other words, according to the 1-loop β-function, the continuum limit of QED is **trivial**. The two-loop contribution proportional to β_2 does not change this conclusion qualitatively.

Instead of the fine structure constant a on the lattice one ussually considers the renormalised coupling squared e_R^2 defined by:

$$e_R^2 \equiv 4\pi a. \tag{7.6}$$

The β-function also determines the change of e_R^2 as a function of the renormalisation scale μ. The differential equation for $e_R^2(\mu)$ is, with $\beta_{e^2} \equiv 4\pi\beta$,

$$\frac{de_R^2(\mu)}{d\log\mu} = \beta_{e^2}(e_R^2(\mu)). \tag{7.7}$$

In the 1-loop approximation we have:

$$e_R^2(\mu) = \frac{e_R^2(\mu_0)}{1 - e_R^2(\mu_0)(\beta_1/4\pi)\log(\mu/\mu_0)}. \tag{7.8}$$

If $e_R^2(\mu) = e_R^2(\mu_0)$ at μ_0 then $e_R^2(\mu)$ becomes infinite at the scale:

$$\mu_{Landau} = \exp\mu_0 \left(\frac{4\pi}{\beta_1 e_R^2(\mu_0)}\right) \tag{7.9}$$

in the 1-loop approximation. The position of the Landau pole on the right hand side of Eqn.(7.8) is changed by the two loop contribution to:

$$\mu_{Landau} = \mu_0 \left(\frac{\beta_2}{4\pi\beta_1} e_R^2(\mu_0)\right)^{\beta_2/\beta_1^2} \exp\left(\frac{4\pi}{\beta_1 e_R^2(\mu_0)}\right)\left(1 + O[e_R^2(\mu_0)]\right). \tag{7.10}$$

The higher order corrections are contained here in the last parentheses. Substituting here the physical value of the renormalised coupling ($e_R^2(\mu_0) = 4\pi/137$) one obtains a very high scale. Therefore, in QED the mathematically inconsistent energy range is very far away from any reasonable scale.

The appearance of the Landau pole shows a mathematical inconsistency of renormalised perturbation theory in QED. This inconsistency can be resolved if the full β-function qualitatively behaves as shown in Fig.(7.1). In this case the zero of the β-function at $e_R^2 = e_*^2$ is an ultraviolet stable fixed point (UVFP). This means that the solution of the differential equation(7.7) for the running coupling constant $e_R^2(\mu)$ always tends to e_*^2, for $\mu \to \infty$. The zero of the Callan-Symanzik β-function in Eqn.(7.4) implies that it is possible to tune the bare coupling a_0 near $a_{0*} \equiv e_*^2/4\pi$ in such a way that for infinite cut-off, a, has an arbitrary finite limit. Therefore, if a UVFP at e_*^2 exists, the continuum limit is non-trivial. Note that the 3-loop β-function looks actually like Fig.(7.1), due to the opposite sign of the

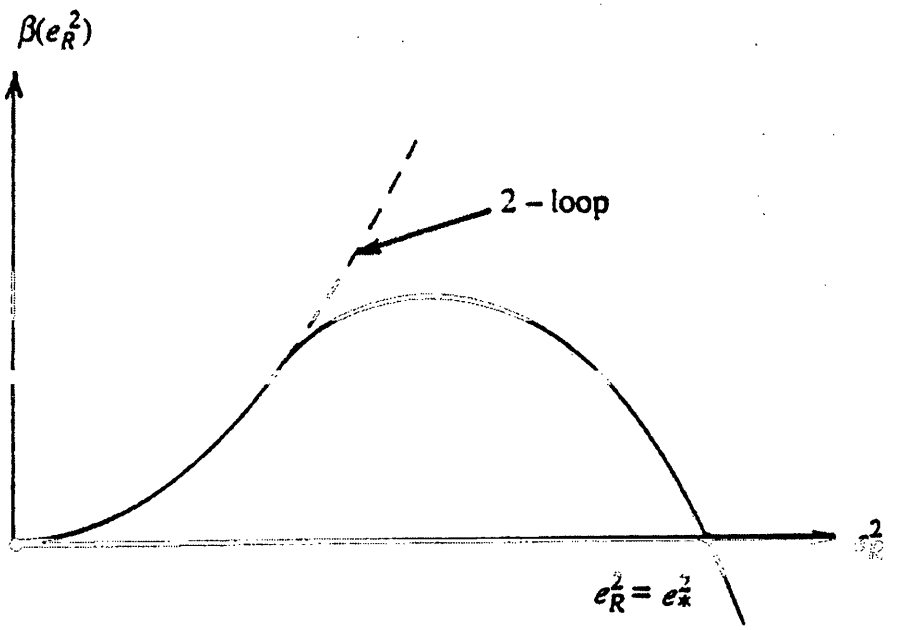

Figure 7.1: The behaviour of the Callan-Symanzik β-function in QED if there is a non-trivial ultraviolet fixed point at $e_R^2 = e_*^2$. The dashed line qualitatively shows the 2-loop β-function.

3-loop term in Eqn.(7.3). Nevertheless, the 3-loop zero is at such large value of e_R^2, that the perturbative approximation is not reliable there. Besides, the 3-loop contribution does also depend on the regularisation scheme, unlike the existence or non-existence of a zero. The zero of the β-function may be associated with a phase transition of QED in the space of bare parameters (m,e).

The first studies in lattice QED concentrated on the question of the chiral phase transition. Numerical simulations of compact QED showed that it undergoes a first order phase transition ([2] and references therein) and therefore a continuum limit cannot be defined. On the other hand, the existence of a continuous phase transition at finite inverse gauge coupling β, separating a strongly coupled phase where chiral symmetry is broken from a weak coupling phase where the symmetry is realised, was found in the non-compact QED(it will be defined later in this chapter) ([41] and references therein). This allows one to take the cut-off to infinity, which is prerequisite to a non-perturbative definition of a continuum theory. There are indications that non-compact QED, like other non-asymptotically free theories, is trivial in the sense that all renormalised couplings vanish as the cut-off is taken to infinity.

However, the various groups that have investigated the ultra-violet behaviour of four flavor non-compact QED disagree in the exact position of the critical point and the critical exponents of the chiral phase transition ([41] and references therein).

The aim in [40] was to investigate the behaviour of the lowest Lee-Yang zeros of the lattice partition function for non-compact QED. These zeros, which are in the complex fermion mass plane, correspond to singularities in the free energy and reflect the phase structure of the theory in the thermodynamic limit. Therefore, an investigation using the Lee-Yang zeros, could help to clarify the position of the critical point and the critical exponent of the transition.

However, exploratory simulations[39] of this theory on a 6^4 lattice showed that

these zeros appeared to depend on the "updating" mass at which the ensemble they are found from is generated. This dependence is incorrect (recall chapter(3)). Our task has been to investigate the nature of this dependence.

7.2 The Model

In the case of Abelian gauge fields it is also possible to define a non-compact formulation of the lattice action[26], which is based on the discretised version of the continuum field strength tensor: (in the following the lattice constant a has been set equal to one, so that all dimensionful quantities are to be understood in units of the (inverse) lattice spacing)

$$F^L_{\mu\nu}(x) = \frac{1}{2}[(A_\nu(x+\hat{\mu}) - A_\nu(x)) - (A_\mu(x+\hat{\nu}) - A_\mu(x))]. \tag{7.11}$$

Hence,

$$S_G^{(non-compact)} = \frac{1}{4}\sum_{x,\mu\nu} F^L_{\mu\nu}(x)F^L_{\mu\nu}(x). \tag{7.12}$$

This is a direct discretization of the Euclidean action of the Abelian gauge field in continuum. Here the real link variables $A_\mu(x)$ have a range $(-\infty, +\infty)$. Therefore, the intergration over gauge variables in the path integral is:

$$\int [dA] \equiv \prod_x \prod_{\mu=1}^{4} \int_{-\infty}^{+\infty} dA_\mu(x). \tag{7.13}$$

As a lattice version of non-compact QED we consider Kogut-Susskind fermions coupled to a non-compact $U(1)$ gauge field A_μ. The action now reads:

$$S = S_G + S_F \tag{7.14}$$

where:

$$S_G = \frac{\beta}{2}\sum_{x,\mu<\nu} (A_\mu(x) + A_\nu(x+\hat{\mu}) - A_\mu(x+\hat{\nu}) - A_\nu(x))^2, \tag{7.15}$$

$$S_F = \sum_{x,y} \overline{\chi}(x) M_{xy} \chi(y) \tag{7.16}$$

and

$$M_{xy} = m_0\delta_{xy} + \frac{1}{2}\sum_{\mu}(-1)^{x_1+\ldots+x_{\mu-1}}[e^{iA_\mu(x)}\delta_{yx+\hat{\mu}} - e^{-iA_\mu(y)}\delta_{yx-\hat{\mu}}]. \tag{7.17}$$

m_0 is the bare fermion mass, M is the fermionic matrix, $\beta = \frac{1}{e^2}$ (e is the bare charge).

In the naive continuum limit the fermionic action describes four Dirac fermions (flavours) coupled to a $U(1)$ gauge field. For finite lattice spacing it has a chiral $U(1) \times U(1)$ symmetry at $m_0 = 0$. The physically interesting region is near the phase transition at $\beta = \beta_c$, where this chiral symmetry is spontaneously broken.

7.2.1 Lee-Yang Zeros

As described in chapter(3), for the $\chi U\phi_3$ model, the GCPF of this model can be written as :

$$Z(\beta, m_0) = \frac{\int dA \det(M + m_0\mathbb{1})e^{-S_G}}{\int dA \det(M + \hat{m}_0\mathbb{1})e^{-S_G}}, \tag{7.18}$$

where $\hat{m}_0$ is the "updating" mass, M is the fermionic matrix at zero fermion mass, and S_G is the non-compact gauge field action. The eigenvalues of M are found using the Lanczos algorithm [42]. The determination of the eigenvalues enables the determination of the coefficients of the characteristic polynomial (recall chapter(3)).

These coefficients, averaged over the ensemble, give the polynomial expansion in m_0^2 for the GCPF:

$$Z(\beta, m_0) = \sum_{n=0}^{\frac{V}{2}} \exp(\overline{C}_n)(m_0^2)^n \tag{7.19}$$

or

$$Z(\beta, m_0) = \sum_{n=0}^{\frac{V}{2}} \exp(\overline{C}_n)(m_0^2 - \bar{m}_i^2)^n \tag{7.20}$$

where $\bar{m}$ is the "mass shift" as we recall from chapter(3).

Finally, the Lee-Yang zeros are found by using a standard root finding algorithm on the equivalent sets of polynomials generated as in the previous equation:

$$\sum_{n=0}^{\frac{V}{2}} A_n^i (m_0^2 - \bar{m}_i^2)^n \tag{7.21}$$

for a set of $\bar{m}_i$ in the region where we expect the lowest zeros to occur. We first used a standard rootfinder[44] in order to find the zeros of the polynomials and then a multi-precision package MPFun[43] which allowed us to consider approximately known coefficients. We used an input precision, d_n, which defined the polynomial neighbourhood of the GCPF polynomial, i.e, the set of all the polynomials with coefficients having d_n common digits with the corresponding coefficients of the GCPF polynomial. For example, we could choose 15 common digits (as in the standard machine precision) up to 500 common digits.

7.3 Strong Coupling Calculations

We first performed simulations on a 6^4 lattice at $\beta = 0.22$ (above β_c ([41] and references therein)). We have used the Hybrid Monte Carlo algorithm, as in [41], for updating the gauge field configurations and we thermalised the system with 250 iterations from a hot start. We chose the molecular dynamics parameters to keep the length of each molecular dynamics trajectory ~ 0.8 and the acceptance rate $\sim 0.9-0.95$. Measurements of the coefficients were made on configurations separated by 6 units of Molecular Dynamics time. In order to investigate the dependence of the edge singularity on the "updating" mass we generated an ensemble of configurations using $\hat{m_0} = 0.04$ as the "updating" mass and a second ensemble using $\hat{m_0} = 0.02$ as the "updating" mass.

On a 6^4 lattice for $\beta = 0.22$, the zeros are imaginary and appear in conjugate pairs. The edge singularity is defined as the zero with the smallest positive imaginary part and we count each pair only once.

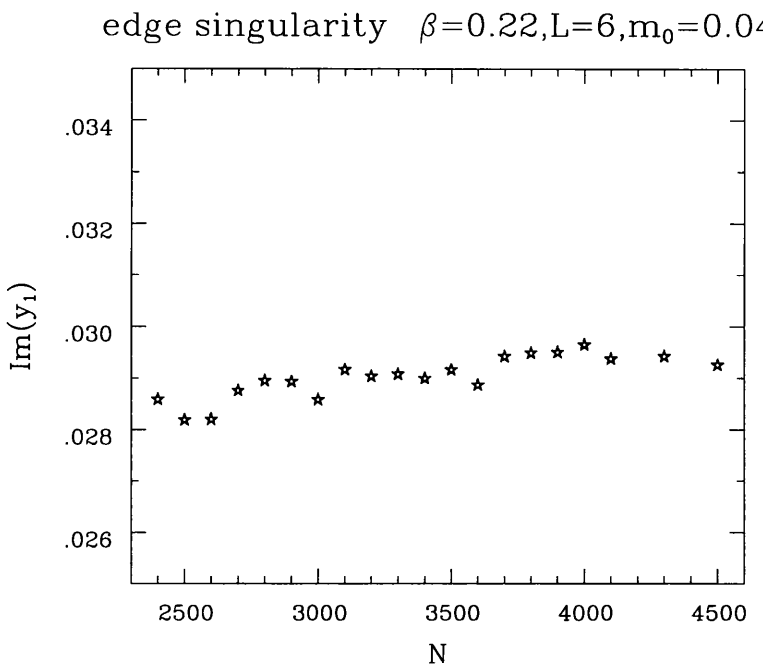

Figure 7.2: The Imaginary part of the lowest zero with increasing number of measurements.

Figs.(7.2,7.3) show the evolution of the edge singularity (every 100 measurements) for $\hat{m_0} = 0.04, \hat{m_0} = 0.02$ "updating" masses, respectively. Fig.(7.4) shows the lowest zeros, plotted in sequence, for the two different "updating" masses. It is obvious that there is a strong dependence of the Lee-Yang zeros on the "updating" mass.

However, one has to notice that for $\hat{m_0} = 0.02$ the first two zeros have imaginary parts so close as to be indistinguishable within statistical error. Assuming that the first two zeros (for $\hat{m_0} = 0.02$) have within the numerical precision identical imaginary part, the lowest Lee-Yang zeros seem to depend now weakly on the "updating" mass as can be shown in Fig.(7.5).

We also performed simulations on a 6^4 lattice at $\beta = 0.19$, (close to β_c ([41] and references therein)). We thermalised the system with 100 iterations from a hot start. We chose the molecular dynamics parameters to keep the length of each

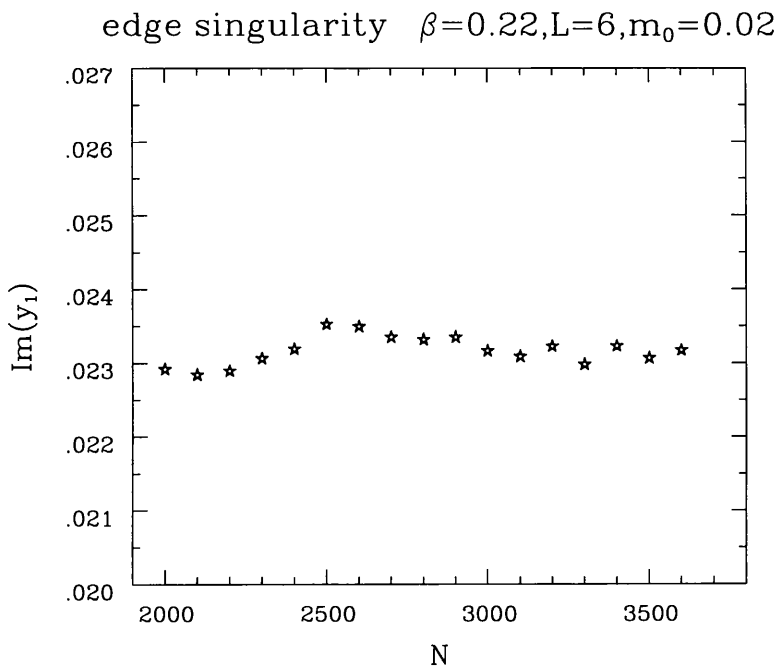

Figure 7.3: The Imaginary part of the lowest zero with increasing number of measurements.

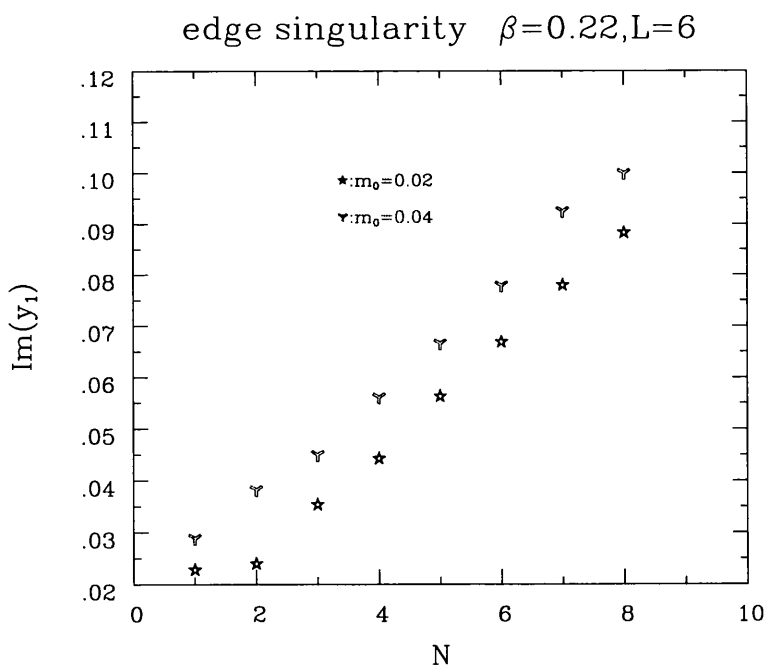

Figure 7.4: The lowest zeros on the 6^4 lattice plotted in sequence.

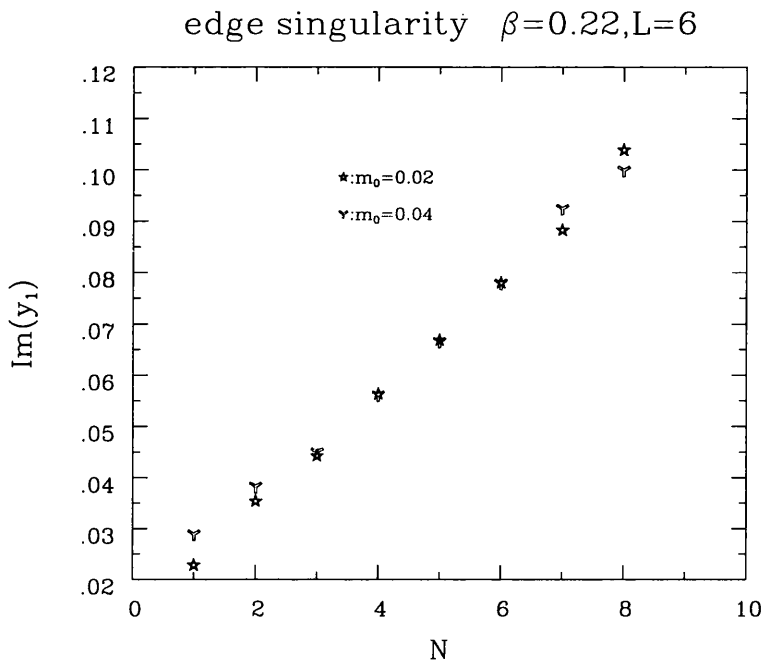

Figure 7.5: The lowest zeros on the 6^4 lattice plotted in sequence. We have assumed that the first two zeros (for $\hat{m_0} = 0.02$) have imaginary parts so close as to be indistinguishable within statistical error.

molecular dynamics trajectory ~ 0.8. In order to investigate again the dependence of the edge singularity on the "updating" mass we generated an ensemble of configurations using $\hat{m_0} = 0.04$ as the "updating" mass and a second enseble using $\hat{m_0} = 0.01$ as the "updating" mass.

We first noticed that the acceptance rate for the enseble of configurations using $\hat{m_0} = 0.01$ as the "updating" mass was $\sim 0.45 - 0.50$ compare to the acceptance rate, for the enseble of configurations using $\hat{m_0} = 0.04$ as the "updating" mass, which was $\sim 0.9 - 0.95$. We also noticed that the simulations with the $\hat{m_0} = 0.01$ "updating" mass gave jumps ("spikes") in the plaquette energy between configurations. A typical examples of these "spikes" is shown in Fig.(7.6). The number of "spikes" decreased when we decreased the time stepsize of the molecular dynamics trajectory. On the other hand no significant jumps in the plaquette enrgy were noticed between configurations for the simulations with the $\hat{m_0} = 0.04$ "updating" mass.

On a 6^4 lattice for $\beta = 0.19$, the zeros near the physical mass region ($m_0 \geq 0$ and real) were imaginary indicating that any phase transition will only occur at zero fermion mass, as expected. Figs.(7.7,7.8) show again the evolution of the edge singularity (every 100 measurements) for $\hat{m_0} = 0.04, \hat{m_0} = 0.01$ "updating" masses, respectively. Fig.(7.9) shows the lowest zeros, plotted in sequence, for the two different "updating" masses. We notice again that there is a weak dependence of the lowest Lee-Yang zeros on the "updating" mass.

Finally, we calculated the Lee-Yang zeros using a multi-precision rootfinder which allowed us to to consider approximately known coefficients. Although we chose from 15 up to 500 digits for the input precision d_n, the value of the edge singularity did not change significantly for both "updating" masses.

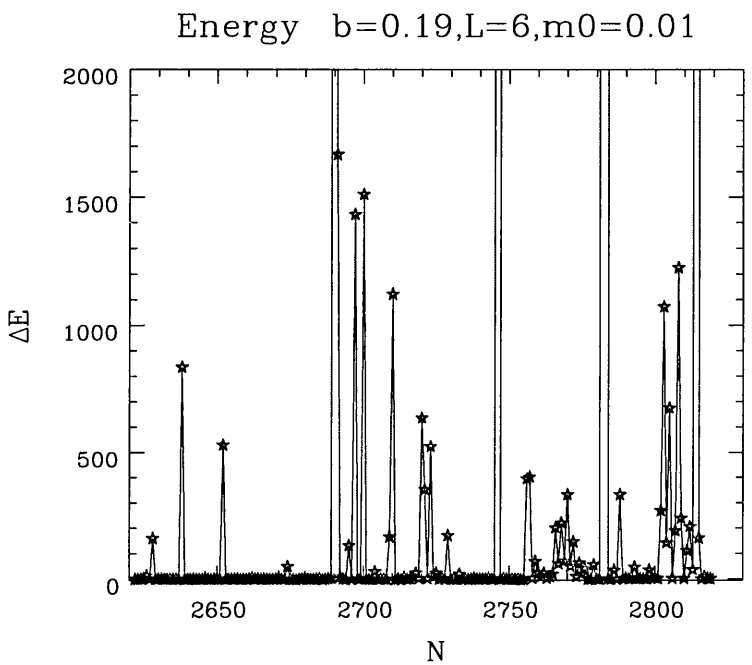

Figure 7.6: The difference in the plaquette energy between configurations with increasing number of configurations.

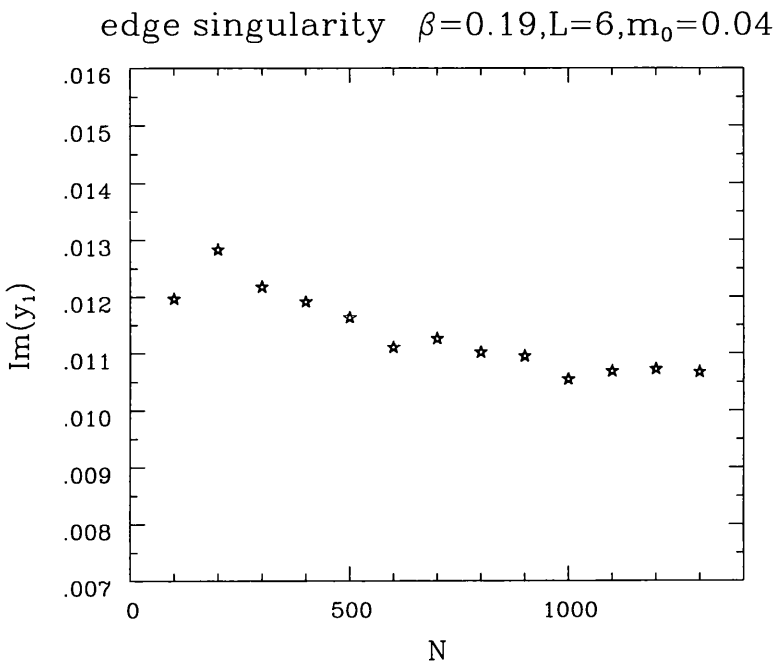

Figure 7.7: The Imaginary part of the lowest zero with increasing number of measurements.

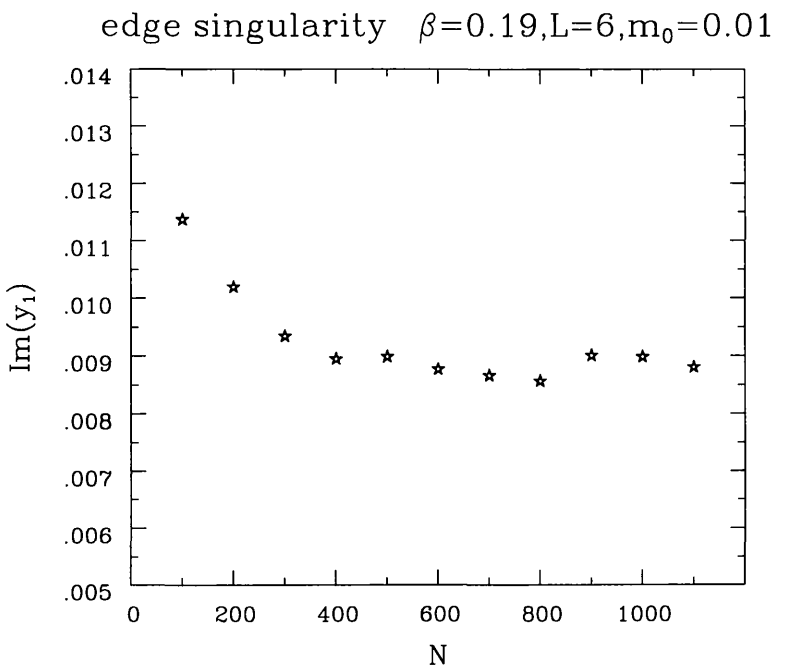

Figure 7.8: The Imaginary part of the lowest zero with increasing number of measurements.

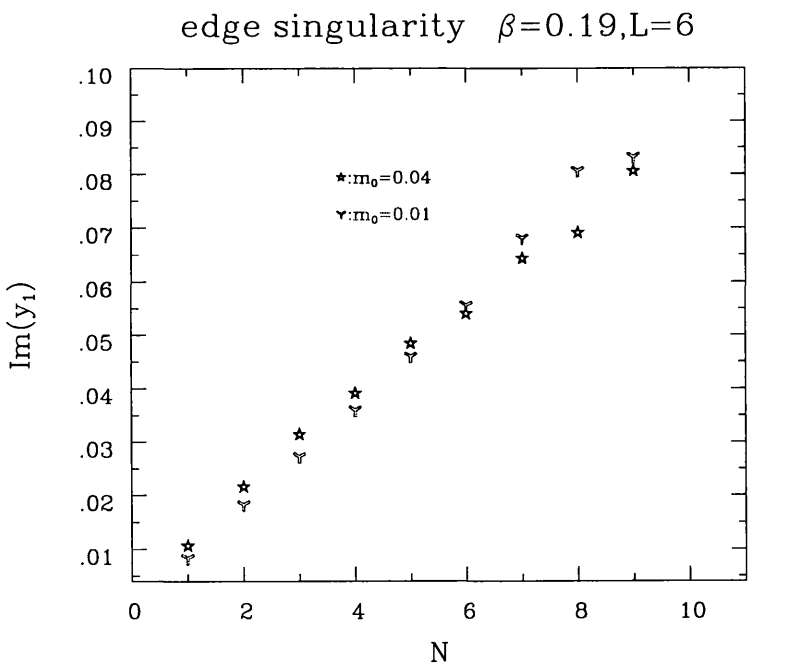

Figure 7.9: The lowest zeros on the 6^4 lattice plotted in sequence.

7.4 Summary

We noticed in our simulations on a 6^4 lattice that there is a dependence of the edge singularity on the "updating" mass at which the ensemble it is found from is generated. This dependence is incorrect (recall chapter(3)).

The simulations on a 6^4 lattice at $\beta = 0.19$ (close to β_c) with $\hat{m_0} = 0.01$ as the "updating" mass gave jumps ("spikes") in the plaquette energy between configurations. The number of "spikes" decreased when we decreased the time stepsize of the molecular dynamics trajectory. The simulations on a 6^4 lattice at $\beta = 0.22$ (above β_c) with $\hat{m_0} = 0.02$ as the "updating" mass showed that the the first two zeros have imaginary parts so close as to be indistinguishable within statistical error. Note that this behaviour is only observed in the edge singularity.

High statistics simulations on large lattices, using a set of different "updating" masses, are probably necessary in order to verify the absence of the dependence of the edge singularity on the update mass at which the ensemble it is found from is generated.

Chapter 8

Summary and Conclusions

The "$\chi U\phi$ model" or QED with scalars and fermions is a model which was suggested as a promising candidate[1] for dynamical fermion mass generation. In two dimensions it seems to be in the universality class of the Gross-Neveu model[10] at least for strong gauge coupling, and so is renormalizable. In four dimensions there is also a strong coupling region in which the model behaves in a very similar manner to the corresponding four-fermion theory, the Nambu–Jona-Lasinio model with a massive fermion whose mass scales at the critical point. Here both models belong to the same universality class and have the same renormalizability properties. But for intermediate coupling there evidently exists a special point. It is a tricritical point at which, together with the composite fermion F, scaling of a particular scalar state was found. This composite scalar can be interpreted as a gauge ball mixing with a $\phi^\dagger$-ϕ state. Thus the gauge degrees of freedom play an important dynamical role and the model belongs to a new universality class of models with dynamical mass generation and whose renormalizability is of much interest[12, 13].

We investigated, in this work, the phase structure of the three-dimensional "$\chi U\phi$ model" or compact lattice QED with scalars and fermions in three dimensions. The analysis has been made possible by the application of two different

methods: 1)fits to an equation of state of the chiral condensate and the mass of the physical neutral fermion and 2)finite size scaling investigations of the Lee-Yang zeros of the partition function in the complex fermion mass plane.

Our investigations showed that there are three regions in the β-κ plane with possibly different critical behaviour in the chiral limit:

a) The region at small κ and strong gauge coupling, where the chiral symmetry is broken and the neutral physical fermion is massive, called the Nambu phase.

b) The region at large κ, where the chiral symmetry is restored and the physical fermion is massless, called the Higgs phase.

c) A third region at weak coupling and small κ, where the chiral condensate is zero within our numerical accuracy but the neutral fermion mass is large, called the X region. This region can analytically be connected with either the Nambu or Higgs phase but it may well be a separate phase. If chiral symmetry is not broken in this region, then the mass observed in the fermion channel is presumably the energy of a two-particle state. Otherwise this region might be an interesting example of dynamical mass generation of unconfined fermions. If the continuum limit is taken at the Higgs phase transition, the gauge fields should play an important dynamical role and the model would not fall into the universality class of the three-dimensional Gross-Neveu model. A further investigation of this possibility is highly desirable.

In the region X of the phase diagram, the chiral condensate is very small, which suggests that the Lee-Yang zeros cannot be near to the physical region. It was of interest to investigate if the closest zeros can be determined with sufficient accuracy to ascertain their finite size scaling behaviour (and hence that of the condensate) in the weak coupling region. Our investigation showed that the edge singularity can be determined with **sufficient accuracy** not only in the **weak**, but also in the **intermediate** and **strong** coupling region and therefore, **we can ascertain its finite size scaling behaviour** in all the regions of the phase

diagram.

At strong gauge coupling, the chiral phase transition was clearly localized, and there are strong indications that it is in one universality class for all $\beta \leq 0.80$ (and probably for all $\beta \leq 1.25$): that of the three-dimensional Gross-Neveu model, which is known to be non-pertubatively renormalizable. This demonstrates that the three-dimensional lattice $\chi U \phi_3$ model is a nonperturbatively renormalizable quantum field theory and the shielded gauge-charge mechanism of fermion mass generation works in three dimensions.

There are indications that non-compact QED, like other non-asymptotically free theories, is trivial in the sense that all renormalised couplings vanish as the cut-off is taken to infinity. The various groups that have investigated the ultra-violet behaviour of four flavor non-compact QED disagree in the exact position of the critical point and the critical exponents of the chiral phase transition ([41] and references therein). The aim in [40] was to investigate the behaviour of the lowest Lee-Yang zeros of the lattice partition function for non-compact QED and help to clarify the position of the critical point and the critical exponent of the transition. However, exploratory simulations[39] of this theory on a 6^4 lattice showed that these zeros appeared to depend on the "updating" mass at which the ensemble they are found from is generated. This dependence is incorrect.

Our task was to investigate the nature of this dependence. Our analysis confirmed the dependence of the Lee-Yang zeros on the "updating" mass on a 6^4 lattice. (Note that we observed jumps ("spikes") in the plaquette energy between configurations on the 6^4 lattice simulations for small "updating" masses at $\beta \sim \beta_c$).

High statistics simulations on large lattices, using a set of different "updating" masses, are probably necessary in order to verify the absence of the dependence of the edge singularity on the update mass at which the ensemble it is found from is generated.

Bibliography

[1] C. Frick and J. Jersák, *Phys. Rev.* **D52** (1995) 340.

[2] V. Azcoiti, I.M. Barbour, R. Burioni, G. Di Carlo, A.F. Grillo, G. Salina Phys. Rev. **D51**, 5199 (1998).

[3] I.M. Barbour, A.J. Bell, M. Bernaschi, G. Salina, A. Vladikas, Nucl.Phys. **B386**, 683 (1992).

[4] H.B. Nielsen and M. Ninomiya, Nucl.Phys. **B185**, 20 (1981).

[5] H.B. Nielsen and M. Ninomiya, Nucl.Phys. **B195**, 541 (1981).

[6] H.B. Nielsen and M. Ninomiya, Nucl.Phys. **B193**, 173 (1981).

[7] H. Kluberg-Stern, A. Morel, O. Napoly and B. Peterson, Nucl.Phys. **B220**, 447 (1983).

[8] L.H. Karsten and J. Smit, Nucl.Phys. **B183**, 103 (1981).

[9] M. Lindner and D. Ross, Nucl.Phys. **B370**, 30 (1992).

[10] W. Franzki, J. Jersák, and R. Welters, *Phys. Rev.* **D54**, 7741 (1996).

[11] I.M. Barbour, A.J. Bell, and E.G. Klepfish, Nucl.Phys. **B389**, 285 (1993).

[12] W. Franzki and J. Jersák, *Strongly coupled U(1) lattice gauge theory as a microscopic model of Yukawa theory*, PITHA 97/42, HLRZ1997_65, hep-lat/9711038, to appear in Phys. Rev. D.

[13] W. Franzki and J. Jersák, *Dynamical fermion mass generation at a tricritical point in strongly coupled U(1) lattice gauge theory*, PITHA 97/43, HLRZ1997_66, hep-lat/9711039, to appear in Phys. Rev. D.

[14] I.M. Barbour, R. Burioni and G. Salina, *Phys. Lett.* **B341**, 355 (1995).

[15] B. Rosenstein, B. J. Warr, and S. H. Park, *Phys. Rev. Lett.* **62**, 1433 (1989).

[16] I.-H. Lee and R. E. Shrock, *Phys. Rev. Lett.* **59**, 14 (1987).

[17] I. M. Barbour, W. Franzki, N. Psycharis, Nucl.Phys. **B63** (Proc. Suppl.) 712 (1998).

[18] I. M. Barbour, E. Focht, W. Franzki, J. Jersak and N.Psycharis, Phys. Rev. **D58**, 074507 (1998).

[19] S.P. Martin, Phys. Rev. **D46**, 2197 (1992).

[20] W.Franzki, *Dynamische Erzeugung von Fermionmassen in stark gekoppelten Eichtheorien auf dem Gitter*, Dissertation RWTH Aachen, Shaker Verlag 1997.

[21] A. M. Polyakov, *Nucl. Phys.* **B120**, 429 (1977).

[22] A. M. Polyakov, *Phys. Lett.* **59B**, 82 (1975).

[23] T. Appelquist, D. Nash, and L. C. R. Wijewardhana, *Phys. Rev. Lett.* **60**, 2575 (1988).

[24] T. Banks and A. Casher, *Nucl. Phys.* **B169**, 103 (1980).

[25] E. Dagotto, J. B. Kogut, and A. Kocic′, *Phys. Rev. Lett.* **62**, 1083 (1989).

[26] E. Dagotto, J. B. Kogut, and A. Kocic′, *Phys. Rev. Lett.* **60**, 772 (1988).

[27] E. Dagotto, J. B. Kogut, and A. Kocic′, *Nucl. Phys.* **B334**, 279 (1990).

[28] S. Hands and J. B. Kogut, *Nucl. Phys.* **B335**, 455 (1990).

[29] L. Del Debbio and S. J. Hands, *Phys. Lett.* **373B**, 171 (1996).

[30] L. Del Debbio, S. J. Hands, and J. C. Mehegan, *Nucl. Phys.* **B502**, 269 (1997).

[31] T. Banks, R. Myerson, and J. Kogut, *Nucl. Phys.* **B129**, 493 (1977).

[32] M. Göpfert and G. Mack, *Commun. Math. Phys.* **82**, 545 (1982).

[33] A. N. Burkitt and A. C. Irving, *Nucl. Phys.* **B295 [FS21]**, 525 (1988).

[34] S. P. Booth, R. D. Kenway, and B. J. Pendleton, *Phys. Lett.* **228B**, 115 (1989).

[35] A. Ali Khan, M. Göckeler, R. Horsley, P. E. L. Rakow, G. Schierholz, and H. Stüben, *Phys. Rev.* **D51**, 3751 (1995).

[36] K.-I. Kondo, *Nucl. Phys.* **B450**, 251 (1995).

[37] W. Franzki, C. Frick, J. Jersák, and X. Q. Luo, *Nucl. Phys.* **B453**, 355 (1995).

[38] B. Rosenstein, B. J. Warr, and S. H. Park, *Phys. Lett.* **219B**, 469 (1989).

[39] A. Ali Khan, I. Barbour and G. Salina, unpublished work.

[40] A. Ali Khan and I. Barbour, Nucl. Phys. **B** (Proc. Suppl.) 42 (1995), 651.

[41] M. Göckeler, R. Horsley, V.Linke, P. Rakow, G. Schierholz and H.Stuben, Nucl.Phys. **B487** (1997) 313.

[42] C. Lanczos, J. Res. Nat. Bur. Standards **45**, 409 (1952).

I.M. Barbour, N. E. Behill, P. Gibbs, G. Schierholz and M. Teper, " The Lanczos Method in Lattice Gauge Theories " in: *The Recursion Method and its Applications*, Lecture notes in Physics, Springer, Berlin (1985).

[43] D.H.Bailey, A Fortran-90 Based Multiprecision System, RNR Technical Report RNR-94-013, NASA Ames Research Center, Moffett Feild, CA 94035 USA, 1995.

[44] D.A.Bini, Numerical computation of polynomial zeros by means of Aberth's method, Munerical Algorithms, **13**, 179, 1996.

[45] C.N.Yang and T.D.Lee, *Phys. Rev.* **87**, 404 (1952).

[46] C.N.Yang and T.D.Lee, *Phys. Rev.* **87**, 410 (1952).

[47] Kerson Huang,Statistical Mechanics, Wiley, 1987.

[48] C.Itzykson, R.B.Pearson and J.-B.Zuber, Nucl.Phys. **B220** (1983) 415.